NAVAL POSTGRADUATE SCHOOL
MONTEREY, CALIFORNIA

THESIS

SIMPLIFIED MICROMECHANICAL MODELS FOR ANALYSIS OF INTERFACE DEBONDING IN A FIBROUS COMPOSITE

by

Guo, Jia-Yuarn

December, 1995

Thesis Advisor:　　　　　　　　Young W. Kwon

Approved for public release; distribution is unlimited.

19960415 079

REPORT DOCUMENTATION PAGE

Form Approved OMB No. 0704-0188

1. AGENCY USE ONLY *(Leave blank)*	2. REPORT DATE December 1995	3. REPORT TYPE AND DATES COVERED Master's Thesis

4. TITLE AND SUBTITLE SIMPLIFIED MICROMECHANICAL MODELS FOR ANALYSIS OF INTERFACE DEBONDING IN A FIBROUS COMPOSITE	5. FUNDING NUMBERS
6. AUTHOR(S) Guo, Jia-Yuarn	

7. PERFORMING ORGANIZATION NAME(S) AND ADDRESS(ES) Naval Postgraduate School Monterey CA 93943-5000	8. PERFORMING ORGANIZATION REPORT NUMBER

9. SPONSORING/MONITORING AGENCY NAME(S) AND ADDRESS(ES)	10. SPONSORING/MONITORING AGENCY REPORT NUMBER

11. SUPPLEMENTARY NOTES The views expressed in this thesis are those of the author and do not reflect the official policy or position of the Department of Defense or the U.S. Government.

12a. DISTRIBUTION/AVAILABILITY STATEMENT Approved for public release; distribution is unlimited.	12b. DISTRIBUTION CODE

13. ABSTRACT *(maximum 200 words)*

The objective of this study is to develop simplified micromechanical models to analyze the interface debonding between fiber and the matrix materials. Both analytical and simplified finite element models are used to predict the effective transverse elastic modules of fibrous composites with a partial interface crack based on the material properties of their constituents. The simplified finite element model uses springs in the connecting nodes between the fiber and matrix. A detailed finite element analysis, which is programmed using the MATLAB engineering software is performed to check the accuracy of the simplified models. The simplified models yield accurate effective transverse elastic modulii of various composites with partial interface cracks when compared to the results obtained from detailed finite element analyses.

14. SUBJECT TERMS Micromechanical Models, Interface Debonding, Fibrous Composite	15. NUMBER OF PAGES 116
	16. PRICE CODE

17. SECURITY CLASSIFICATION OF REPORT Unclassified	18. SECURITY CLASSIFICATION OF THIS PAGE Unclassified	19. SECURITY CLASSIFICATION OF ABSTRACT Unclassified	20. LIMITATION OF ABSTRACT UL

NSN 7540-1-280-5500 Standard Form 298 (Rev. 2-89)
Prescribed by ANSI Std. 239-18 298-102

SIMPLIFIED MICROMECHANICAL MODELS FOR ANALYSIS OF INTERFACE DEBONDING IN A FIBROUS COMPOSITE

Guo, Jia-Yuarn
Major, Republic of China Army
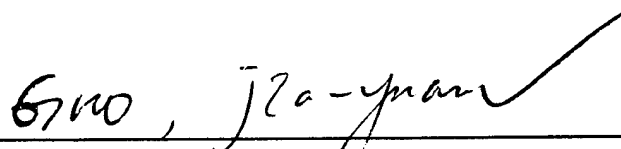B.S., Chung Cheng Institute of Technology - 1986

Submitted in partial fulfillment
of the requirements for the degree of

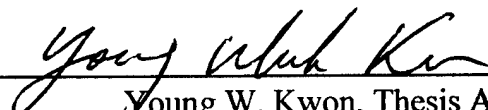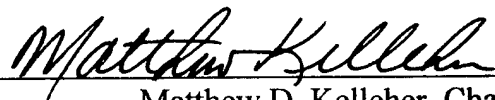## MASTER OF SCIENCE IN ENGINEERING SCIENCE

from the

NAVAL POSTGRADUATE SCHOOL
December 1995

Author: _____
Guo, Jia-Yuarn

Approved by: _____
Young W. Kwon, Thesis Advisor

_____
Matthew D. Kelleher, Chairman
Mechanical Engineering Department

iii

ABSTRACT

The objective of this study is to develop simplified micromechanical models to analyze the interface debonding between fiber and the matrix materials. Both analytical and simplified finite element models are used to predict the effective transverse elastic modules of fibrous composites with a partial interface crack based on the material properties of their constituents. The simplified finite element model uses springs in the connecting nodes between the fiber and matrix. A detailed finite element analysis, which is programmed using the MATLAB engineering software is performed to check the accuracy of the simplified models. The simplified models yield accurate effective transverse elastic modulii of various composites with partial interface cracks when compared to the results obtained from detailed finite element analyses.

TABLE OF CONTENTS

viii

LIST OF FIGURES

xii

LIST OF TABLES

I. INTRODUCTION

Use of fibrous composite material is expanding rapidly, especially in structural application because properties of fibrous composite materials are beneficial such as high ratios of stiffness-to-weight and strength-to-weight.

Prediction of effective modulii of fibrous composites from material properties of their constituents has been a main topic, especially when there are micro-cracks. There are many different micromechanics models which have been proposed to predict effective moduli. However, most of them did deal with neither damages nor 3-D models. Broutman and Sahn observed the transverse matrix cracking in cross-ply composites [Ref. 1]. After the observation, the phenomenon has been studied analytically and experimentally by several investigators. Highsmith and Reifsnider [Ref. 2] conducted an experiment to measure the longitudinal stiffness reductions of various laminates. Talreja [Ref. 3,4] used continuum damage mechanics to represent damage as internal variables in a phenomenological approach, and Kwon [Ref. 5] used an analytical micromechanics model to predict the effective modulii of composites. Kwon and Berner [Ref. 6] also used a micromechanics model to investigate matrix cracking in laminated fibrous composite, and predict matrix cracking and its effect on stiffness reduction.

An analysis of a fibrous composite structure requires information of material properties of the composite. To determine the material properties of a composite, it is necessary to conduct experiments that will allow measurement of those properties. Even though some of the material properties can be determined with physical tests, it is difficult to obtain some other properties of the composite.

This study will develop simplified micromechanical models to analyze the interface debonding between the fiber and the matrix materials using an analytical model and a simple two-dimensional finite element model with which the effective transverse elastic modulii of fibrous composites with partial interface cracks can be predicted. Since modeling an interface crack in the simplified finite element model is limited by a

1

minimum number of node points, the model uses springs in the connecting nodes between the fiber and matrix. In order to check the accuracy of the two simplified micromechanics models, a detailed finite element analysis is performed.

Using properties of the fiber and matrix materials as well as their fiber volume fractions, it can be determined the relationship between the elastic modulus and the crack length. Figure 1 shows a micromechanical modeling process. In later chapters, both analytical and finite element micromechanical models will be presented, and followed by the results and discussion. The last chapter has conclusions and recommendations.
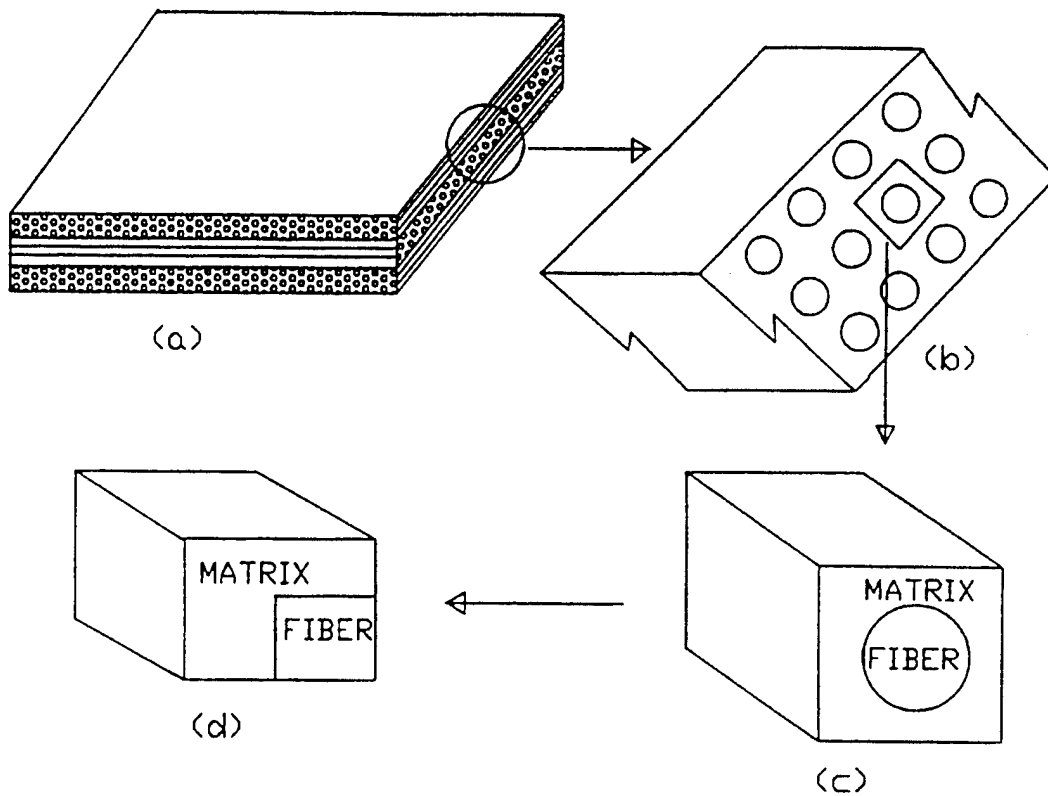
Figure 1. Modeling Process of a Micromechanical Model From a Fibrous
Composite.

II. MICROMECHANICS MODELS

A.   ANALYTICAL MICROMECHANICS MODEL

This micromechanics model, which considers a unit cell consisting of the fiber and surrounding matrix material, was developed by Kwon [Ref. 5], and is shown in Figure 2. The cross-section of the fiber is assumed to be square, for simplicity, and the unit cell is divided into four subcells a,b,c and d. Subcell 'a' represents the fiber section and other subcells are the matrix. The size of the unit cell is unity, and the size of the subcell varies with the fiber volume fraction. The stress continuity at the subcell interfaces is expressed as:

$$\sigma_{22}^a = \sigma_{22}^b, \sigma_{22}^c = \sigma_{22}^d, \sigma_{33}^a = \sigma_{33}^c, \sigma_{33}^b = \sigma_{33}^d$$

$$\sigma_{12}^a = \sigma_{12}^b, \sigma_{12}^c = \sigma_{12}^d, \sigma_{13}^a = \sigma_{13}^c, \sigma_{13}^b = \sigma_{13}^d \qquad \text{(2-1)}$$

$$\sigma_{23}^a = \sigma_{23}^b = \sigma_{23}^a = \sigma_{23}^b \quad ,$$

and the strain compatibility is assumed as:

$$\varepsilon_{11}^a = \varepsilon_{11}^b = \varepsilon_{11}^c = \varepsilon_{11}^d$$

$$\varepsilon_{22}^a + \varepsilon_{22}^b = \varepsilon_{22}^c + \varepsilon_{22}^d, \varepsilon_{33}^a + \varepsilon_{33}^c = \varepsilon_{33}^b + \varepsilon_{33}^d \qquad \text{(2-2)}$$

$$\varepsilon_{2}^a + \varepsilon_{12}^b = \varepsilon_{12}^c + \varepsilon_{12}^d, \varepsilon_{13}^a + \varepsilon_{13}^c = \varepsilon_{13}^b + \varepsilon_{13}^d \quad .$$

The constitutive relation within each subcell can be expressed as:

$$\sigma_{ij}^\alpha = E_{ijkl}^\alpha \varepsilon_{kl}^\alpha \quad , \qquad \text{(2-3)}$$

where $i,j,k,l = 1,2,3$ and $\alpha = a,b,c,d$.

From Figure 2 (before crack), Kwon [Ref. 5] expressed the composite stresses and strains as a function of the subcell stresses, subcell strains and the fiber volume fraction as follows:

$$\overline{\sigma}_{ij} = V_f \sigma_{ij}^a + \sqrt{V_f}\left(1 - \sqrt{V_f}\right)\sigma_{ij}^b + \sqrt{V_f}\left(1 - \sqrt{V_f}\right)\sigma_{ij}^c + \sqrt{V_f}\left(1 - \sqrt{V_f}\right)^2 \sigma_{ij}^d \quad , \qquad \text{(2-4)}$$

5

$$\overline{\varepsilon}_{ij} = V_f \varepsilon_{ij}^a + \sqrt{V_f}\left(1 - \sqrt{V_f}\right)\varepsilon_{ij}^b + \sqrt{V_f}\left(1 - \sqrt{V_f}\right)\varepsilon_{ij}^c + \sqrt{V_f}\left(1 - \sqrt{V_f}\right)^2 \varepsilon_{ij}^d \ \cdot, \qquad (2\text{-}5)$$

where $\overline{\sigma}_{ij}$ and $\overline{\varepsilon}_{ij}$ are composite stresses and strains, σ^{α}_{ij} and $\varepsilon^{\alpha}_{ij}$ are stresses and strains of each subcell, and V_f is the fiber volume fraction that determines the size of the subcell. The composite stresses and strains are determined from the volume average of the stresses and strains of the subcells.

a - Fiber Subcell
b, c and d - Matrix Subcells
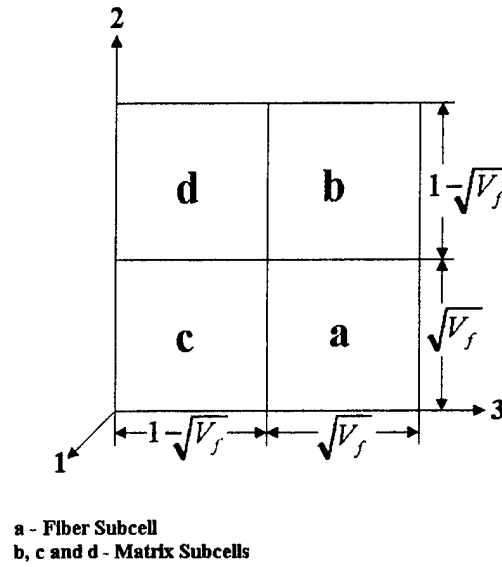
Figure 2. Subcells of a Unit Cell.

When there is an interface crack between the fiber and the matrix as shown in Figure 3, some volume portions of subcells a and c cannot sustain a load applied in the 3-direction. As a result, equation (2-4) is rewritten as

6

$$\bar{\sigma}_{ij} = \sqrt{V_f}\left(\sqrt{V_f} - \frac{\ell}{2}\right)\sigma_{ij}^a + \sqrt{V_f}\left(1 - \sqrt{V_f}\right)\sigma_{ij}^b +$$
$$\left(2\sqrt{V_f} - \frac{\ell}{2}\right)\frac{\left(1 - \sqrt{V_f}\right)}{2}\sigma_{ij}^c + \left(1 - \sqrt{V_f}\right)^2 \alpha_{ij}^d \quad , \tag{2-6}$$

a - Fiber Subcell
b, c and d - Matrix Subcells ℓ Crack Length
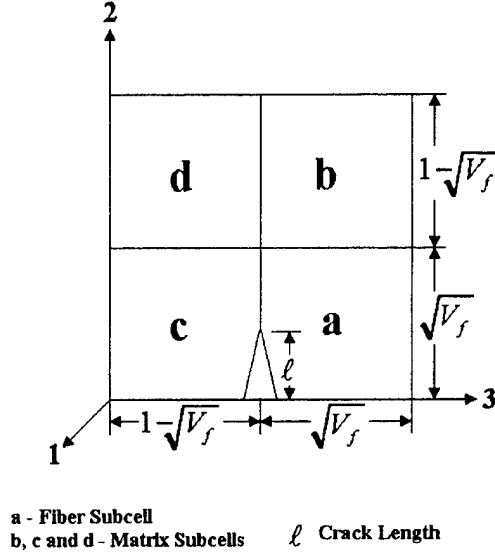
Figure 3. Crack Situation in Unit Cell.

In order to find the relation between composite stresses and composite strains, first of all equations (2-1) through (2-3) and (2-5) are solved together. Then, the following matrix equation can be obtained.

$$[A]\{\varepsilon_{ij}^\alpha\} = \{\bar{\varepsilon}_{ij}\} \quad i,j = 1,2,3 \quad , \tag{2-7}$$

where $[A]$ is a constant coefficient matrix and is invertible.

Pre-multiplying $[A]^{-1}$ on both sides of equation 2-7, we get:

$$\{\varepsilon_{ij}\} = [A]^{-1}\{\bar{\varepsilon}_{ij}\} \quad . \tag{2-8}$$

7

Finally, combining equation 2-4 and equation 2-8 along with equation 2-3 yields the relationship between composite stresses and strains:

$$\left\{\overline{\sigma}_{ij}\right\} = [C]\left\{\overline{\varepsilon}_{ij}\right\} \quad , \tag{2-9}$$

where [C] is the smeared material property matrix of the composite. In case of the interface crack, equation (2-6) is used instead of equation (2-4) with the same procedures.

In Kwon's model, he assumed the fiber and matrix were orthotropic materials. This means the normal stress (strain) components and the shear stress (strain) components are uncoupled. Appendix A shows the equations relating the subcell strains to the composite strains for the normal strains.

B.   FINITE ELEMENT MICROMECHANICS MODEL

The finite element method (FEM) is a numerical procedure for solving differential equations of physics and engineering. A continuous quantity such as displacements, temperature, or pressure can be approximated by a piece-wise continuous function spanned over a finite number of subdomains into which the problem domain is divided. For each subdomain, nodal variables are defined as unknowns which satisfy the governing equation in an approximate manner. The nodal unknowns are assembled into a system of matrix equation for the whole domain. The matrix equation is solved for the unknowns with prescribed boundary conditions.

1.   Finite Element Method

In this study, one of the finite element methods called the weighted residual method (WRM) has been selected for the micromechanical model. The concept of this method is to minimize the residual multiplied by a weighting function (W). The WRM has many forms, and one that is very useful for solving boundary value problems is Galerkin's method. This is the method used in this study. The procedure for this method is given below:

The equilibrium equations for two dimensional elasticity are:

$$\frac{\partial \sigma_x}{\partial x} + \frac{\partial \tau_{xy}}{\partial y} = 0 \quad ,$$

$$\frac{\partial \tau_{yx}}{\partial x} + \frac{\partial \sigma_y}{\partial y} = 0 \quad ,$$

(2-10)

and the shear stresses satisfy:

$$\tau_{xy} = \tau_{yx} \quad ,$$

(2-11)

The two-dimensional strain-displacement relationships i.e. (kinemetic equations) are:

$$\varepsilon_x = \frac{\partial u}{\partial x}, \quad \varepsilon_y = \frac{\partial v}{\partial y}, \quad \gamma_{xy} = \frac{\partial u}{\partial y} + \frac{\partial v}{\partial x} \quad ,$$

(2-12)

where u and μ represent the displacements in x and y direction.

The stress-strain relationships i.e. (constitutive equation) for the plane stress condition are:

$$\begin{Bmatrix} \sigma_x \\ \sigma_y \\ \tau_{xy} \end{Bmatrix} = \frac{E}{1-\mu^2} \begin{bmatrix} 1 & v & 0 \\ v & 1 & 0 \\ 0 & 0 & \frac{1-\mu}{2} \end{bmatrix} \begin{Bmatrix} \varepsilon_x \\ \varepsilon_y \\ \gamma_{xy} \end{Bmatrix} \quad ,$$

(2-13a)

or

$$[\sigma] = [D] \, [\varepsilon] \quad .$$

(2-13b)

Where E and μ are elastic modulus and Poisson's ratio.

The traction boundary conditions are:

$$\phi_x = \sigma_x n_x + \tau_{xy} n_y$$

$$\phi_y = \tau_{xy} n_x + \sigma_y n_y \quad .$$

(2-14)

The basic formulation of the weighted residual method is:

$$I = \int_\Omega R W_i d\Omega = 0 \quad (i = 1,2) \quad ,$$

(2-15)

where R is residual of the governing equation, and W_i is a weight function.

By applying equation 2-10 to the weighted residual equation we get:

9

$$I_1 = \int_\Omega \left(\frac{\partial \sigma_x}{\partial x} + \frac{\partial \tau_{xy}}{\partial y} \right) W_1 d\Omega = 0$$

$$I_2 = \int_\Omega \left(\frac{\partial \tau_{xy}}{\partial x} + \frac{\partial \sigma_y}{\partial y} \right) W_2 d\Omega = 0 \quad .$$

(2-16)

Using integrations by parts and combining the two I functions yields:

$$\int_\Omega \begin{bmatrix} \sigma_x \dfrac{\partial W_1}{\partial x} + \tau_{xy} \dfrac{\partial W_1}{\partial y} \\ \tau_{xy} \dfrac{\partial W_2}{\partial x} + \sigma_y \dfrac{\partial W_2}{\partial y} \end{bmatrix} d\Omega = \int_\Gamma \begin{Bmatrix} \phi_x W_1 \\ \phi_y W_2 \end{Bmatrix} dP \quad , \qquad (2\text{-}17)$$

or

$$\int_\Omega \begin{bmatrix} \dfrac{\partial W_1}{\partial x} & 0 & \dfrac{\partial W_1}{\partial y} \\ 0 & \dfrac{\partial W_2}{\partial y} & \dfrac{\partial W_2}{\partial x} \end{bmatrix} \begin{Bmatrix} \sigma_x \\ \sigma_y \\ \tau_{xy} \end{Bmatrix} d\Omega = \int_\Gamma \begin{Bmatrix} \phi_x W_1 \\ \phi_y W_2 \end{Bmatrix} dP \quad , \quad (2\text{-}18)$$

where ϕ_x and ϕ_y are boundary tractions as stated in equation 2-14. Here, Ω denotes the domain and Γ indicates the boundary.

Plugging the strain-displacement equations into the constitutive equations and substituting the resultant equation into 2-18 yields:

$$\int_\Omega \begin{bmatrix} \dfrac{\partial W_1}{\partial x} & 0 & \dfrac{\partial W_1}{\partial y} \\ 0 & \dfrac{\partial W_2}{\partial y} & \dfrac{\partial W_2}{\partial x} \end{bmatrix} [D] \begin{bmatrix} \dfrac{\partial}{\partial x} & 0 \\ 0 & \dfrac{\partial}{\partial y} \\ \dfrac{\partial}{\partial y} & \dfrac{\partial}{\partial x} \end{bmatrix} \begin{Bmatrix} u \\ v \end{Bmatrix} d\Omega = \int_\Gamma \begin{Bmatrix} \phi_x W_1 \\ \phi_y W_2 \end{Bmatrix} dP \quad . \quad (2\text{-}19)$$

In this model, linear triangular elements are used for the formulation. That is, each triangular element has three nodes and each node has two displacements u, v in the x and y direction so that each element has six degrees of freedom. The shape function that is

10

used for the triangular element is H_i (x,y). The displacements are interpolated using the shape functions.

$$u = \sum_{i=1}^{3} H_i u_i$$

$$v = \sum_{i=1}^{3} H_i v_i \quad ,$$

(2-20)

or in matrix form:

$$\begin{Bmatrix} u \\ v \end{Bmatrix} = \begin{bmatrix} H_1 & 0 & H_2 & 0 & H_3 & 0 \\ 0 & H_1 & 0 & H_2 & 0 & H_3 \end{bmatrix} \begin{Bmatrix} u_1 \\ v_1 \\ u_2 \\ v_2 \\ u_3 \\ v_3 \end{Bmatrix} \quad .$$

(2-21)

The displacement vector is 2 x 1, and can be expressed as the shape function matrix (2x6) times the nodal displacement vector (6x1); as shown above. We define a matrix [B] that is obtained by taking first partial derivatives of the shape functions with respect to the coordinates, that is:

$$[B] = \begin{bmatrix} \dfrac{\partial H_1}{\partial x} & 0 & \dfrac{\partial H_2}{\partial x} & 0 & \dfrac{\partial H_3}{\partial x} & 0 \\ 0 & \dfrac{\partial H_1}{\partial y} & 0 & \dfrac{\partial H_2}{\partial y} & 0 & \dfrac{\partial H_3}{\partial y} \\ \dfrac{\partial H_1}{\partial y} & \dfrac{\partial H_1}{\partial x} & \dfrac{\partial H_2}{\partial y} & \dfrac{\partial H_2}{\partial x} & \dfrac{\partial H_3}{\partial y} & \dfrac{\partial H_3}{\partial x} \end{bmatrix} \quad .$$

(2-22)

Because the weighting function (W_i) of the Galerkin method is the same as the shape function:

$$W_1 = W_2 = \begin{bmatrix} H_1 \\ H_2 \\ H_3 \end{bmatrix} \quad ,$$

(2-23)

the weighting function matrix in equation 2-19 can be written as:

$$\begin{bmatrix} \dfrac{\partial W_1}{\partial x} & 0 & \dfrac{\partial W_2}{\partial y} \\[2ex] 0 & \dfrac{\partial W_2}{\partial y} & \dfrac{\partial W_2}{\partial x} \end{bmatrix} = \begin{bmatrix} \dfrac{\partial H_1}{\partial x} & 0 & \dfrac{\partial H_1}{\partial y} \\[2ex] 0 & \dfrac{\partial H_1}{\partial y} & \dfrac{\partial H_1}{\partial x} \\[2ex] \dfrac{\partial H_2}{\partial x} & 0 & \dfrac{\partial H_2}{\partial y} \\[2ex] 0 & \dfrac{\partial H_2}{\partial y} & \dfrac{\partial H_2}{\partial x} \\[2ex] \dfrac{\partial H_3}{\partial x} & 0 & \dfrac{\partial H_3}{\partial y} \\[2ex] 0 & \dfrac{\partial H_3}{\partial y} & \dfrac{\partial H_3}{\partial x} \end{bmatrix} = [B]^T \quad . \tag{2-24}$$

From equations 2-22 and 2-24, we can simplify equation 2-19 to the 2-D element stiffness matrix equation:

$$\int_{\Omega} [B]^T [D]\, [B] d\Omega \{d\} = \int_{\Gamma} \begin{bmatrix} \phi_x W_1 \\ \phi_y W_2 \end{bmatrix} d\mathrm{P} \quad . \tag{2-25}$$

where $\{d\}$ is the nodal displacement vector shown in equation (2-21).

For the triangular element, matrix [B] can be simplified as shown in Appendix B, and the element stiffness matrix equation can be written as:

$$[K_e]\{d\} = [B]^T [D]\, [B]\Omega\{d\} = \{F_e\} \quad , \tag{2-26}$$

or

$$[K_e]\{d\} = [B]^T [D]\, [B] At \{d\} = \{F_e\} \quad , \tag{2-27}$$

where A is the area of the triangular element, t is the thickness of the element. For unit thickness, t is equal to 1.

The right hand side of the equation 2-27 is called the element force vector $\{F_e\}$ which is dependent on the surface traction boundary conditions and represents the total force at the nodal points in the x and y directions. Combining the element stiffness matrices into the system global matrix equation gives:

$$[KK] \ \{dd\} \ = \{FF\} \ . \tag{2-28}$$

The FEM used in this study is to calculate the elastic modulus of the composite material, whether there is a crack or not. From equation (2-28) we can solve for the nodals displacement $\{dd\}$ by applying the displacement boundary condition. After we get the nodals displacements, stresses are computed for each element. The elastic modulus can be calculated from:

$$E = \frac{\overline{\sigma}_c}{\overline{\varepsilon}_c} \ . \tag{2-29}$$

where $\overline{\sigma}_c$ is the composite average stress and $\overline{\varepsilon}_c$ is the composite average strain. In this study, we applied a uniform displacement to the micromechanics model as shown in **Figure 4** as the displacement boundary condition.
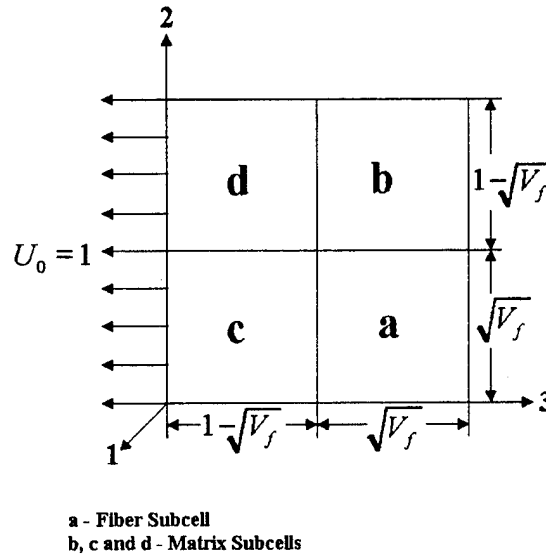

a - Fiber Subcell
b, c and d - Matrix Subcells

Figure 4. Unit Displacement Model.

Two different kinds of finite element analyses are performed. The first one is a simplified model in which each subcell in Figure 4 is divided into two triangular elements. The other one is a detailed model for which each subcell is divided into many

13

number of finite elements. The latter model was used to check the accuracy of the simplified analytical and finite element models.

2.   Interface Crack

When a partial interface crack between the fiber and the matrix exists, the crack cannot be modeled explicitly for the simplified finite element model because there is no node to represent the crack tip. As a result, it is assumed that there are elastic springs at the two corner nodes, which connect the fiber and the matrix. The double node technique is used for this purpose. Since the nodes have two degrees of freedom (x and y directions), the spring constants at every node are k_x and k_y. The stiffness matrix for the two dimensional spring element is:

$$\begin{bmatrix} k_x & 0 & -k_x & 0 \\ 0 & k_y & 0 & k_y \\ -k_x & 0 & k_x & 0 \\ 0 & -k_y & 0 & k_y \end{bmatrix} . \tag{2-30}$$

By adding the stiffness matrix into the global system matrix, springs connect the fiber to the matrix. The spring constant determines the status of a partial interface crack. For example, if the spring constant is very large, there is no crack and if the spring constant is zero, there is a complete crack at the interface. An intermediate value of spring constant represents a partial crack. The proper spring constants need to be determined later for a given size of interface crack.

C.   MATLAB COMPUTER PROGRAM DEVELOPMENT

The MATLAB engineering software is chosen to program the finite element procedure, and to calculate the composite material property of a composite with perfect bonding or partial cracks between the fiber and matrix. The following procedures are the outline of the MATLAB program development:

1. Define the numbers of elements and nodes and input x, y coordinates of the nodes associated with each element using 'GRID'.

2. Input the material properties (*E* & *v*) of the fiber and matrix, and calculate the kinematic matrix [B], the material property matrix [D] and the element stiffness matrix [K_e] using 'TESTT'.

3. Use 'CHECK' to assemble each element stiffness matrix [K_e] into the system stiffness matrix [KK].

4. Use 'MODTT' to apply the geometric boundary conditions and to modify the system global stiffness matrix [KK].

5. Compute the displacement {dd} and stresses using "STRES."

6. From the main program "MAIN," we obtain the composite material property, and compare the results by plotting.

7. For the interface crack model, we add the spring stiffness matrix to the system stiffness matrix before step 5, and follow the remaining steps.

III. RESULTS AND DISCUSSION

In this study, we considered three kinds of composites, Graphite/Epoxy, Glass/Epoxy and Boron/Epoxy. The properties of these composites are listed in Table 1. The relationship between the transverse elastic modulus (E) of each composite and the fiber volume fraction (V_f) for these three composites is shown in Figure 5. The fiber transverse elastic moduli of Glass and Boron are higher than that of Graphite, while the matrix transverse elastic moduli are the opposite. Therefore, when the volume fraction is less than 0.5, the transverse elastic modulus of Graphite/Epoxy is higher than the others, but when the volume fraction is greater than 0.5 the situation is reversed. Figure 6 shows the function that best fit the relation between transverse elastic modulus and the fiber volume fraction in graphite/epoxy materials. The figures of the other materials are shown in Appendix C. (See Figure 36,Figure 37)

Table 1. The Properties of Matrix and Fiber in the Graphite/Epoxy, Glass/Epoxy, and Boron/Epoxy Composites Materials.

Property	Composite					
	Graphite/Epoxy		Glass/Epoxy		Boron/Epoxy	
	Graphite Fiber	Epoxy Matrix	Glass Fiber	Epoxy Matrix	Boron Fiber	Epoxy Matrix
Transverse Elastic Modulus (Gpa)	15	5.35	72.38	2.75	400	2.75
Poisson's Ratio	0.49	0.354	0.2	0.35	0.3	0.35

When the interface between the matrix and fiber begins cracking, the interface will be separated partially, as shown in Figure 7a. Figure 7b. In order to understand the stress distribution within the fiber when there is a partial interface crack, a uniform displacement was applied along the uncracked interface of the fiber as shown in Figure 7b. Stress distributions for the three fibers with 50% or 60% crack length are shown in Figure 8 to Figure 13. The figures for other crack lengths are shown in Appendix D. (See

Figure 38 through Figure 43) From the figures, it is found that the stress distribution for a half of the crack length of the fiber down to the bottom is much lower when compared to other regions. The same results can be shown in the stress distribution over the both fiber and matrix with 50% of crack length ratio and 0.36 of fiber volume fraction for the three composites as seen in Figure 14 to Figure 16. The figures of other cases are shown in Appendix E, Figure 44 through Figure 49. Besides the part of the fiber we mentioned above, the stress distribution at the lower region of the left-hand side of the matrix is also negligible. Therefore, for the analytical model, the lower stress regions were removed as shown in Figure 17, and equation (2-6) was used to calculate the average composite stresses and transverse elastic modulus for a different crack length.

The results of the analytical model and the detailed FEM model with $V_f = 0.36$ for the three composites are shown in Figure 18 to Figure 20. The results for other fiber volume fractions are shown in Appendix F, Figure 50 through Figure 55. They compare the reduced transverse elastic modulus ratio (E_C/E_O) for different crack length ratios and different fiber volume fractions. According to the results, when the crack length ratio increases, the transverse elastic modulus decreases, and the error between the FEM model and the analytical model for the Graphite/Epoxy composite is larger than those for the other two composites. This is a result of the stress ratio of the region which is neglected in the analytical model. The stress ratio at these regions for the Graphite/Epoxy composite is higher than those for the other two composites. So the error between the FEM and analytical models for the Graphite/Epoxy composite is somewhat larger. Nevertheless, these two models produce very compatible results and the analytical model can be used to predict the effective transverse elastic modulus for different fibrous composites with a partial interface crack length.

As mentioned in Chapter II, we model springs in the connection nodes between the fiber and the matrix by adding the spring stiffness matrix into the system global matrix, as shown in Figure 21. For this model, the spring constants k_x and k_y are chosen from 5×10^{10} to 10^6. When the spring constant is equal to or larger than 5×10^{10}, it's

assumed that there is no interface crack between the fiber and matrix, and when the spring constant is less than 10^6, the complete debonding between the fiber and matrix would take place. Otherwise there is a partial debonding.

Based on the above concept, we define two crack cases, low crack case and upper crack case, as shown in Figure 22. When there is no crack at point "A" and point "B" starts to crack, ka is equal to 5×10^{10} and kb changes from 5×10^{10} to 10^6. This is the low crack case. On the other hand, when point "B" totally debonds, this means kb is equal to 10^6, and ka changes from 5×10^{10} to 10^6. This is the upper crack case. The results of these two cases for different materials with 0.36 of the fiber volume fraction are shown in Figure 23 through Figure 28. Appendix G, Figure 56 through Figure 67 shows the other fiber volume fractions. These figures illustrate that the spring constant and the crack length ratio form an exponential relationship. The best fitting function for each relationship is also shown in the figures.

When the spring constant decreases, no matter what the case is, upper or lower, the partial crack ratio increases, and the elastic modulus will decrease. Figure 29 through Figure 31 show the relationship of the transverse elastic modulus ratio and the crack length ratio for the three models. The other results for different fiber volume fractions are shown in Appendix H, Figure 68 through Figure 73. According to these results, the simplified FEM micromechanical model with a proper spring constant can also predict the effective elastic modulus where there is a partial interface crack.

In the above results, it is assumed the shape of the fiber is rectangular. If we change the shape of the fiber to be octagon instead, then we consider a new micromechanical model. Figure 32 shows the two different micromechanical models. We calculate the effective transverse elastic modulii of the new micromechanical model with the same material properties that used in the first simplified model, and compared the results with the first model.

Table 2 shows the effective modulii (undamage) of these two simplified models for the three different composites in which fiber volume fraction is 0.36, and Figure 33

through Figure 35 shows the effective modulii of the new micromechanical model in cracking condition.

Table 2. Effective Modulis (Undamage).

Modulis	Model	
	Rectangular Fiber Shape	Octagon Fiber Shape
Transverse Elastic Modulus of Graphite/Epoxy	7.638×10^9	7.503×10^9
Transverse Elastic Modulus of Glass/Epoxy	6.098×10^9	5.2147×10^9
Transverse Elastic Modulus of Boron/Epoxy	6.538×10^9	5.5310×10^9
Fiber Volume Fraction	0.36	0.365
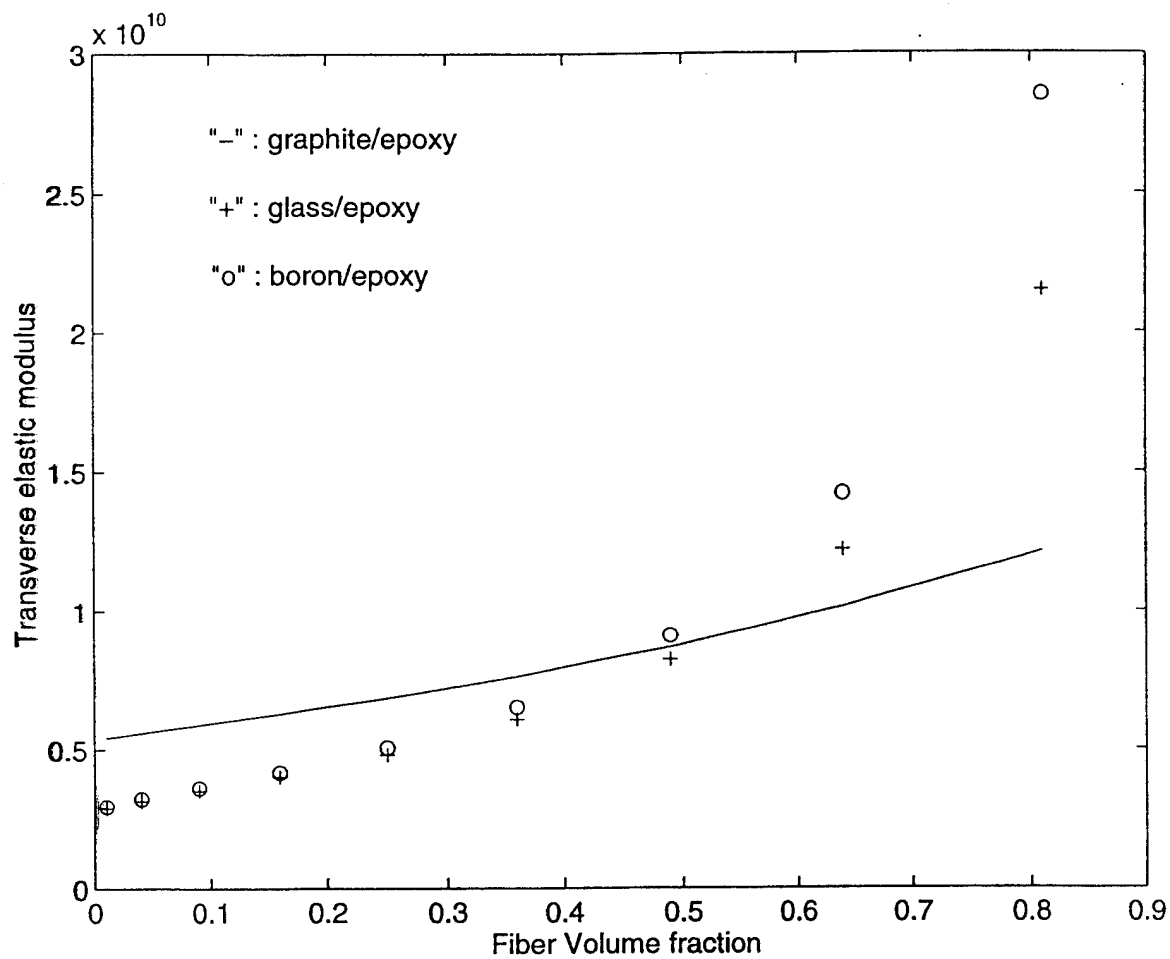
Figure 5. Transverse Elastic Modulis Of Three Composites.
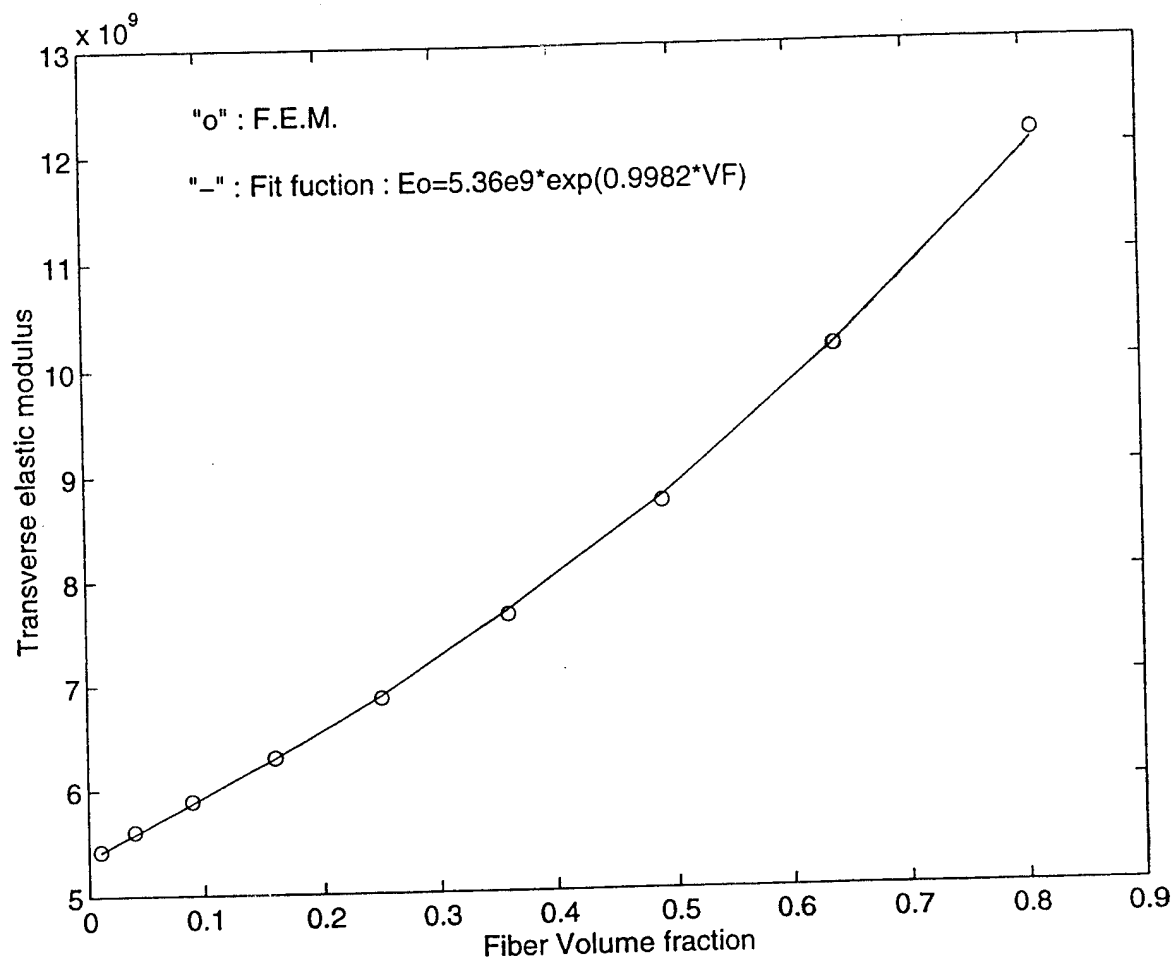
Figure 6. Transverse Elastic Modulis Of Graphite/Epoxy And Best Fitting Function.
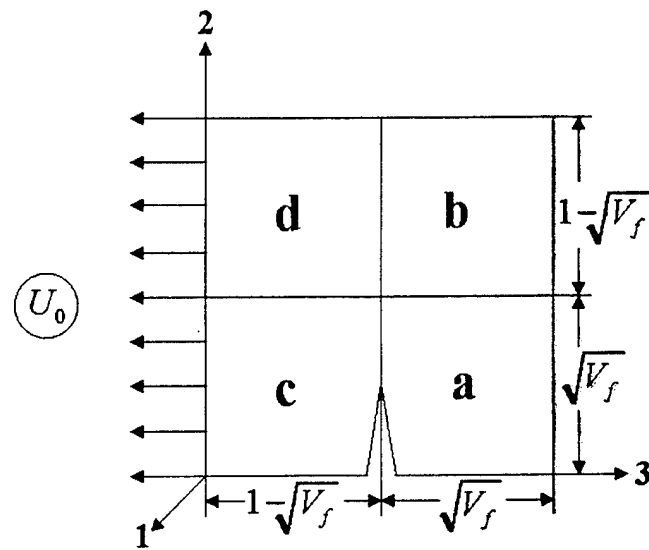
a - Fiber Subcell
b, c and d - Matrix Subcells

(a) A Partial Crack Situation of Subcells
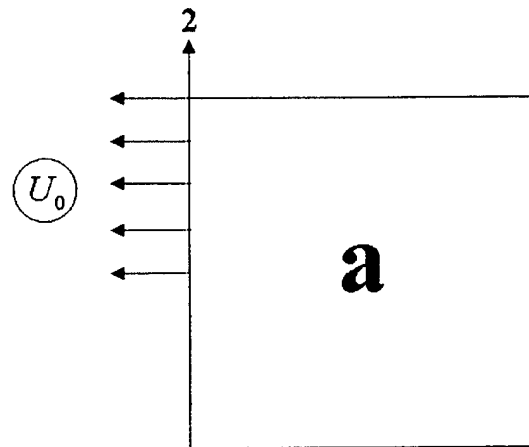
(b) Fiber Part of Subcell in Cracking

Figure 7. Partially Separated.
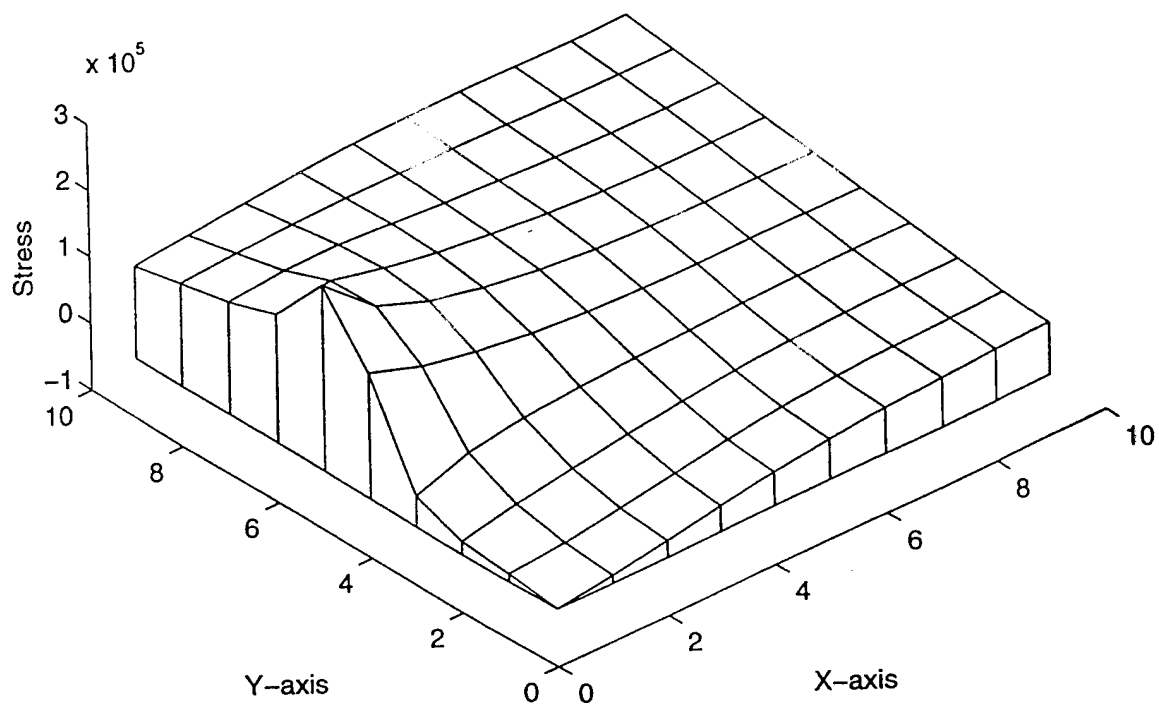
Figure 8. Stresses Distribution Of Graphite Fiber With 50% Crack Length.
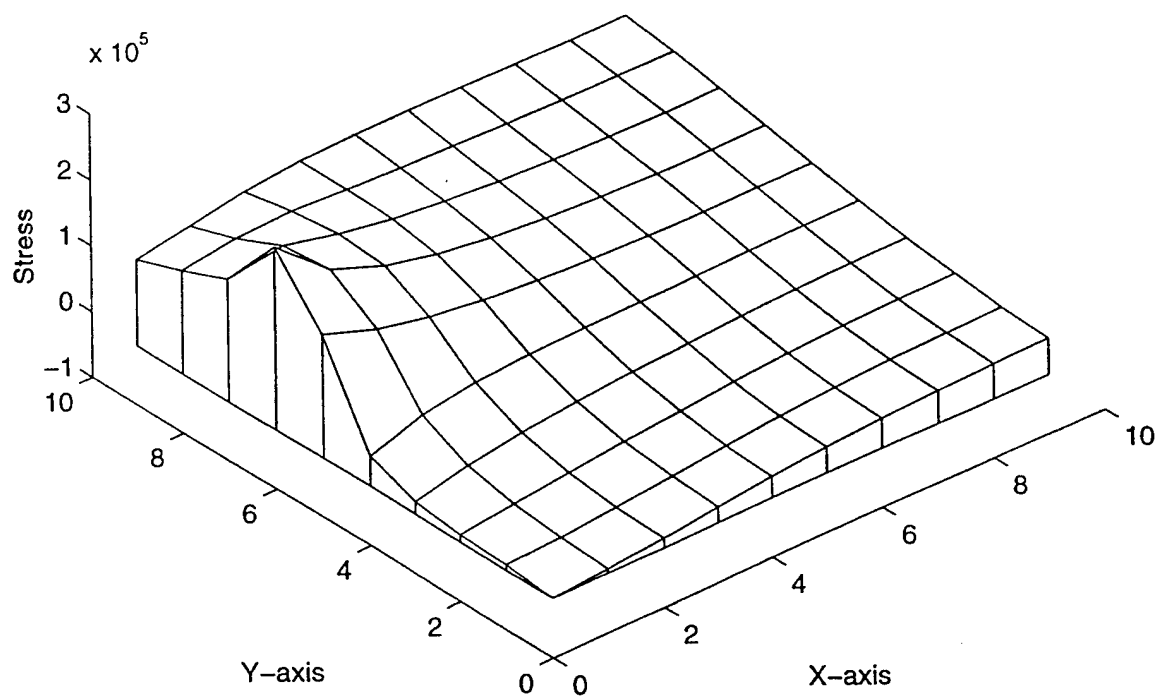
Figure 9. Stresses Distribution Of Graphite Fiber With 60% Crack Length.
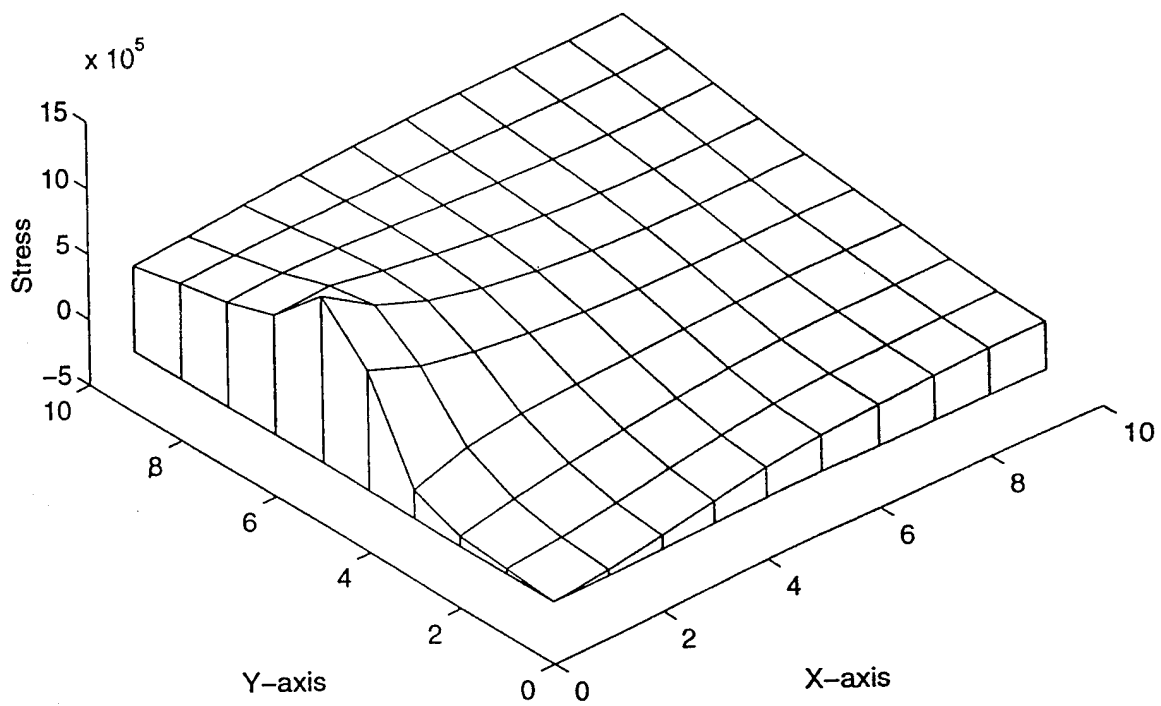
Figure 10. Stresses Distribution Of Glass Fiber With 50% Crack Length.
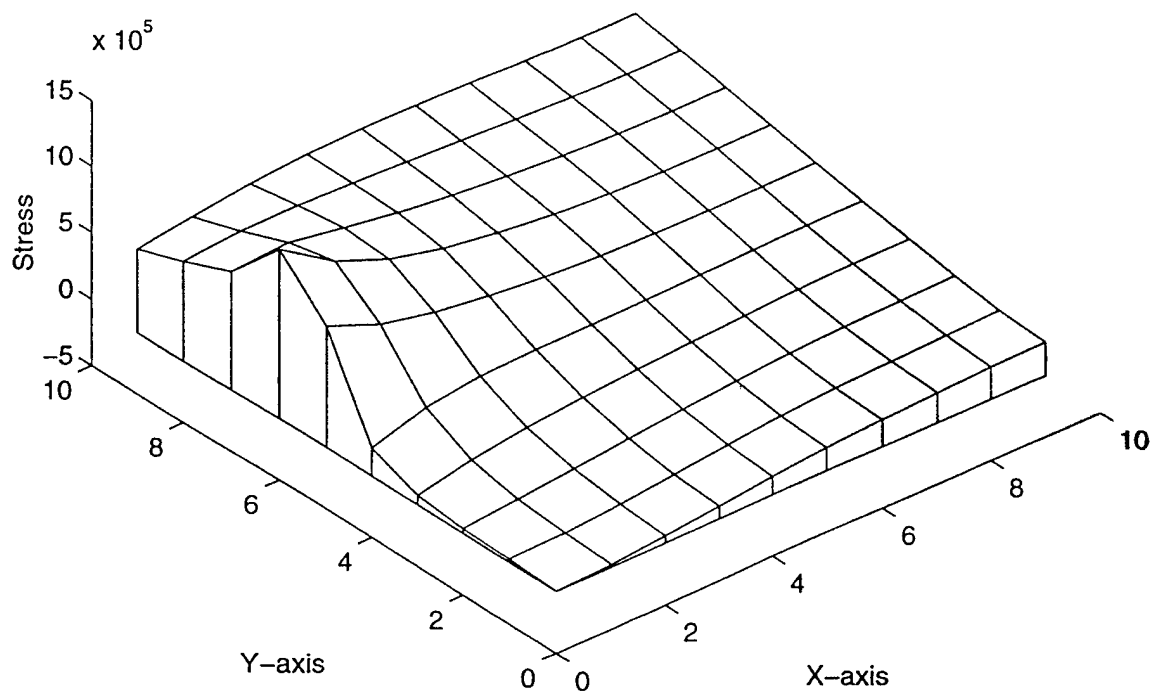
Figure 11. Stresses Distribution Of Glass Fiber With 60% Crack Length.
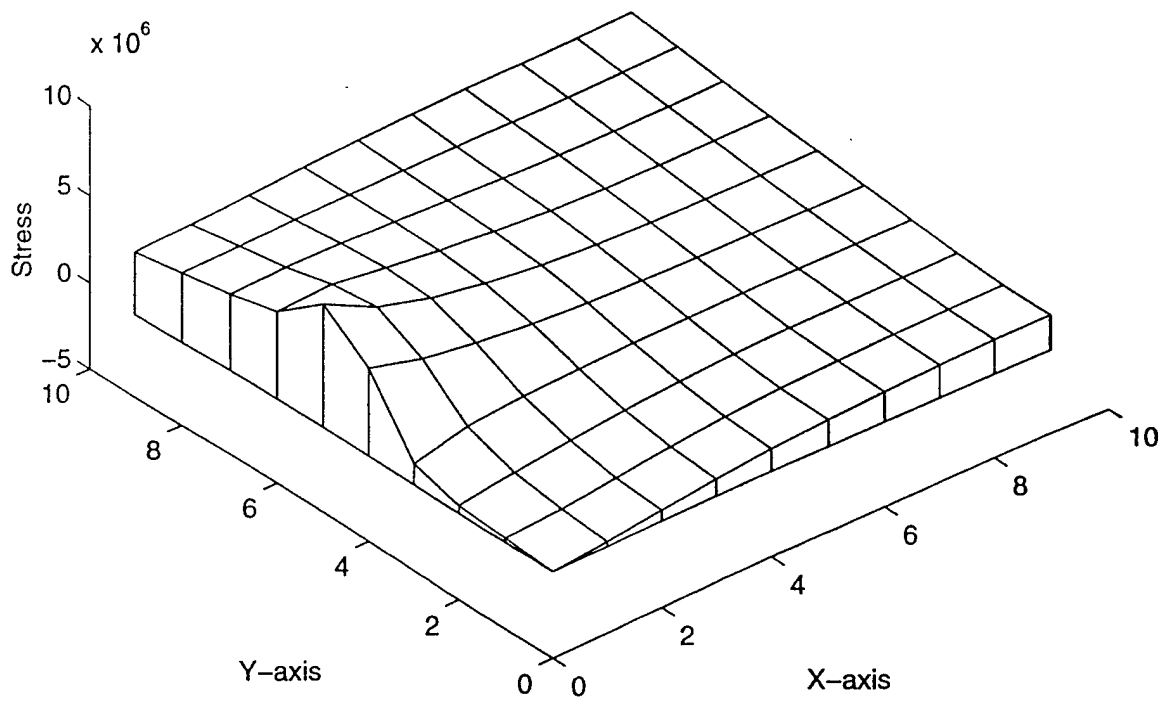
Figure 12. Stresses Distribution Of Boron Fiber With 50% Crack Length.
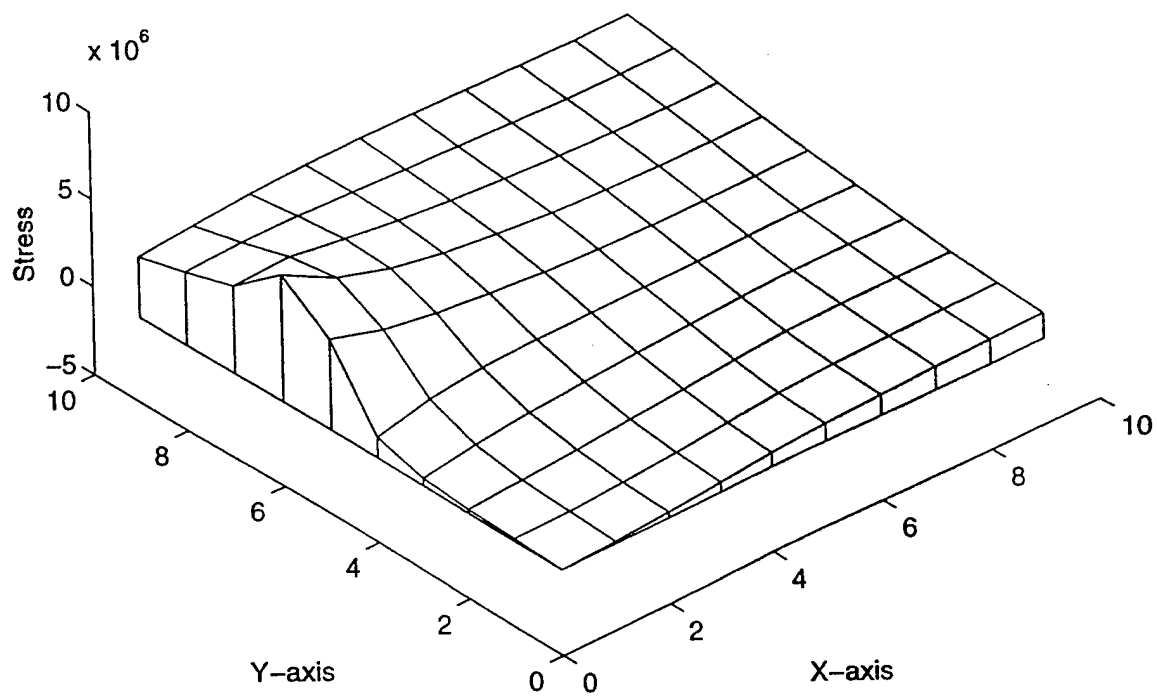
Figure 13. Stresses Distribution Of Boron Fiber With 60% Crack Length.
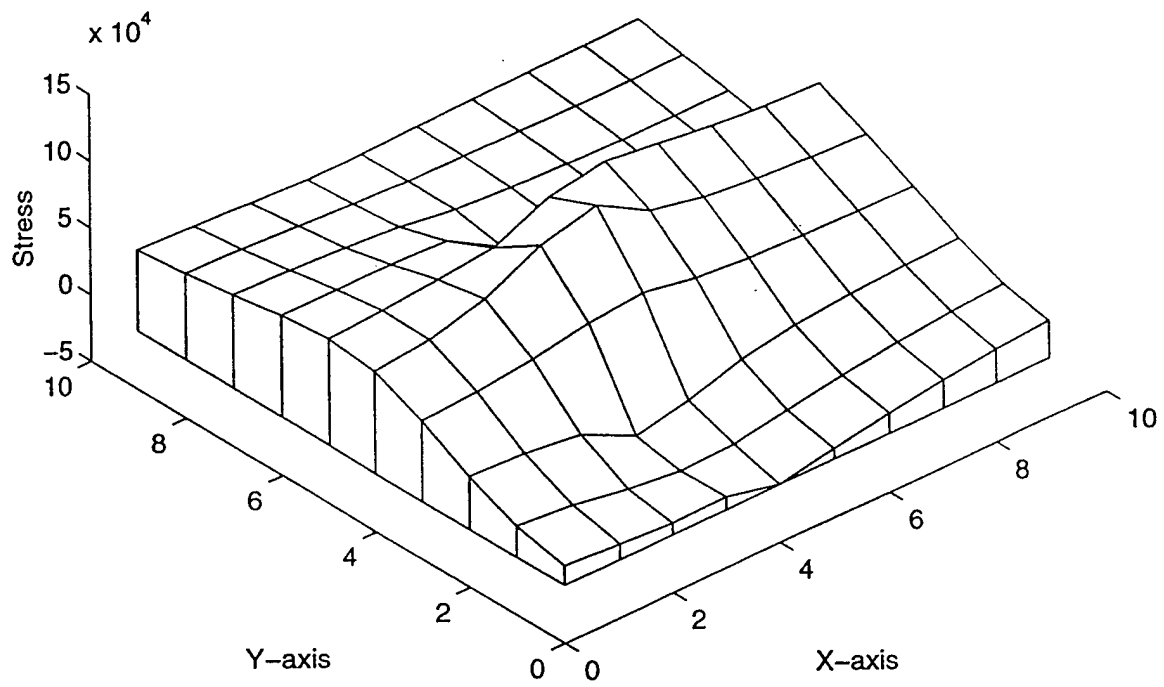
Figure 14. Stresses Distribution Of Graphite/Epoxy With 50% Crack Length. (V_f = 0.36)
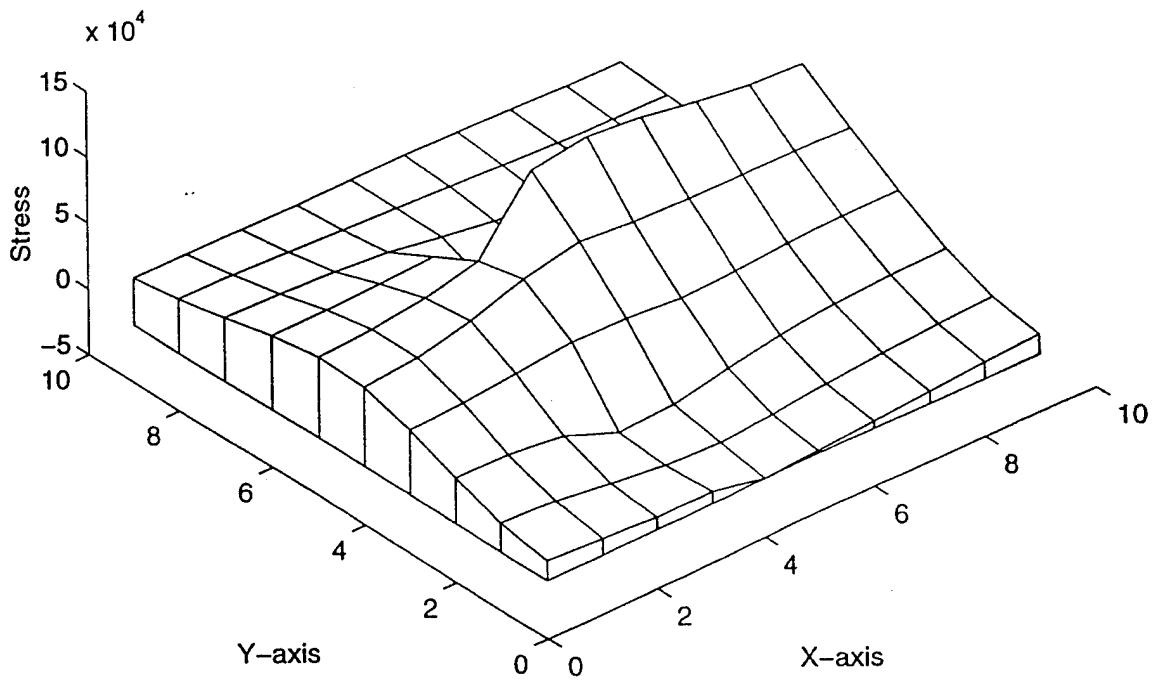
Figure 15. Stresses Distribution Of Glass/Epoxy With 50% Crack Length. (V_f = 0.36)
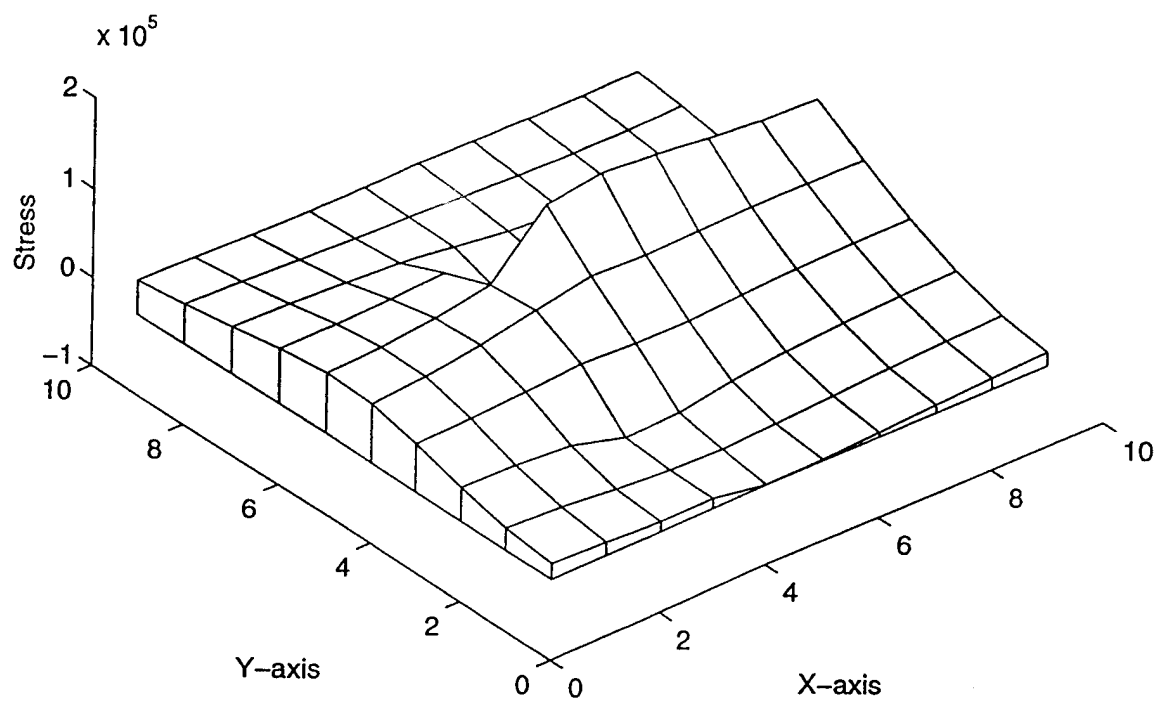
Figure 16. Stresses Distribution Of Boron/Epoxy With 50% Crack Length. ($V_f =$ 0.36)
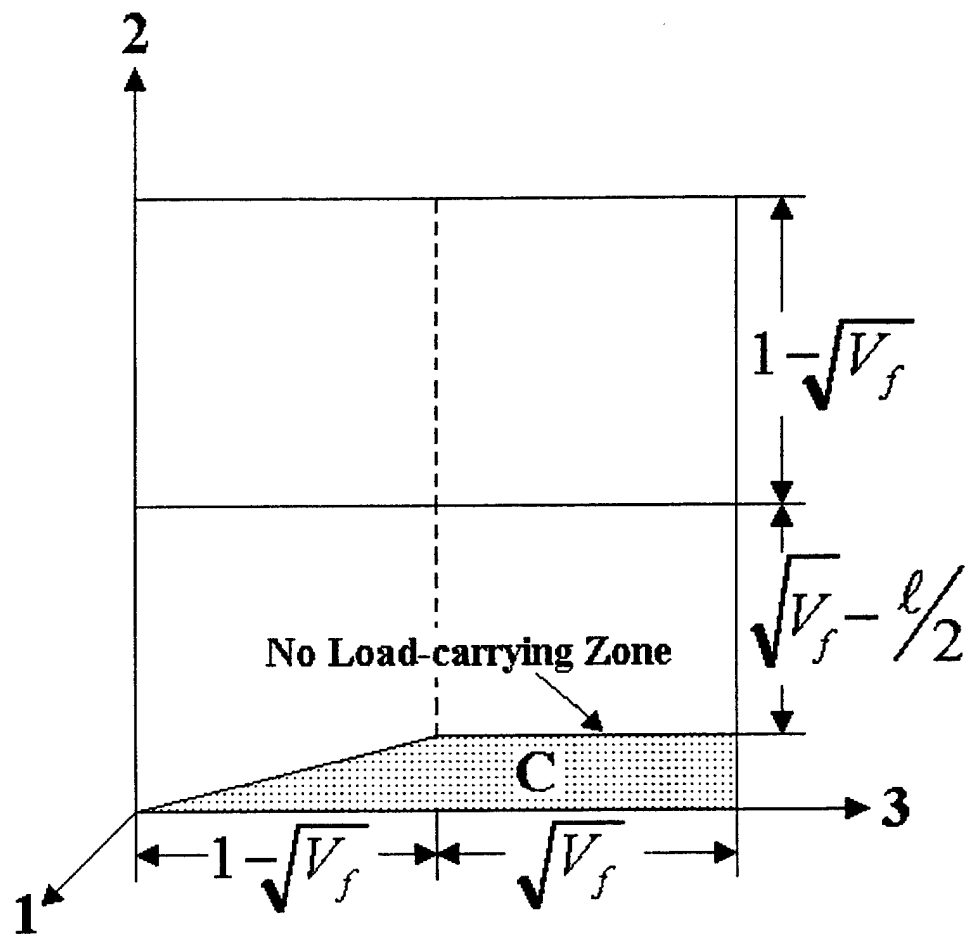
a - Fiber Subcell
b, c and d - Matrix Subcells

Figure 17. Effective Load Carrying Area.
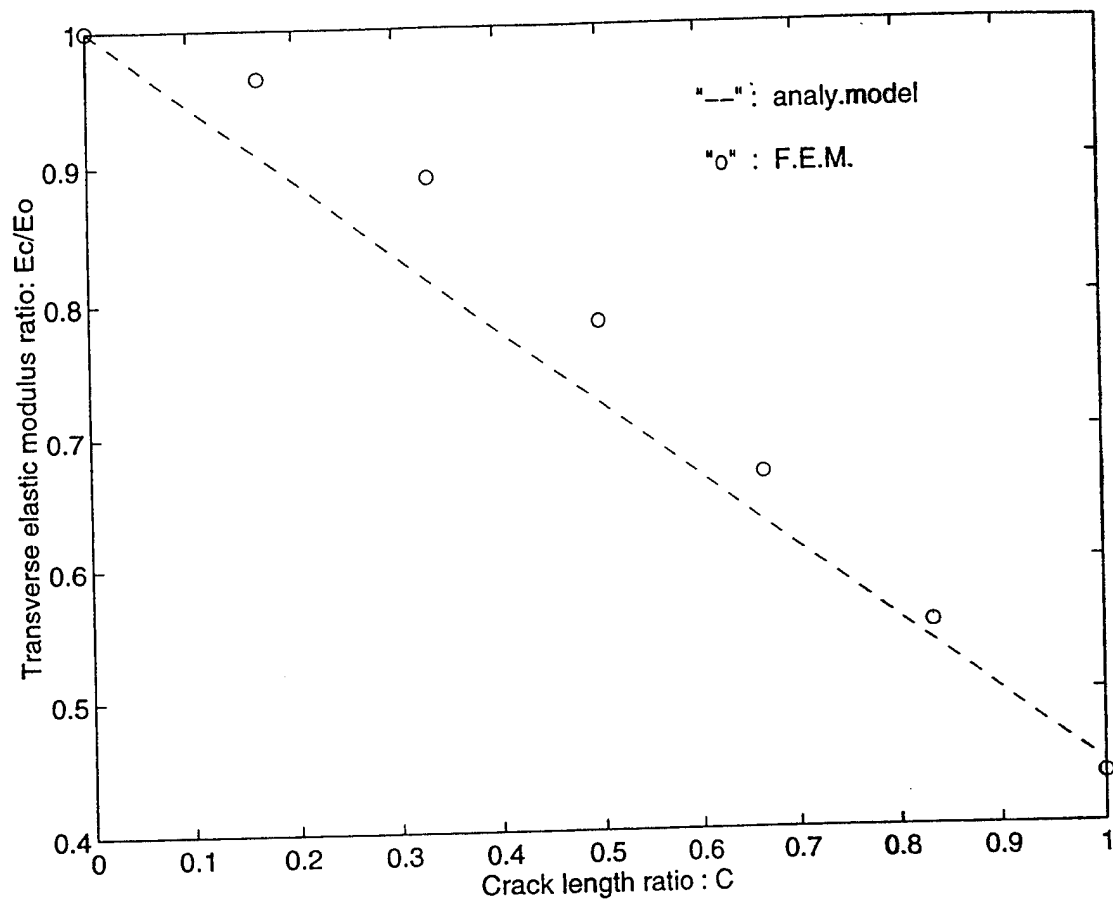
Figure 18. Transverse Elastic Modulis Ratio Of A Graphite/Epoxy Composite. ($V_f = 0.36$)

34
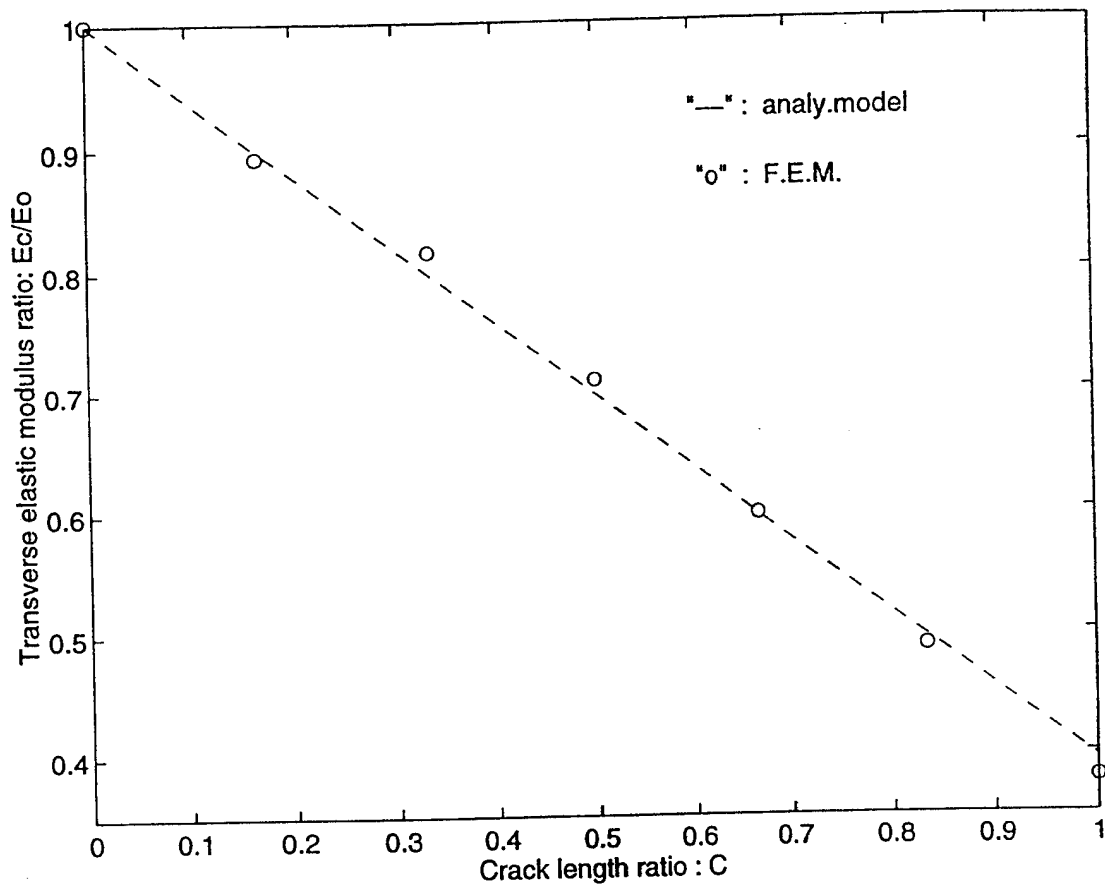
Figure 19. Transverse Elastic Modulis Ratio Of A Glass/Epoxy Composite. (V_f =0.36)
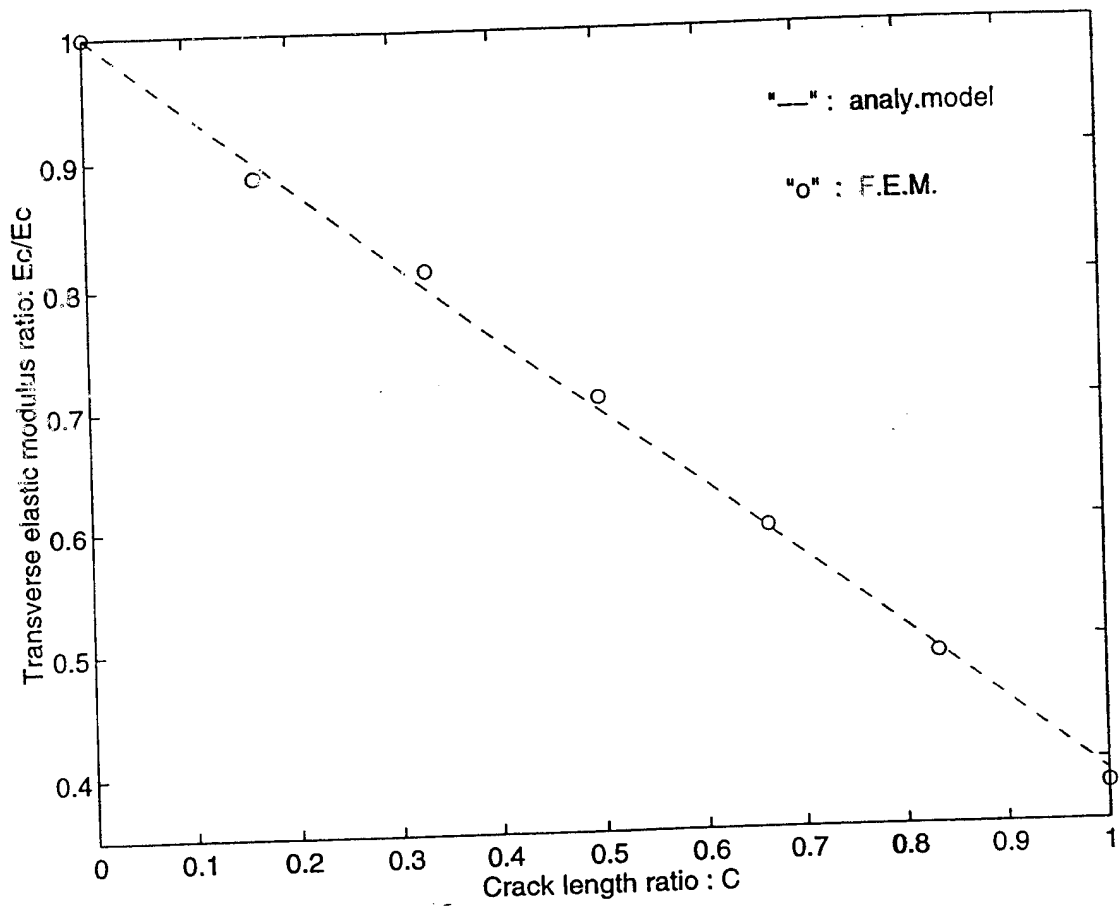
**Figure 20. Transverse Elastic Modulis Of A Boron/Epoxy Composite. ($V_f = 0.36$)**

2

d   **b**

Ⓐ K_{Ax} Ⓒ K_{Cx}

K_{Ay} K_{Cy}

c

Ⓑ K_{Bx}

K_{By}

a - Fiber Subcell
b, c and d - Matrix Subcells

K_{Ax} K_{Ay} K_{Cx} K_{Cy}

Ⓐ   Ⓒ

a

K_{Bx} Ⓑ

K_{By}
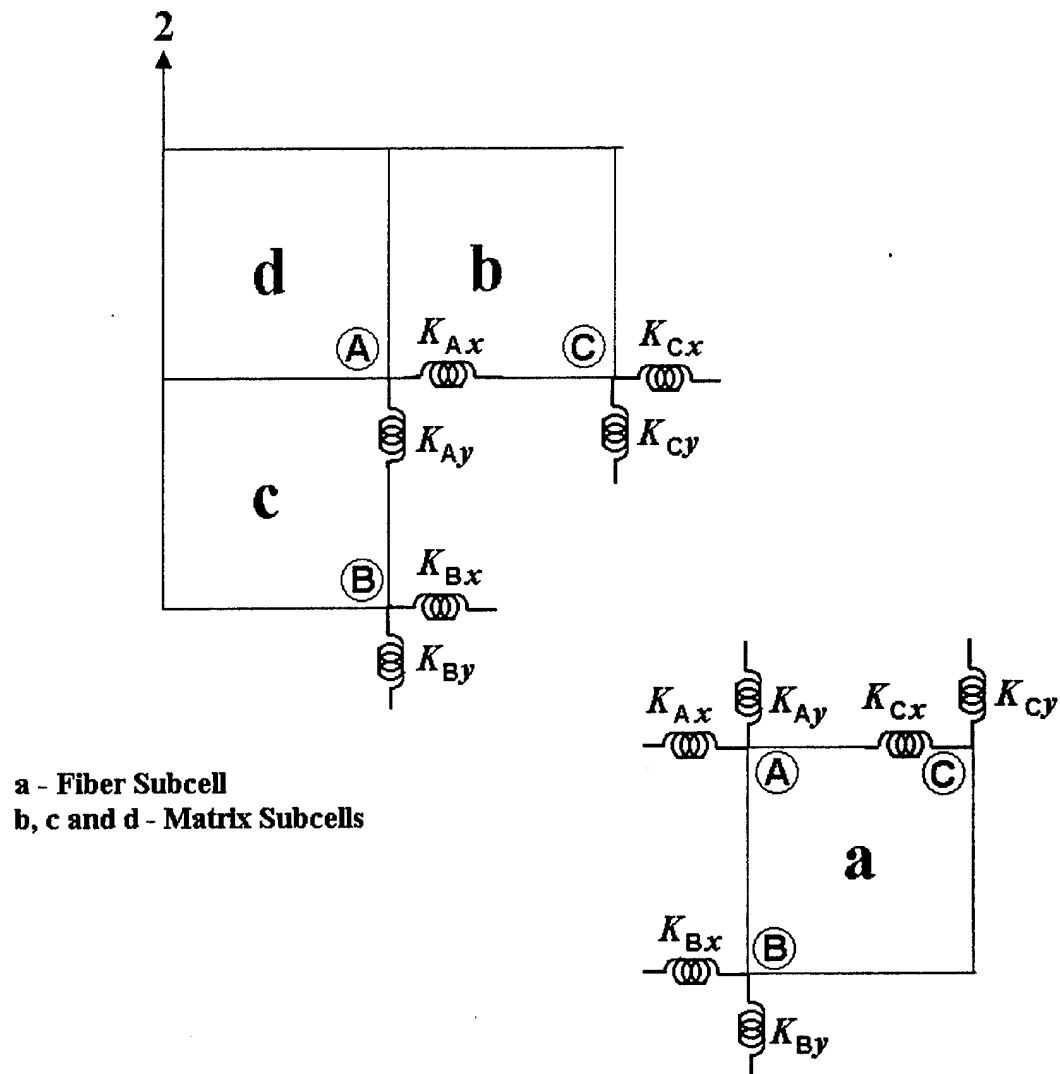
Figure 21. Simplified Finite Element Model With Interface Springs.

37
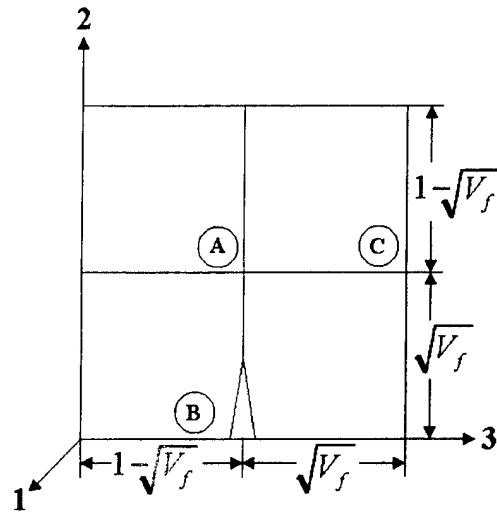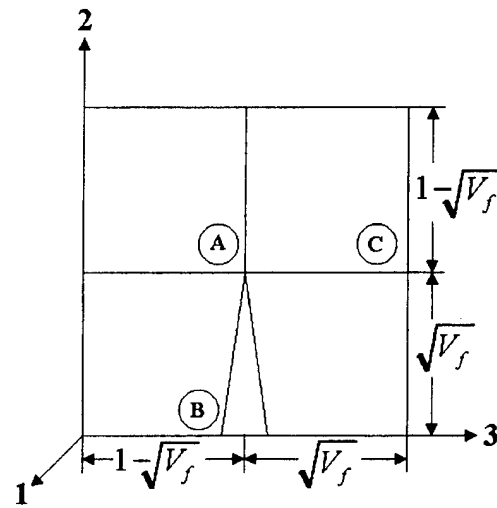
Figure 22. (A) Low Crack Case; (B) Upper Crack Case.
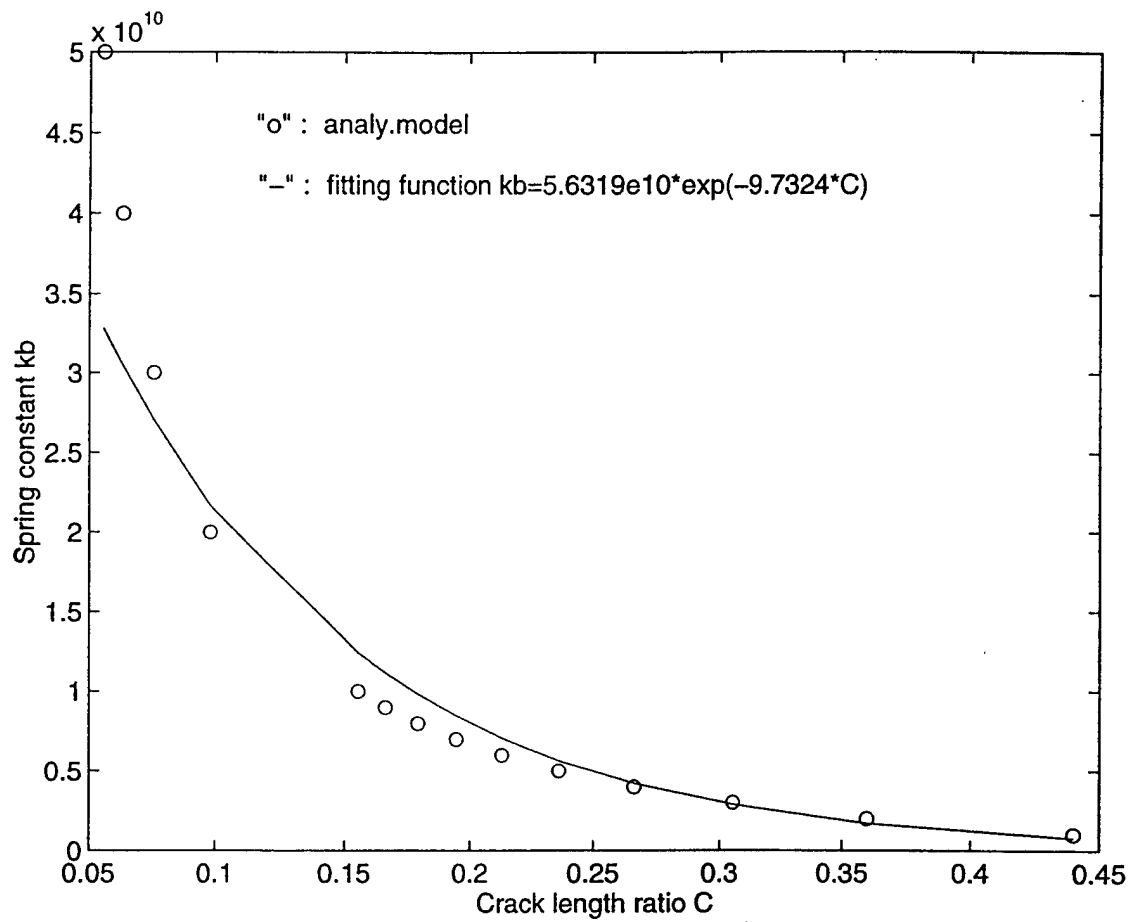
Figure 23. Spring Constant Of A Graphite/Epoxy Composite With $V_f = 0.36$ (Low Crack Case).

39
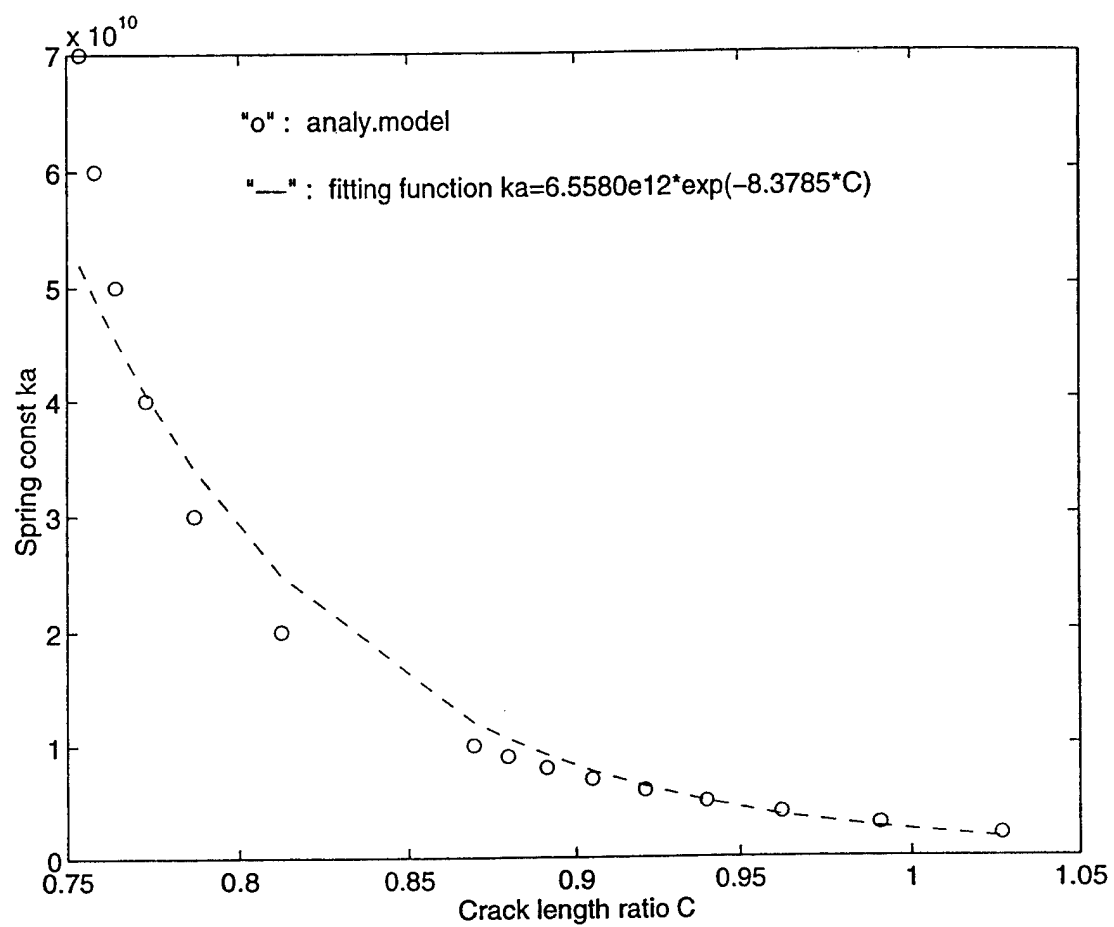
Figure 24. Spring Constant Of A Graphite/Epoxy Composite With V_f = 0.36 **(Upper Crack Case).**
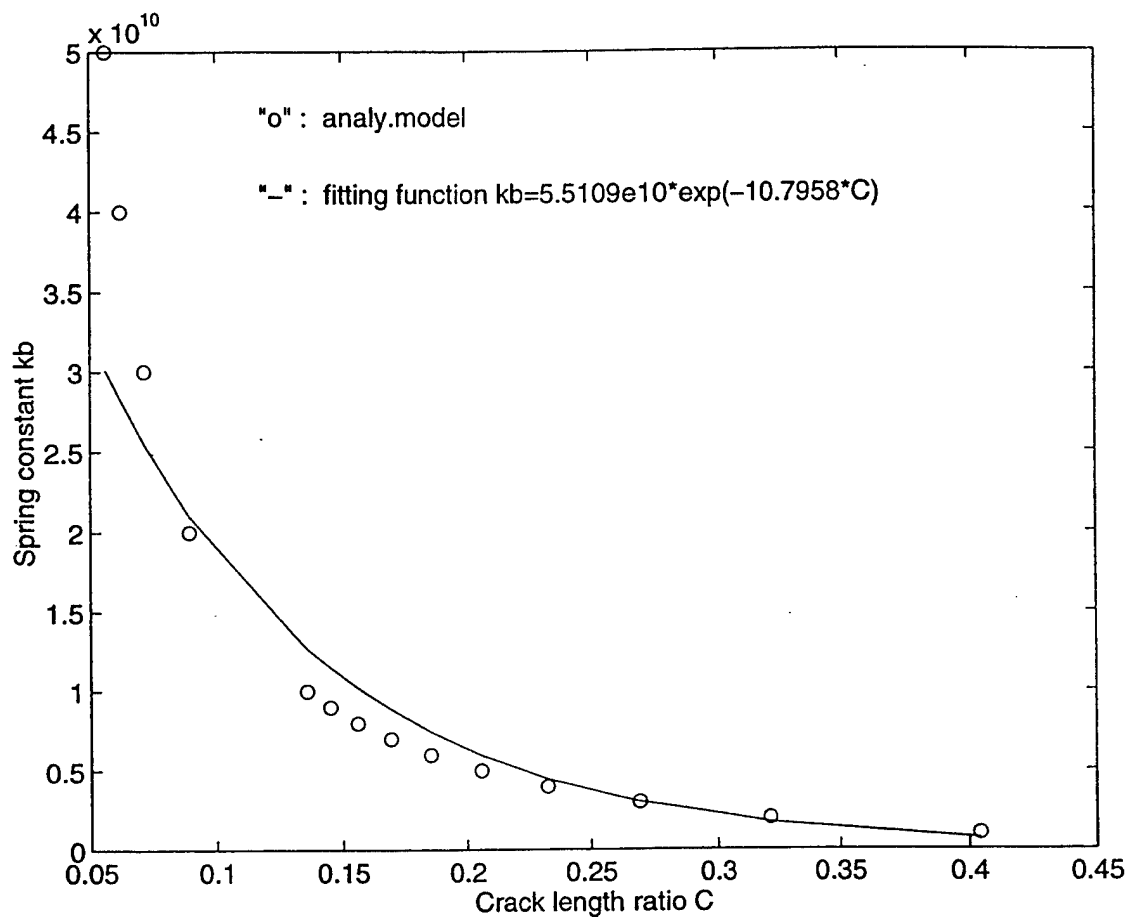
Figure 25. Spring Constant Of A Glass/Epoxy Composite With $V_f = 0.36$ (Low Crack Case).

41
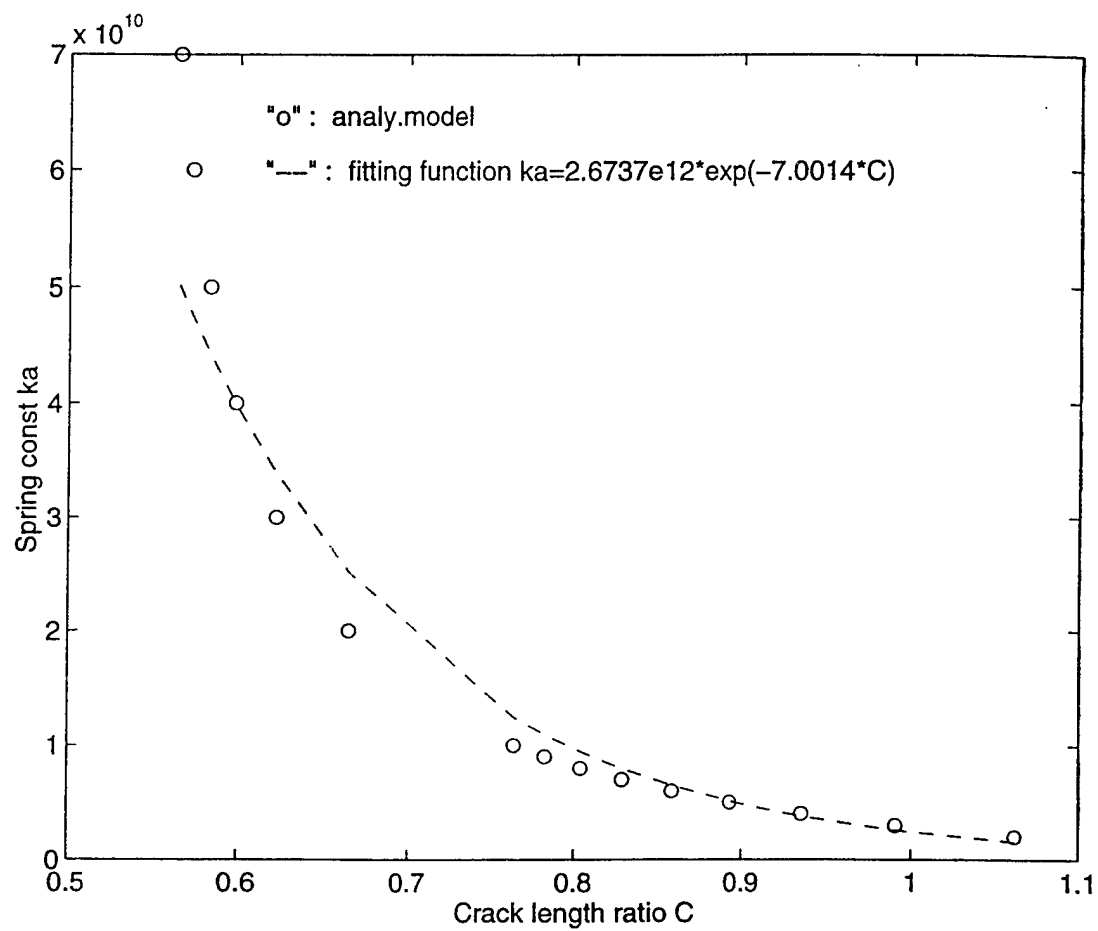
Figure 26. Spring Constant Of A Glass/Epoxy Composite With V_f = 0.36 (Upper Crack Case).
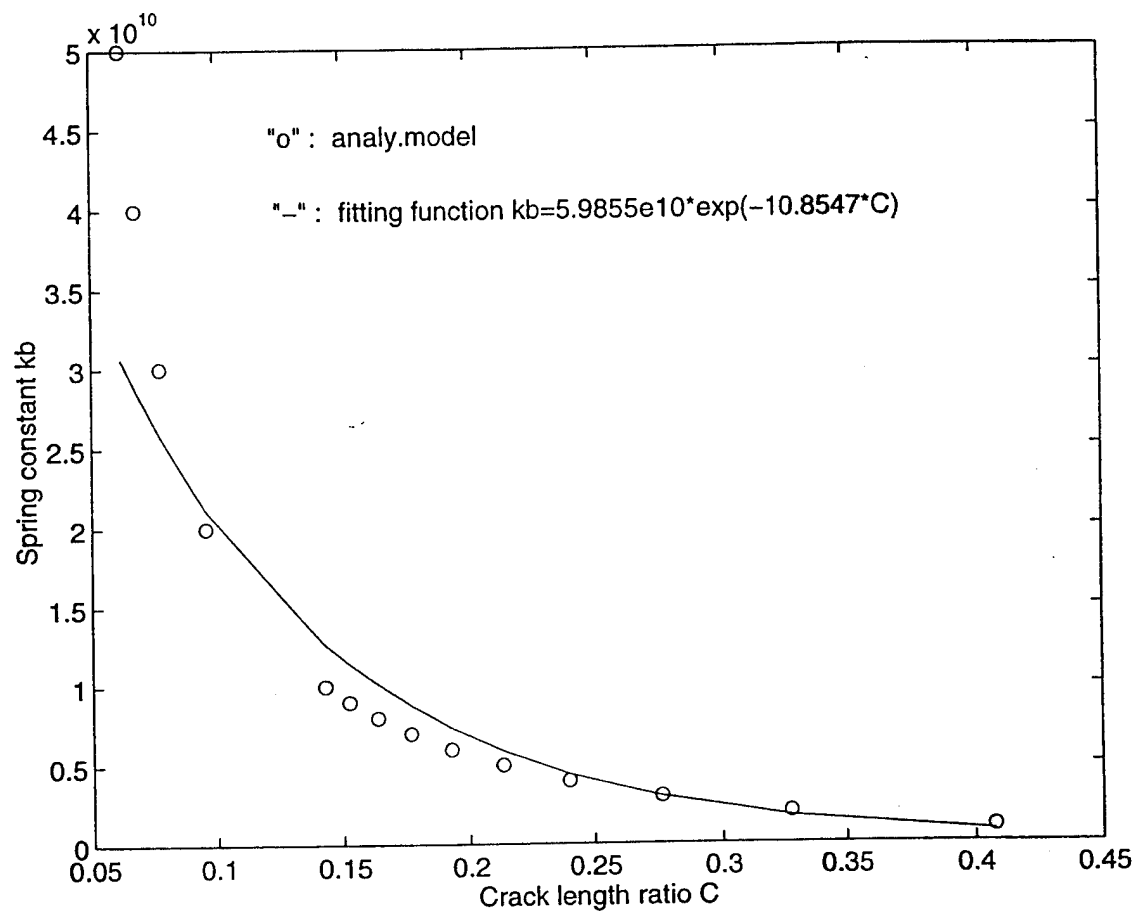
Figure 27. Spring Constant Of A Boron/Epoxy Composite With $V_f = 0.36$ (Low Crack Case)
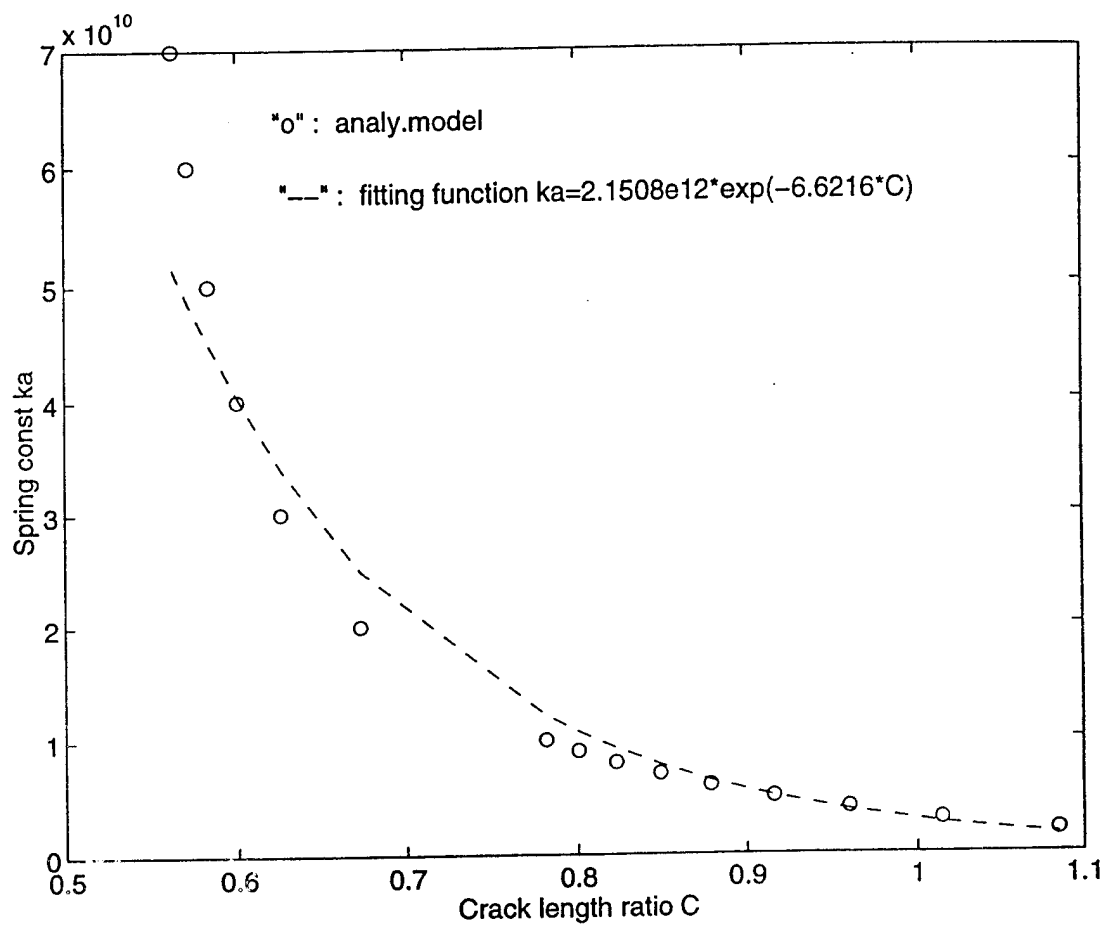
Figure 28. Spring Constant Of A Boron/Epoxy Composite With V_f = 0.36 (Upper Crack Case).
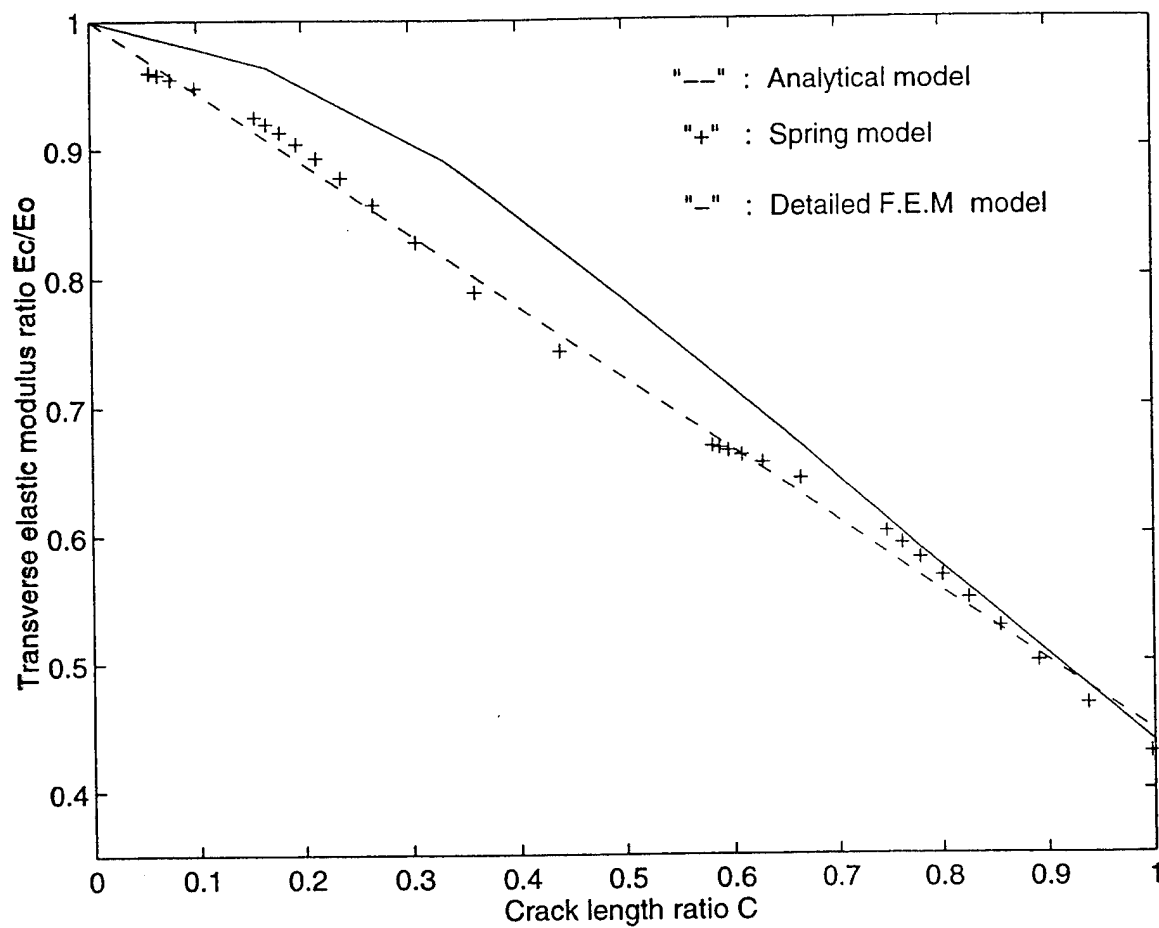
Figure 29.Transverse Elastic Modulis Of Graphic/Epoxy Composite (V_f =0.36).
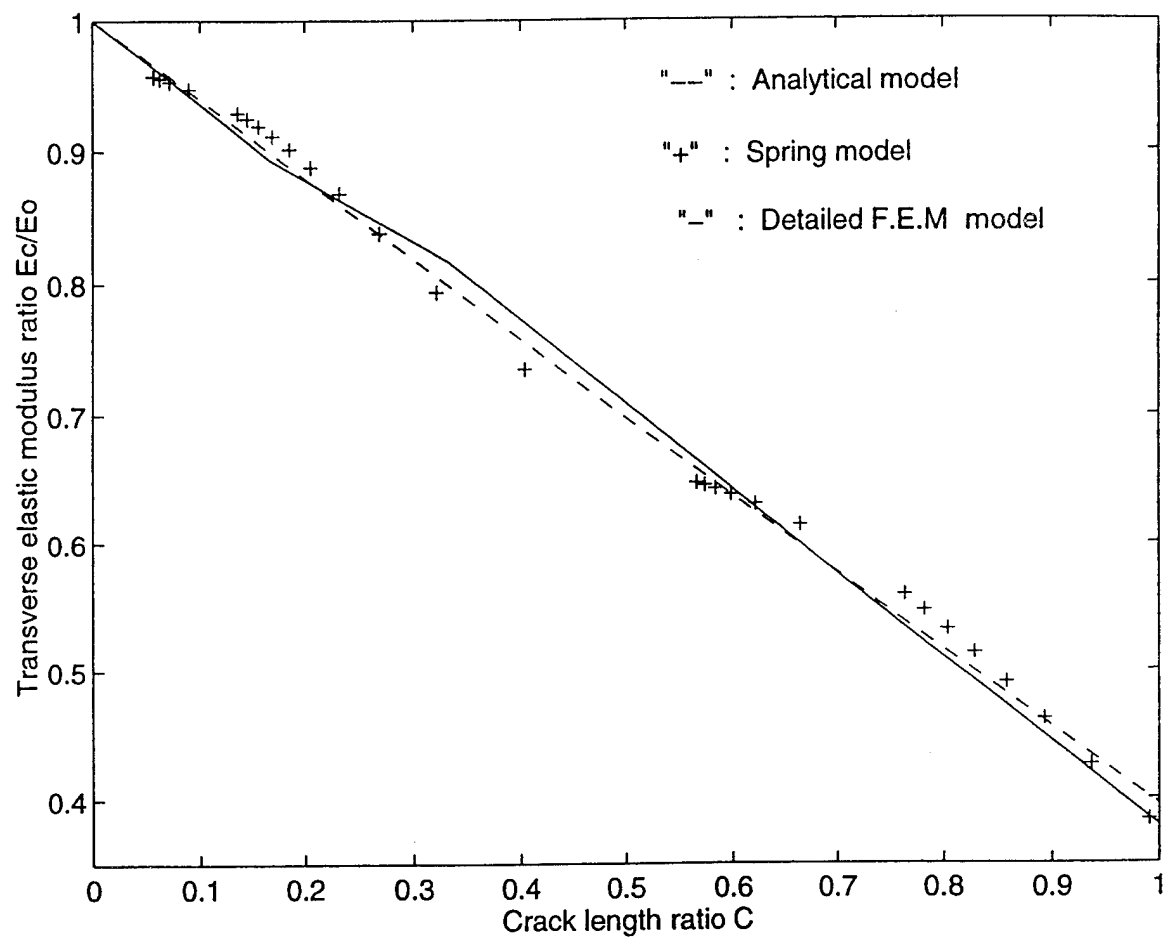
Figure 30. Transverse Elastic Modulis Of A Glass/Epoxy Composite ($V_f = 0.36$).

46
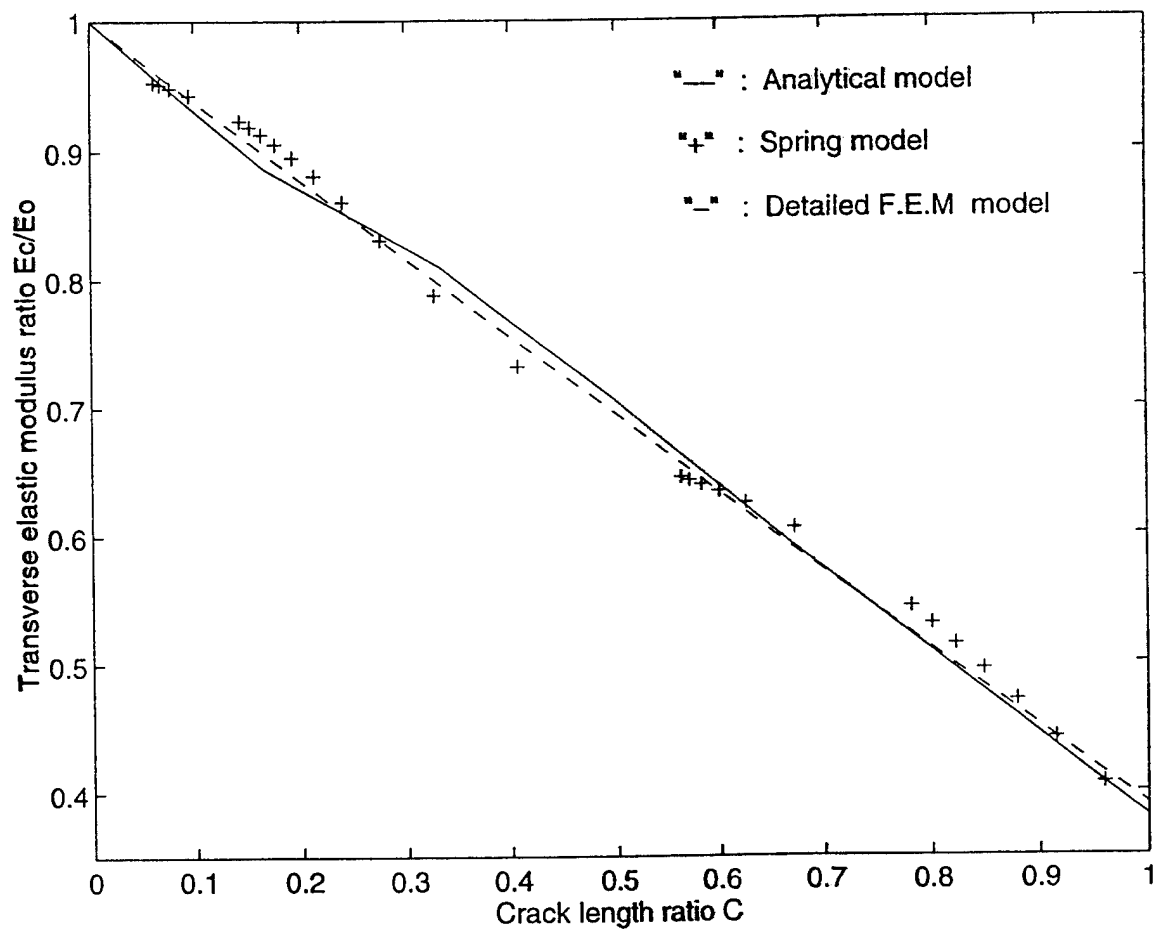
Figure 31. Transverse Elastic Modulis Of A Boron/Epoxy Composite ($V_f = 0.36$).
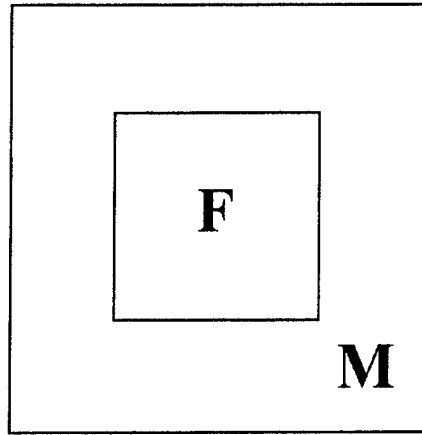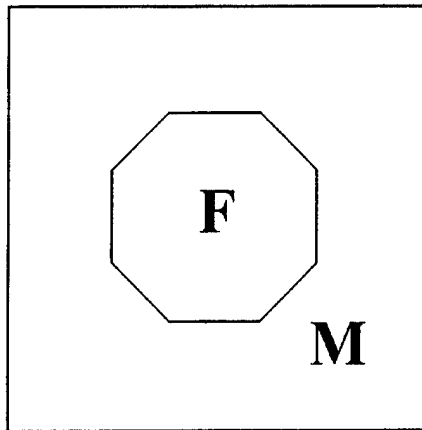
Figure 32. Composite Material Fiber. (a) Rectangular (b) Octagon Fiber.
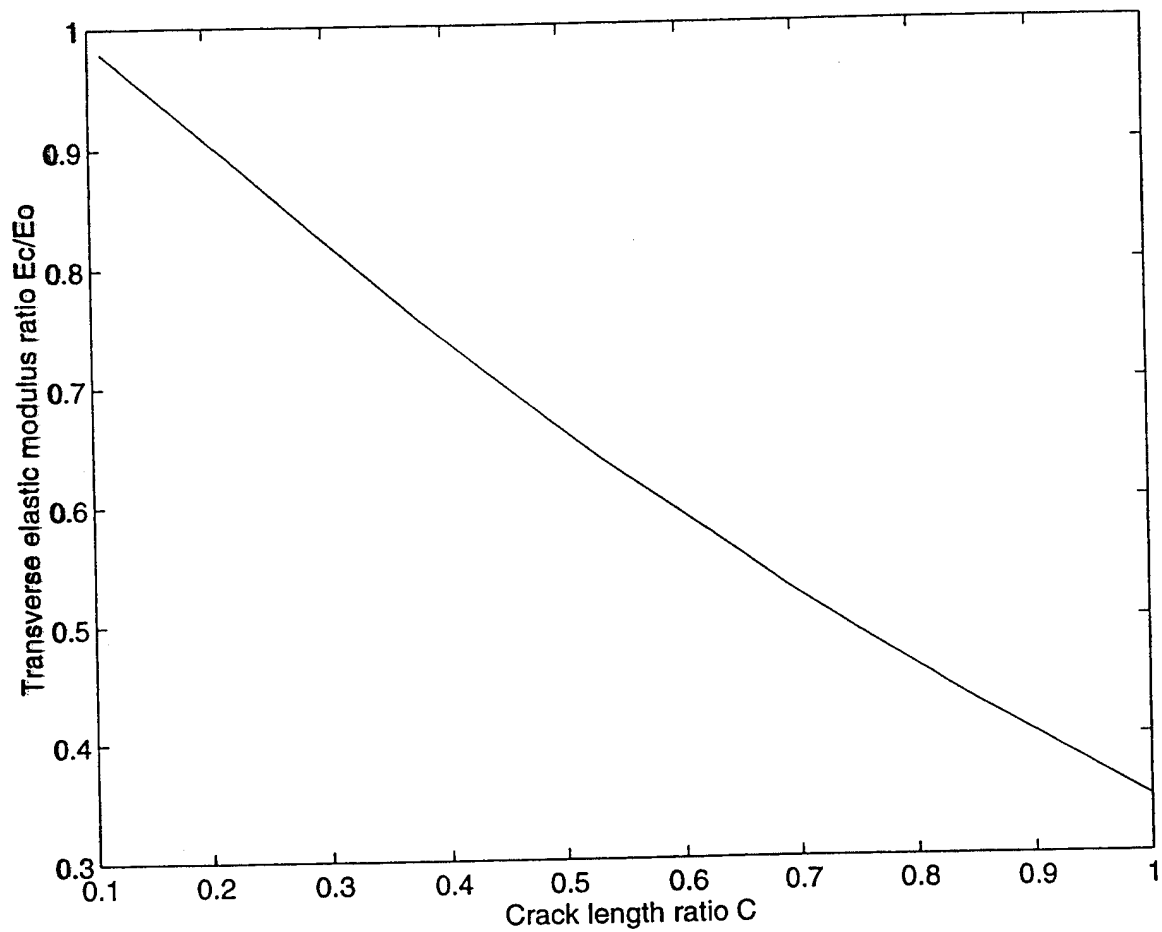
Figure 33. Transverse Elastic Modulis Of Graphite/Epoxy For New Model (V_f = 0.365)
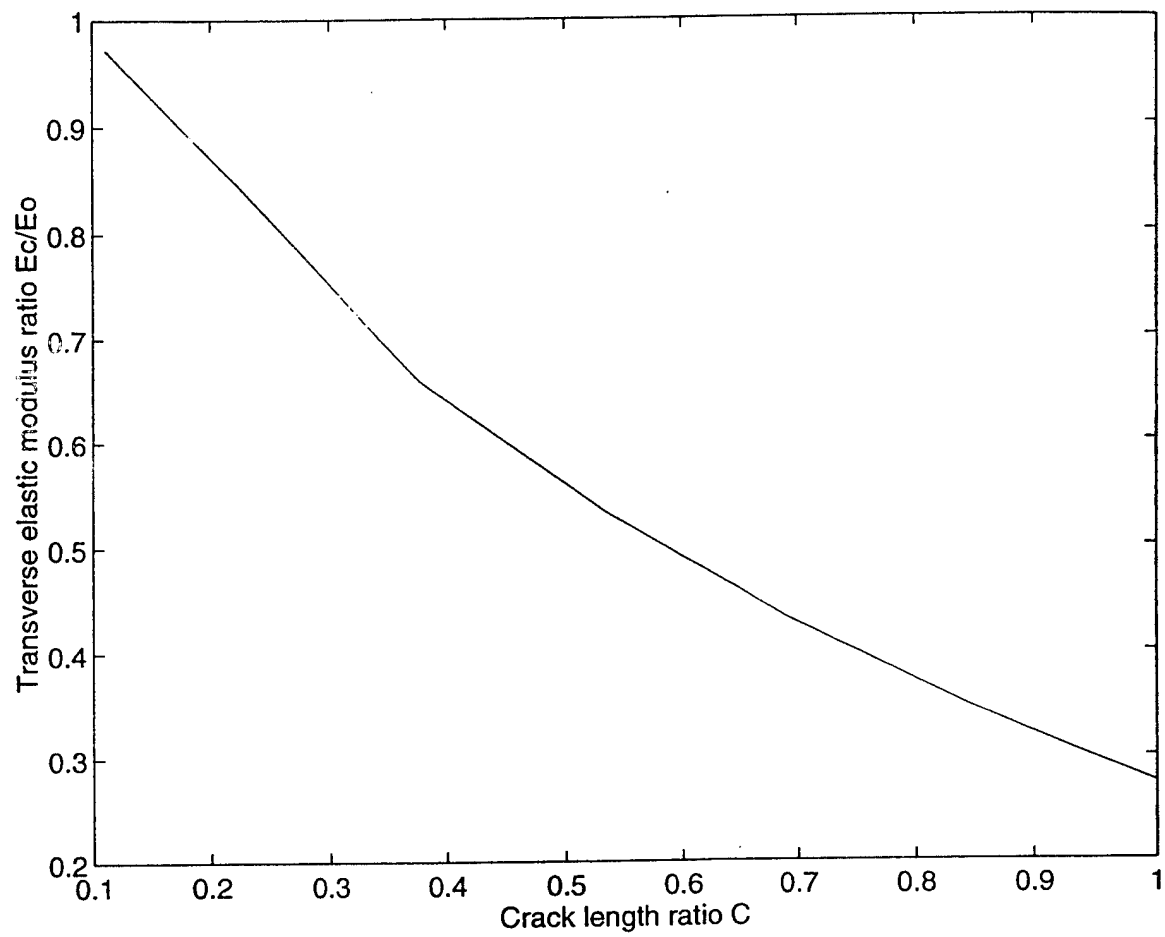
Figure 34. Transverse Elastic Modulis Of Glass/Epoxy For New Model ($V_f = 0.365$).

50
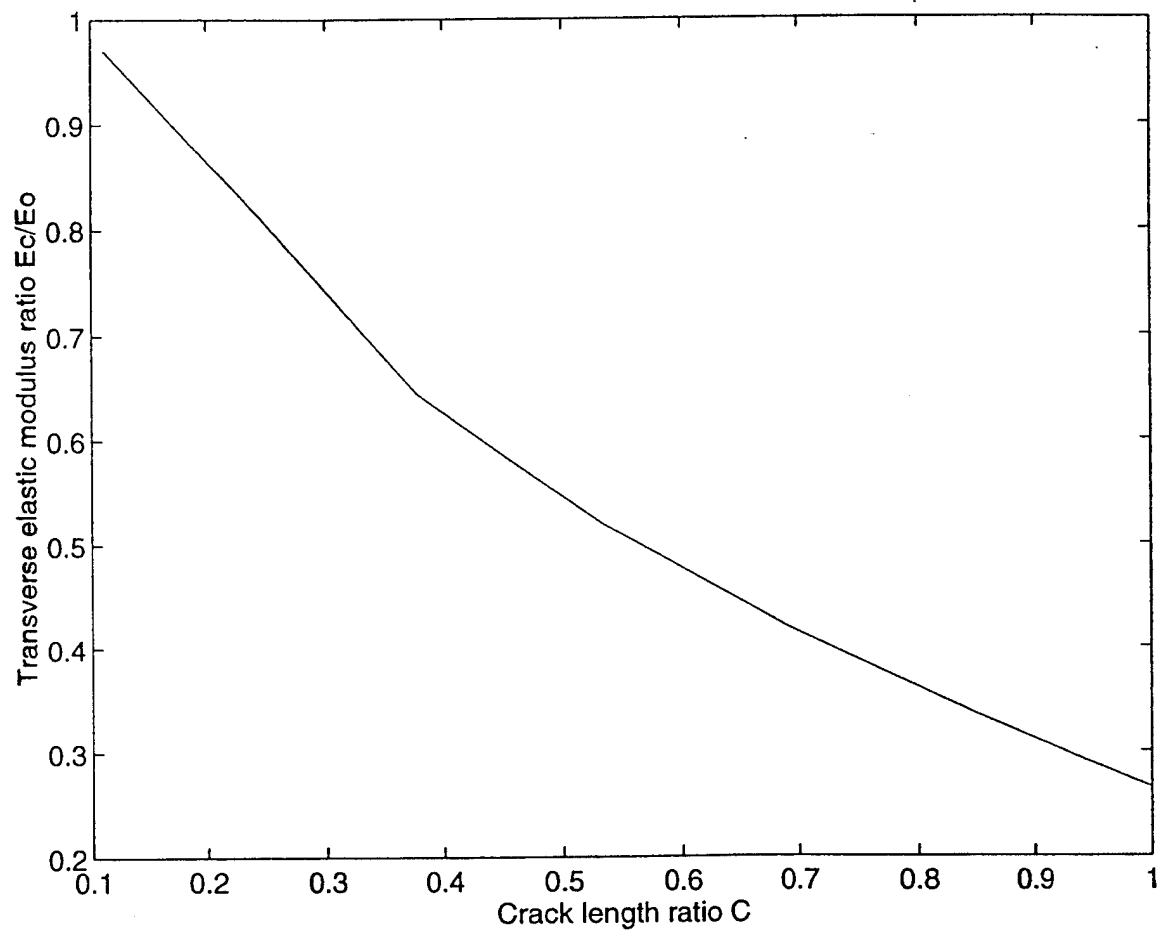
Figure 35. Transverse Elastic Modulis Of Boron/Epoxy For New Model ($V_f = 0.365$).

IV. CONCLUSIONS AND RECOMMENDATIONS

Both modified analytical and simplified FEM micromechanical models developed in this study can predict the effective elastic modulii of composite materials with a partial interface crack between the fiber and matrix. As a result of this study, the following conclusions and recommendations are made.

A. CONCLUSIONS

- A simple, analytical, micromechanical model that neglects the non-effective load-carrying zone, can predict the effective elastic modulii accurately.

- A simplified finite element micromechanical model that contains interface springs can also predict the effective elastic modulii accurately.

- Different fiber shape micromechanical models which have the same fiber volume fraction, and the same material properties, yield comparable results.

- When the fiber elastic modulus is much larger than the matrix elastic modulus, the results of the simplified models are more accurate than those for the case where the fiber and matrix elastic modulii are not much different.

B. RECOMMENDATIONS

- The micromechanics models need to be coupled with an analysis computer program for general composite structures.

- Non-elastic deformations of composites need to be included in the present models.

- A follow-up research from this study would be to develop an algorithm for determining spring constants, dependend on the state of the interface crack.

APPENDIX A. SUBCELL STRAINS EQUATIONS

1. $\sigma_{22}^a = \sigma_{22}^b$

2. $\sigma_{22}^c = \sigma_{22}^d$

3. $\sigma_{22}^a = \sigma_{22}^c$

4. $\sigma_{22}^b = \sigma_{22}^d$

5. $\sigma\varepsilon_{22}^a + (1-a)\varepsilon_{22}^b - \sigma\varepsilon_{22}^c - (1-a)\varepsilon_{22}^d = 0$

6. $\sigma\varepsilon_{33}^a + (1-a)\varepsilon_{33}^b - \sigma\varepsilon_{33}^c - (1-a)\varepsilon_{33}^d = 0$

7. $\varepsilon_{11}^a - \varepsilon_{11}^b = 0$

8. $\varepsilon_{11}^c - \varepsilon_{11}^d = 0$

9. $\varepsilon_{11}^b - \varepsilon_{11}^c = 0$

10. $\bar{\varepsilon}_{11} = a^2\varepsilon_{11}^a + a(1-a)\varepsilon_{11}^b + a(1-a)\varepsilon_{11}^c + a(1-a)\varepsilon_{11}^d$

11. $\bar{\varepsilon}_{22} = a^2\varepsilon_{22}^a + a(1-a)\varepsilon_{22}^b + a(1-a)\varepsilon_{22}^c + a(1-a)\varepsilon_{22}^d$

12. $\bar{\varepsilon}_{33} = a^2\varepsilon_{33}^a + a(1-a)\varepsilon_{33}^b + a(1-a)\varepsilon_{33}^c + a(1-a)\varepsilon_{33}^d$

*Equations 10 through 12 $a = \sqrt{V_f}$, for a subscript "a,b,c,d" are subcells

APPENDIX B. MATRIX [B]

$$[B] = \begin{bmatrix} \dfrac{y_2 - y_3}{2A} & 0 & \dfrac{y_3 - y_1}{2A} & 0 & \dfrac{y_1 - y_2}{2A} & 0 \\[3mm] 0 & \dfrac{x_3 - x_2}{2A} & 0 & \dfrac{x_1 - x_3}{2A} & 0 & \dfrac{x_2 - x_1}{2A} \\[3mm] \dfrac{x_3 - x_2}{2A} & \dfrac{y_2 - y_3}{2A} & \dfrac{x_1 - x_3}{2A} & \dfrac{y_3 - y_1}{2A} & \dfrac{x_2 - x_1}{2A} & \dfrac{y_1 - y_2}{2A} \end{bmatrix}$$

A: Triangular Area

APPENDIX C. TRANSVERSE ELASTIC MODULUS AND BEST FITTING FUNCTION.
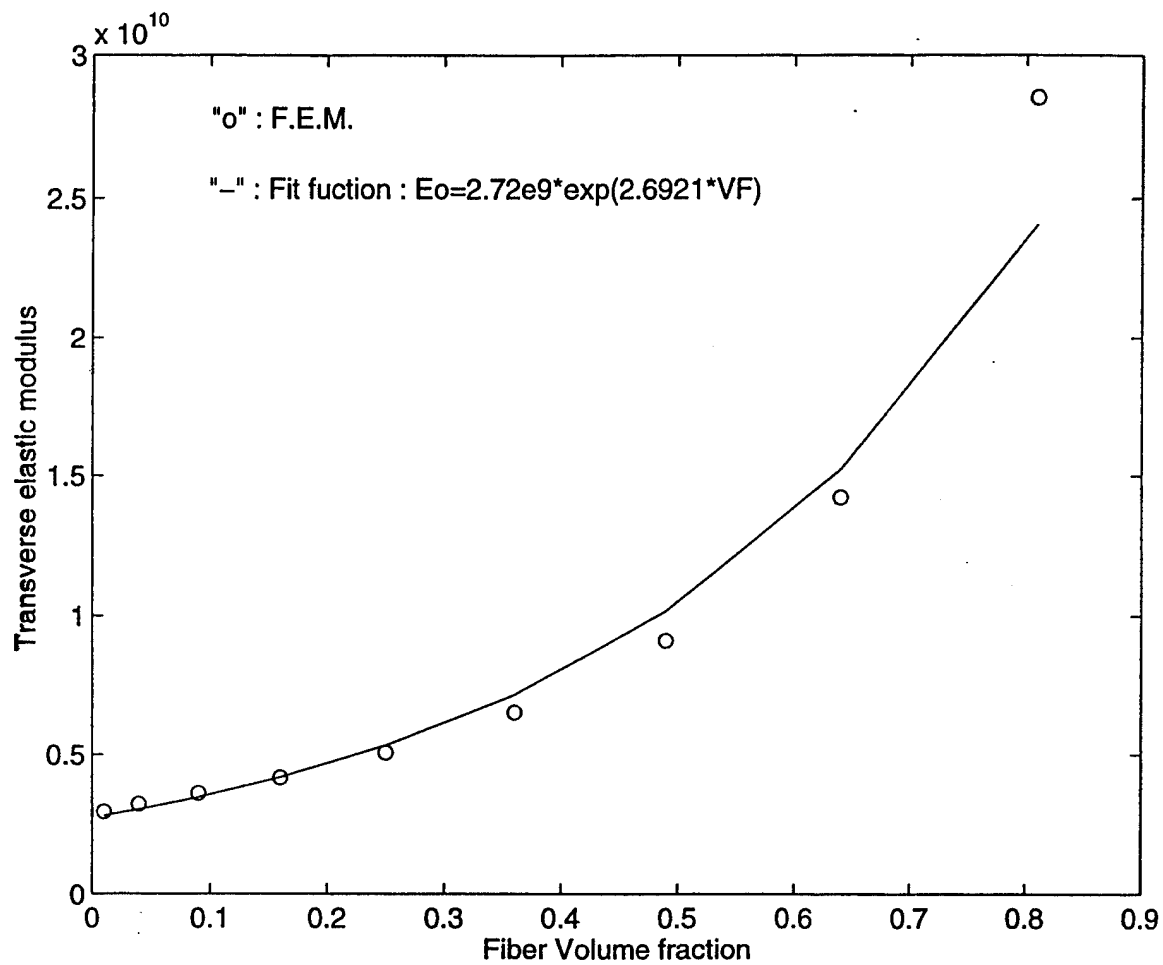
Figure 36. Transverse Elastic Modulus of Glass/Epoxy and Best Fitting Function
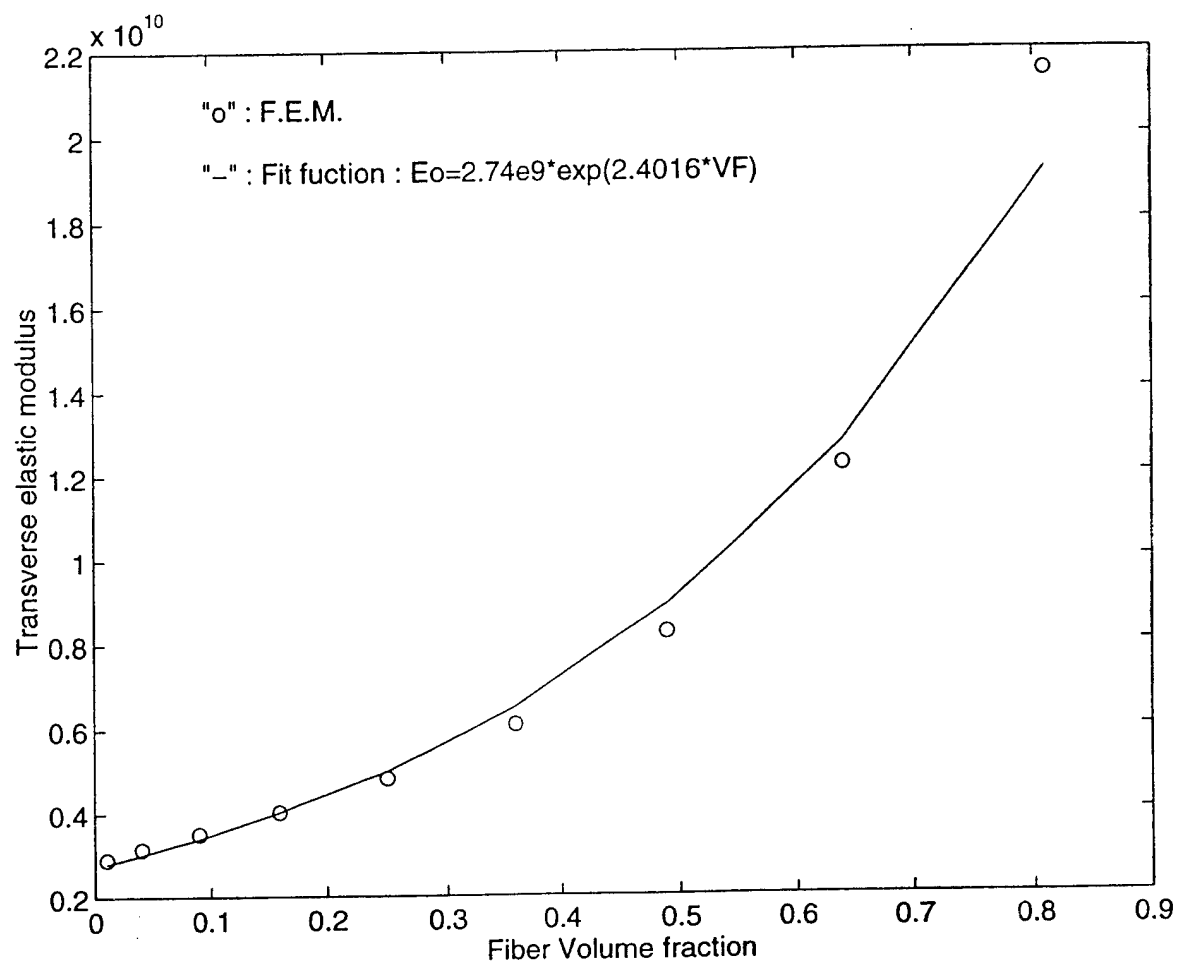
Figure 37. Transverse Elastic Modulus Boron/Epoxy and Best Fitting Function

APPENDIX D. STRESSES DISTRIBUTION OF A FIBER.
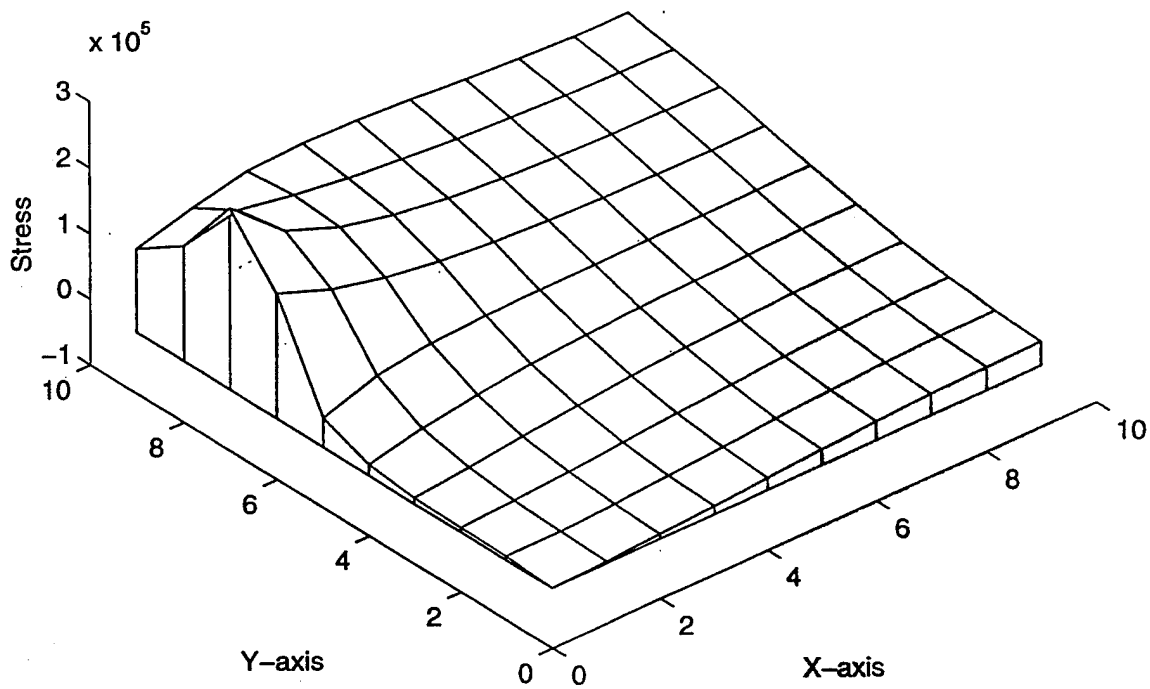
Figure 38. Stresses Distribution of a Graphite Fiber With 70% Crack Length
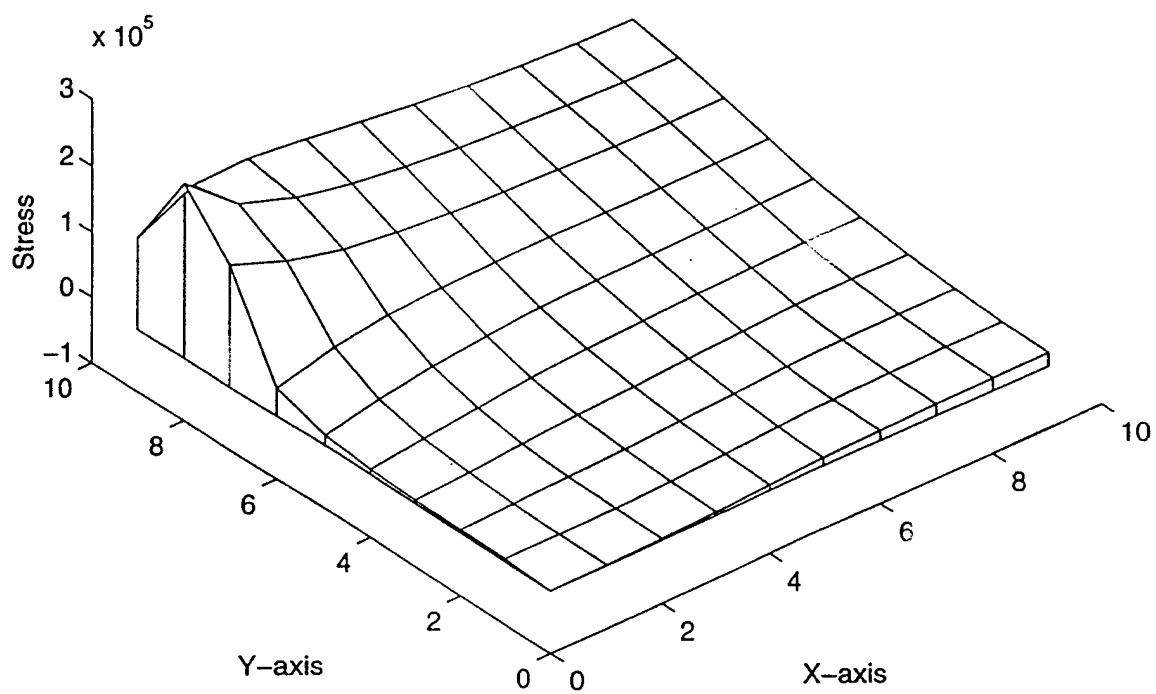
Figure 39. Stresses Distribution of a Graphite Fiber With 80% Crack Length
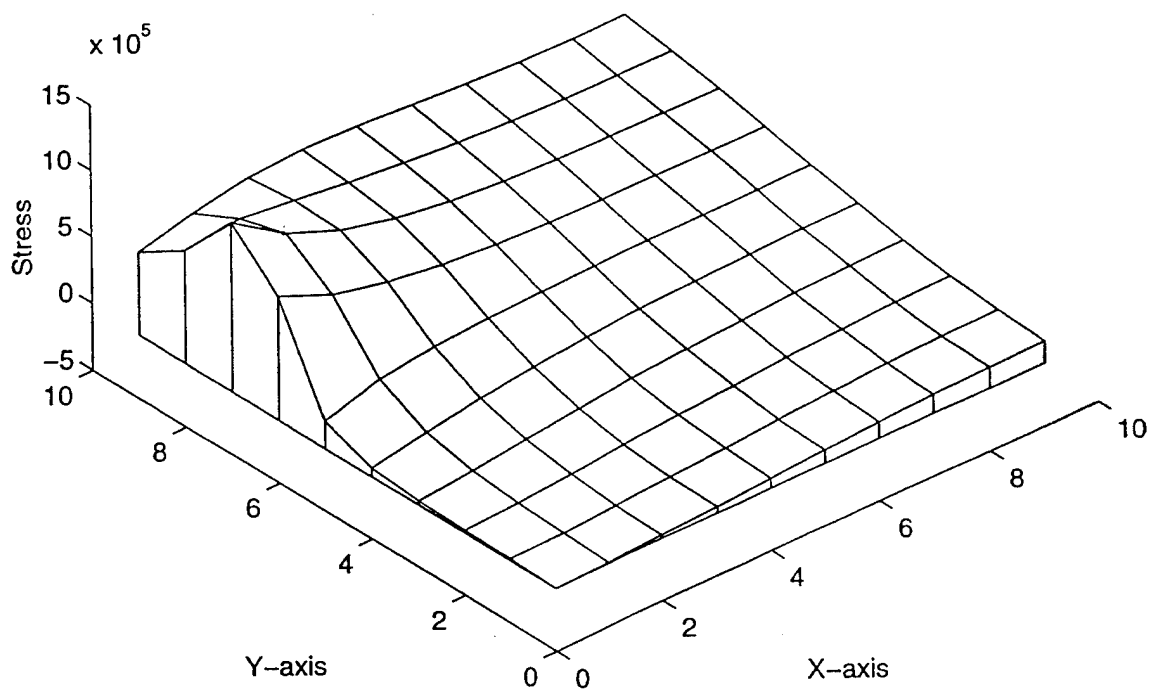
Figure 40. Stresses Distribution of a Glass Fiber With 70% Crack Length
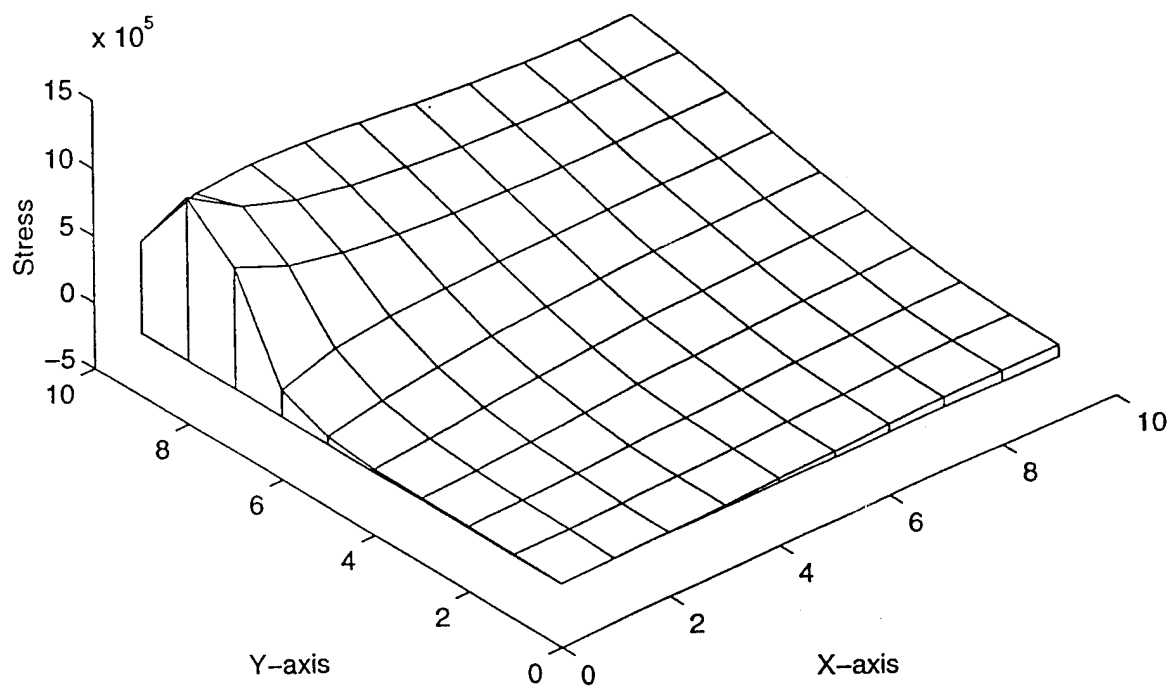
Figure 41. Stresses Distribution of a Glass Fiber With 80% Crack Length
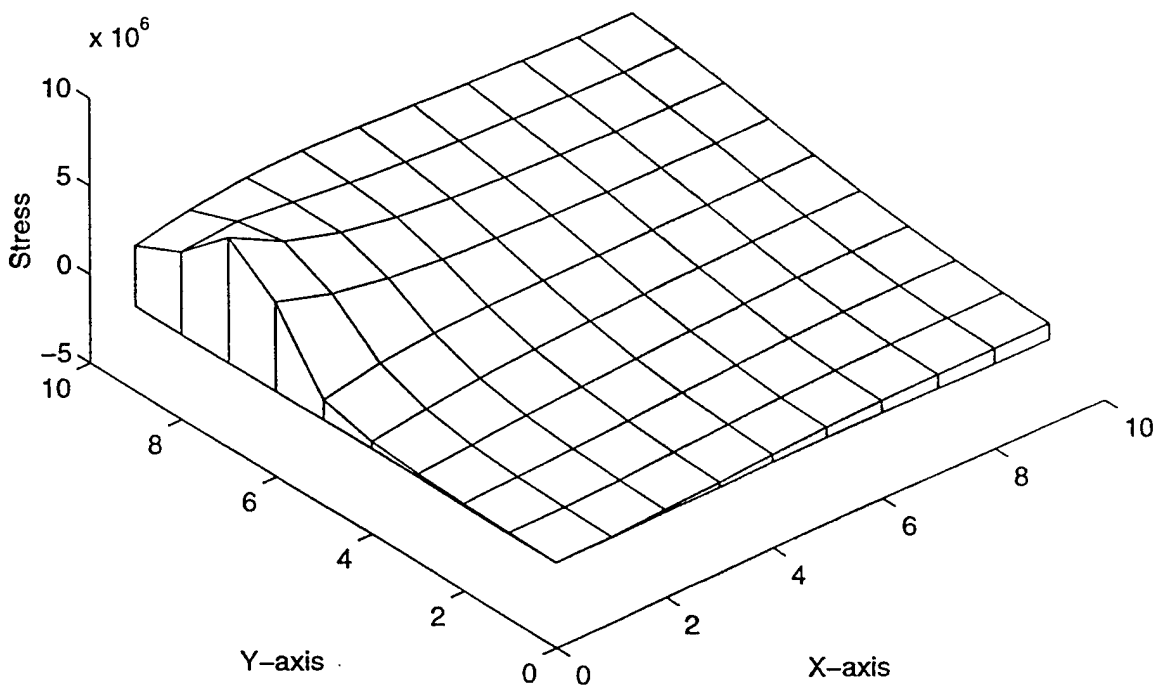
Figure 42. Stresses Distribution of a Boron Fiber With 70% Crack Length
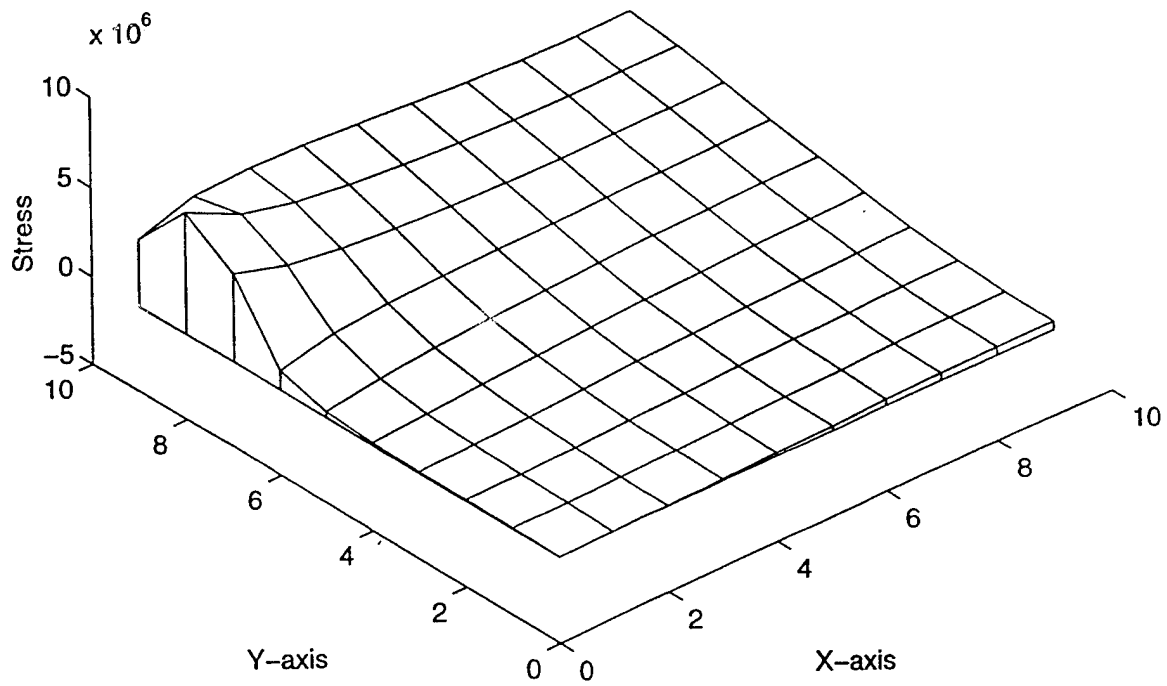
Figure 43. Stresses Distribution of a Boron Fiber With 80% Crack Length

APPENDIX E. STRESSES DISTRIBUTION OF A COMPOSITE.
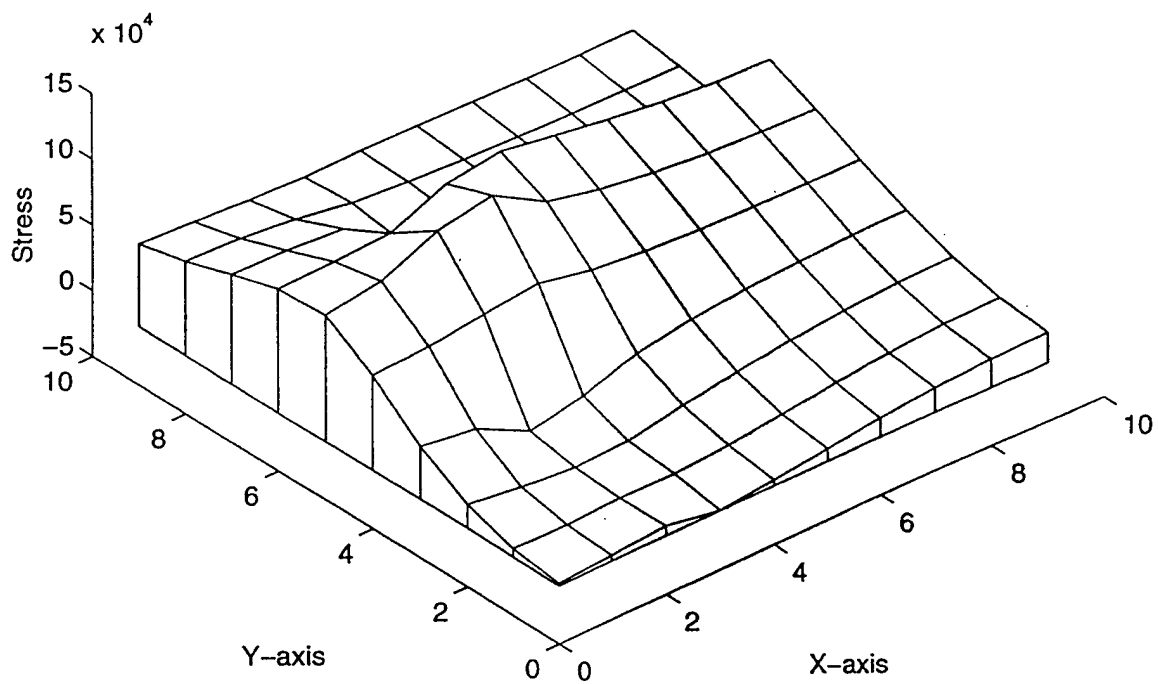
Figure 44. Stresses Distribution of a Graphite/Epoxy Composite With 50% Crack Length ($V_f = 0.49$)
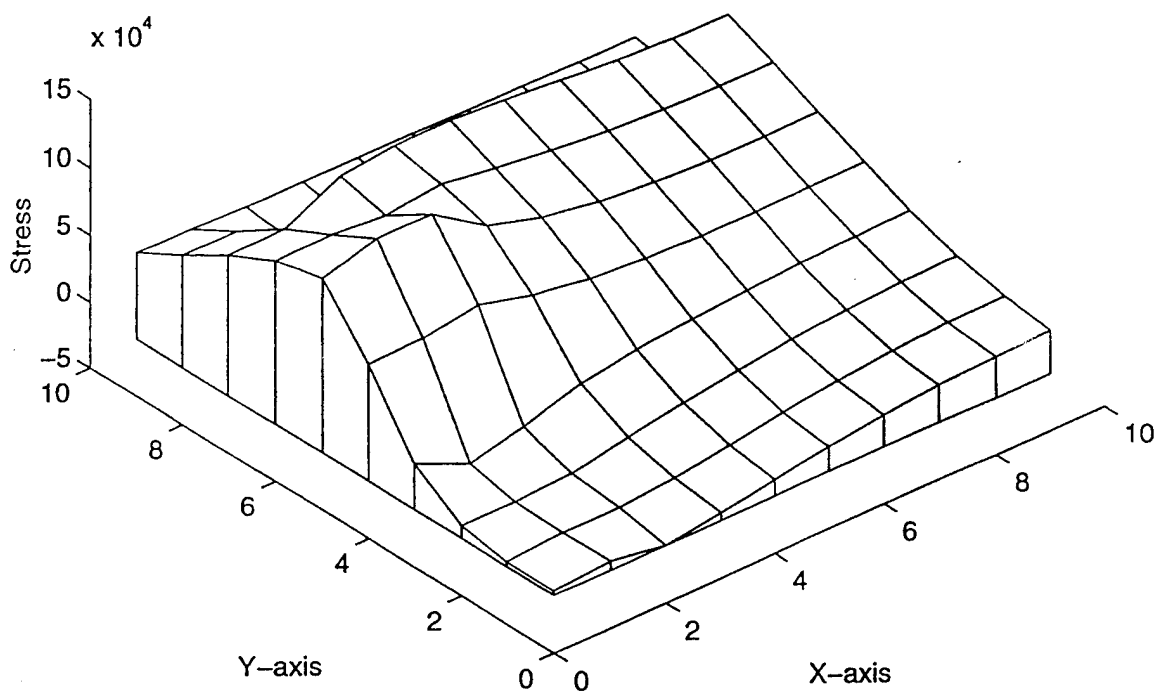
Figure 45. Stresses Distribution of a Graphite/Epoxy Composite With 50% Crack Length ($V_f = 0.64$)
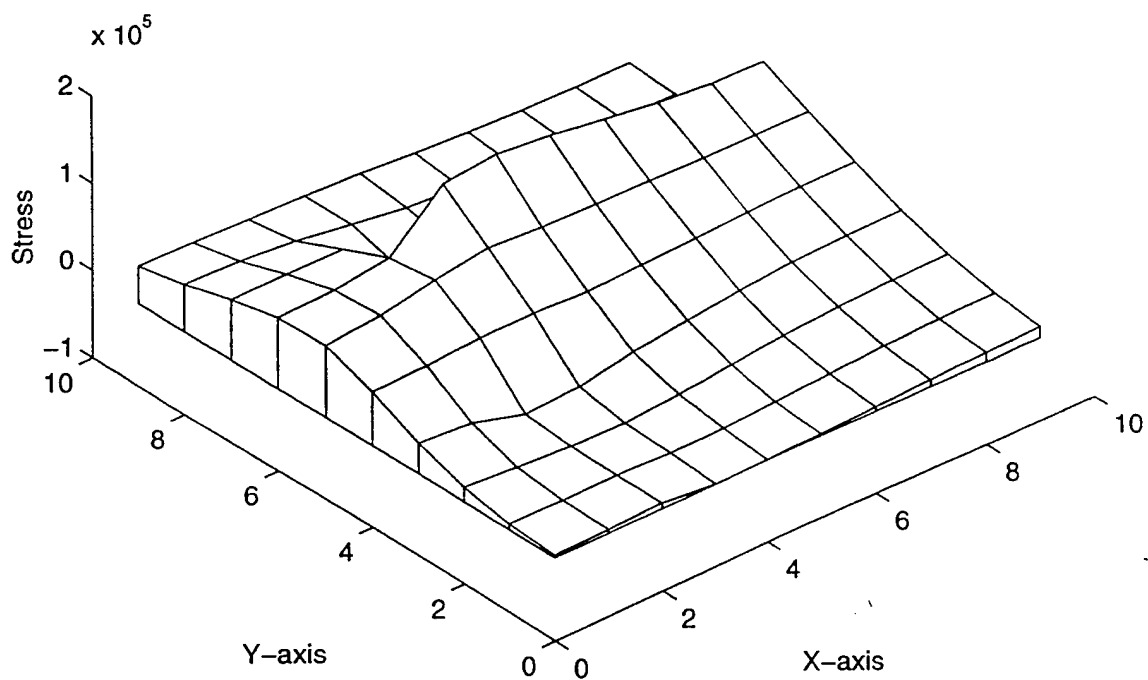
Figure 46. Stresses Distribution of a Glass/Epoxy Composite With 50% Crack Length ($V_f = 0.49$)
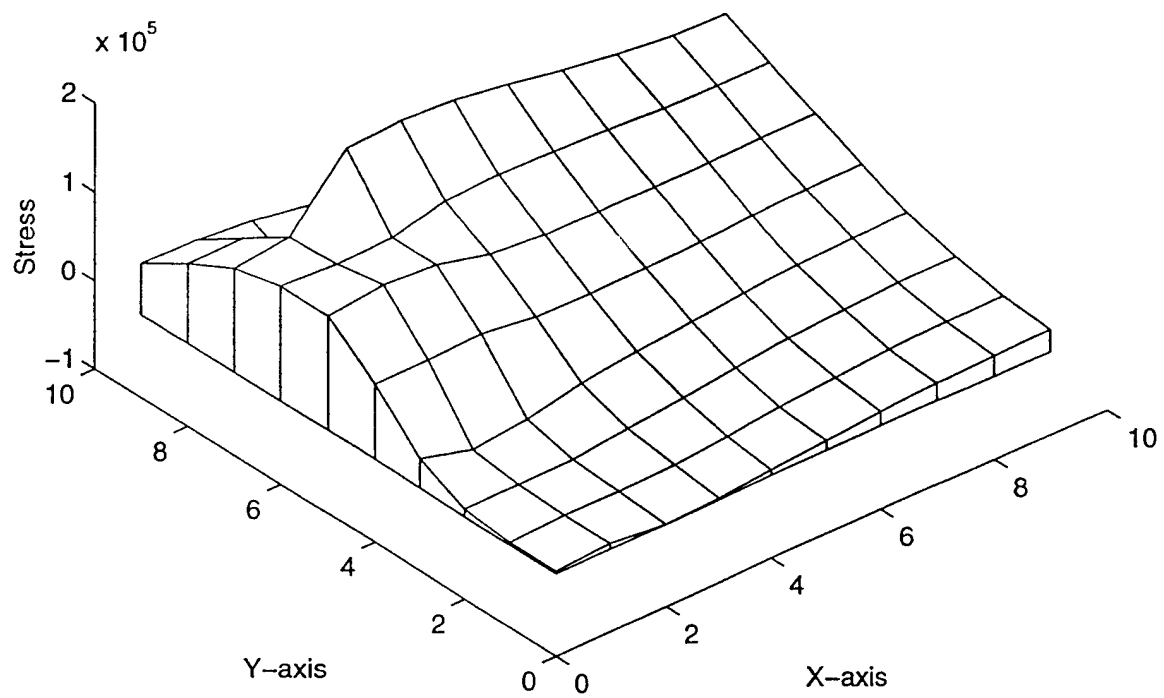
Figure 47. Stresses Distribution of a Glass/Epoxy Composite With 50% Crack Length ($V_f = 0.64$)
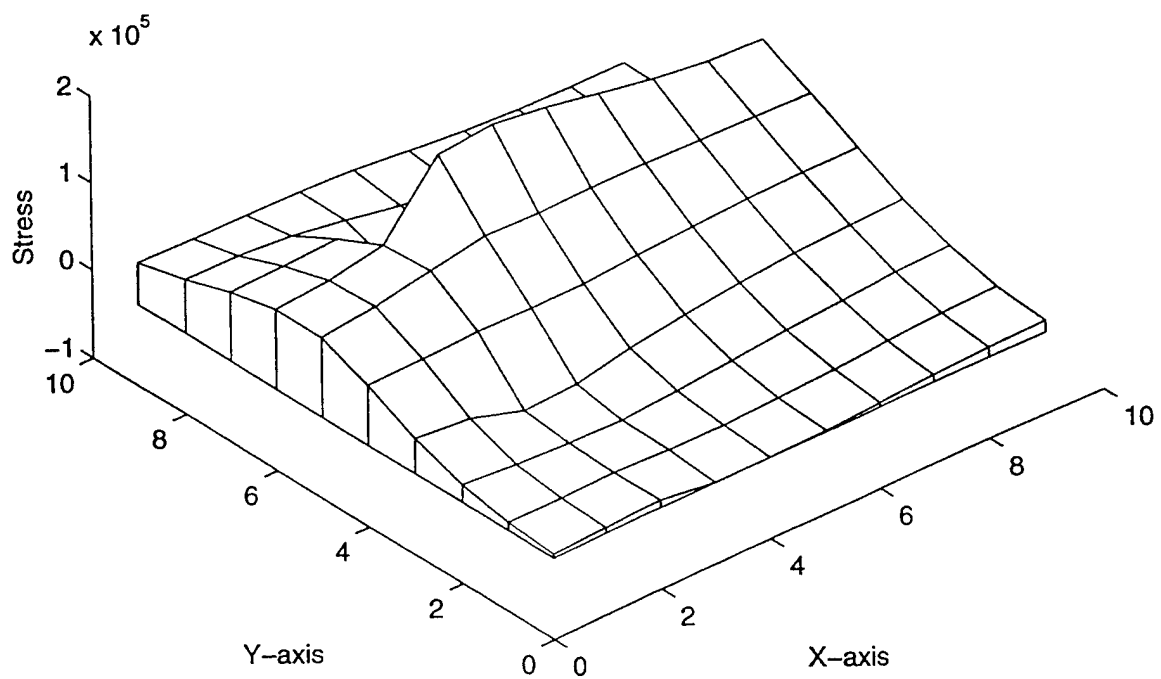
Figure 48. Stresses Distribution of a Boron/Epoxy Composite With 50% Crack
Length ($V_f = 0.49$)
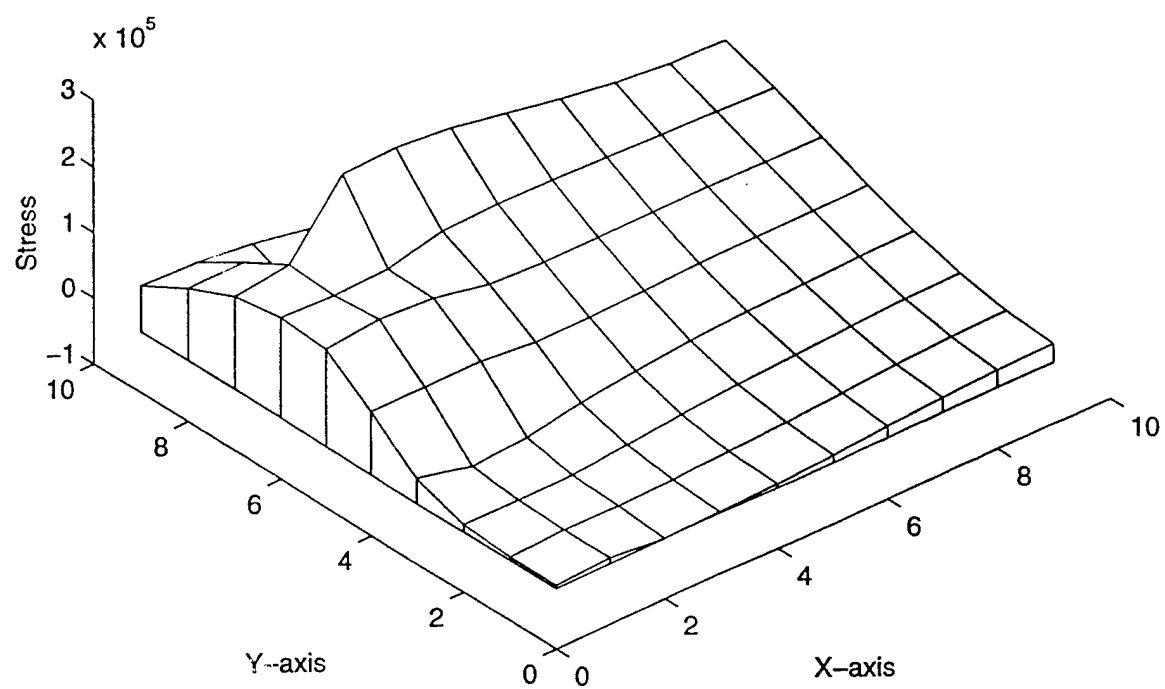
Figure 49. Stresses Distribution of a Boron/Epoxy Composite With 50% Crack Length ($V_f = 0.64$)

72

APPENDIX F. TRANSVERSE ELASTIC MODULUS RATIO.
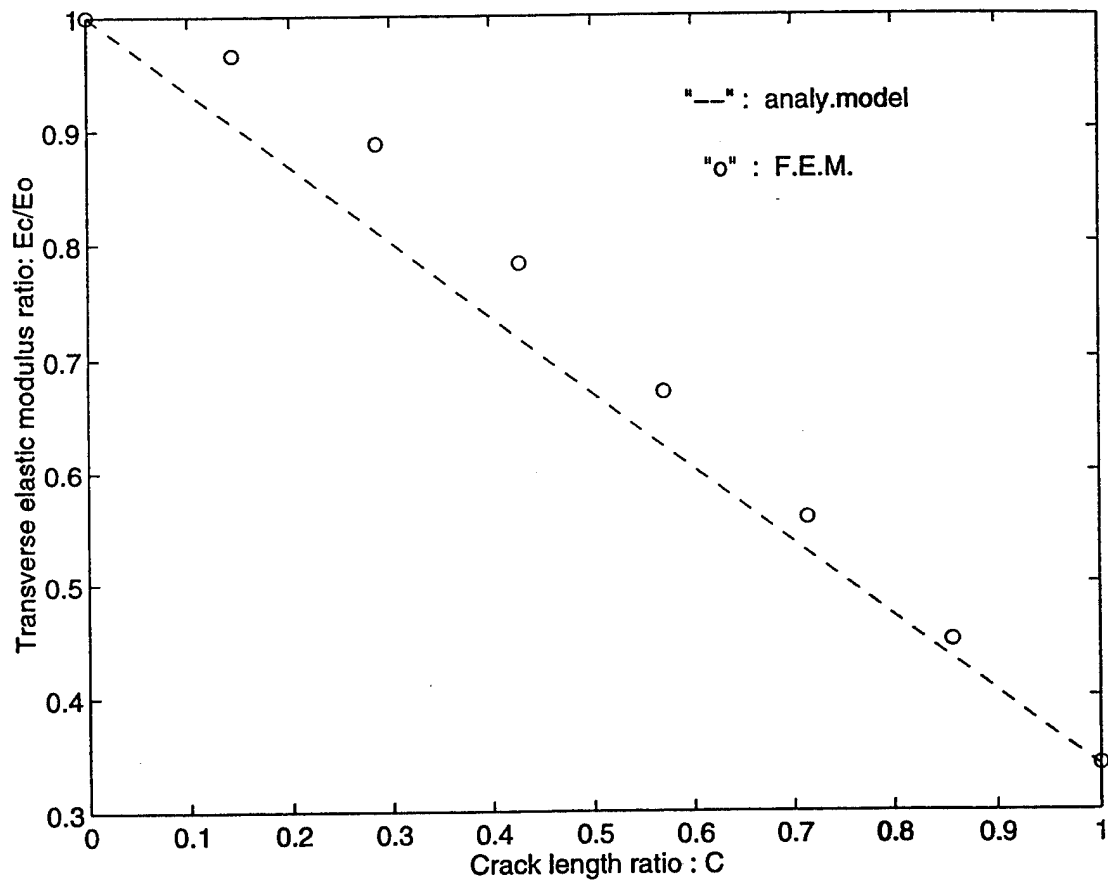
Figure 50. Transverse Elastic Modulus Ratio of a Graphite/Epoxy Composite With
V_f=0.49
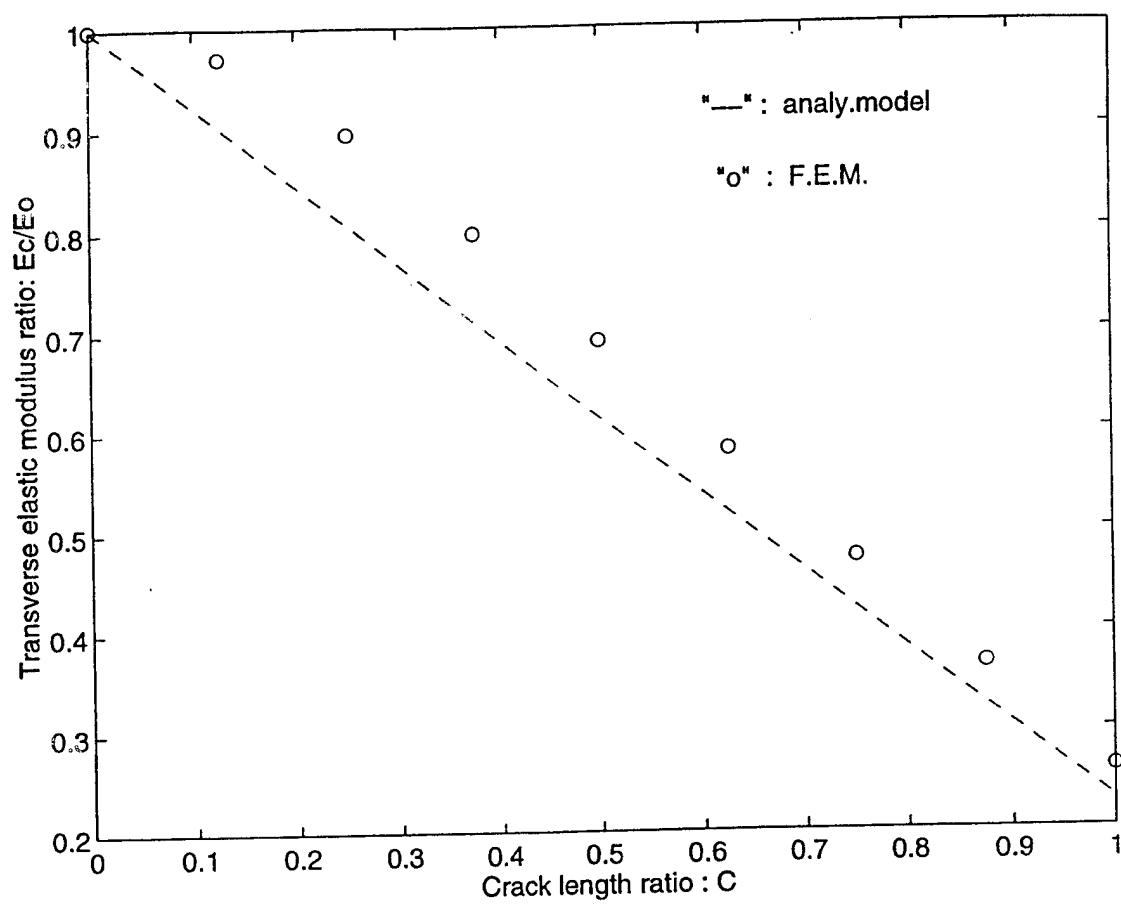
Figure 51. Transverse Elastic Modulus Ratio of a Graphite/Epoxy Composite With V_f=0.64
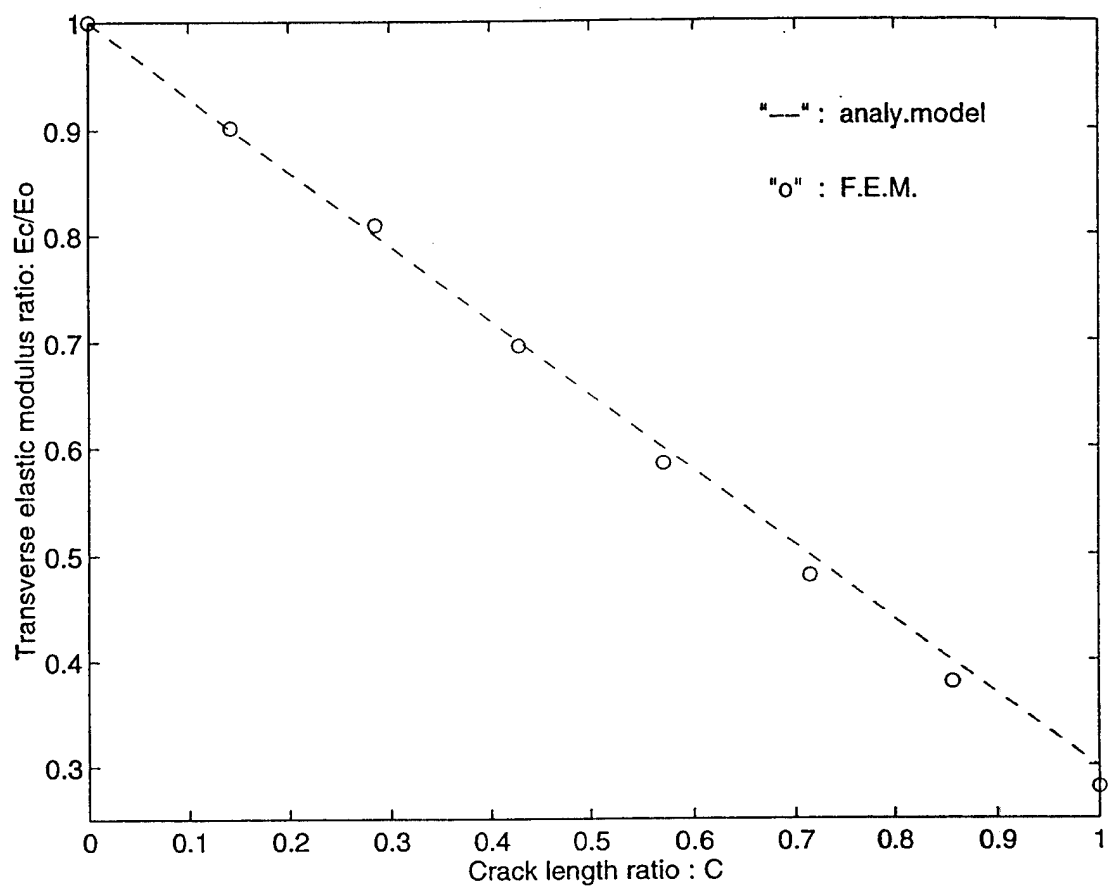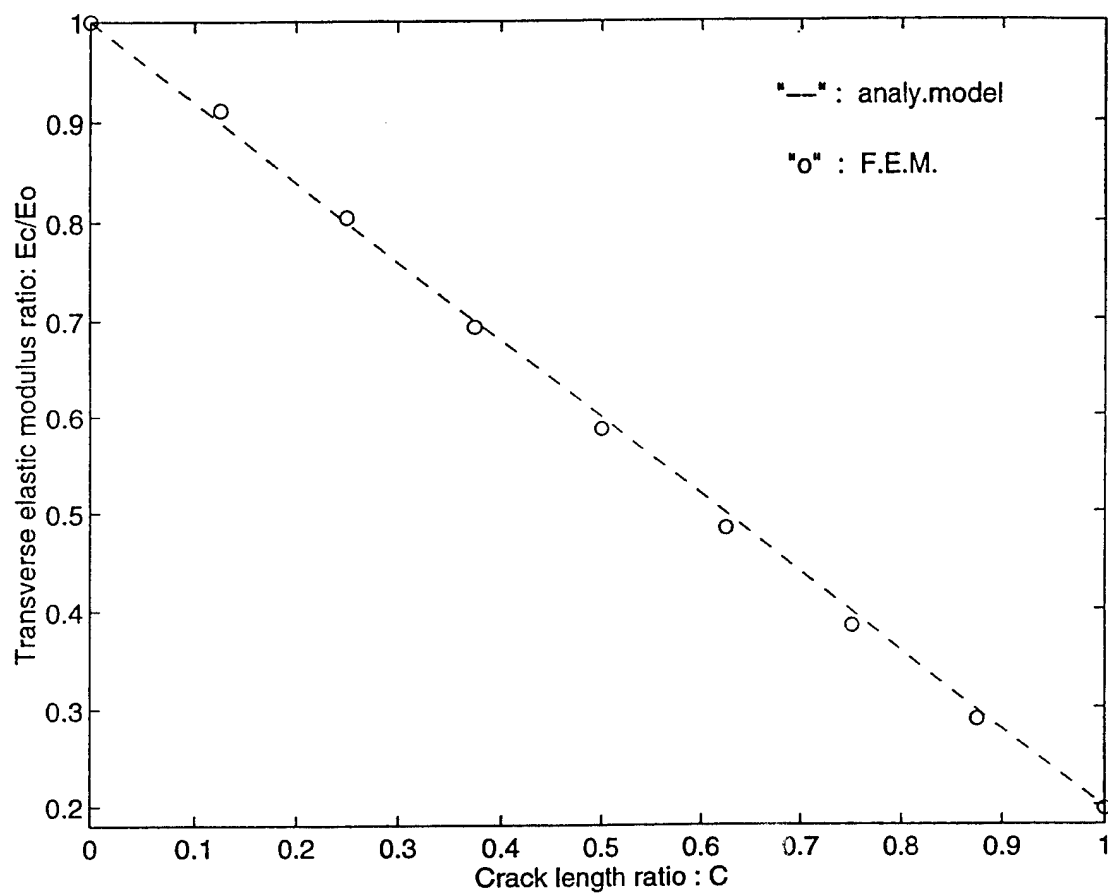
Figure 52. Transverse Elastic Modulus Ratio of a Glass/Epoxy Composite With V_f **=0.49**
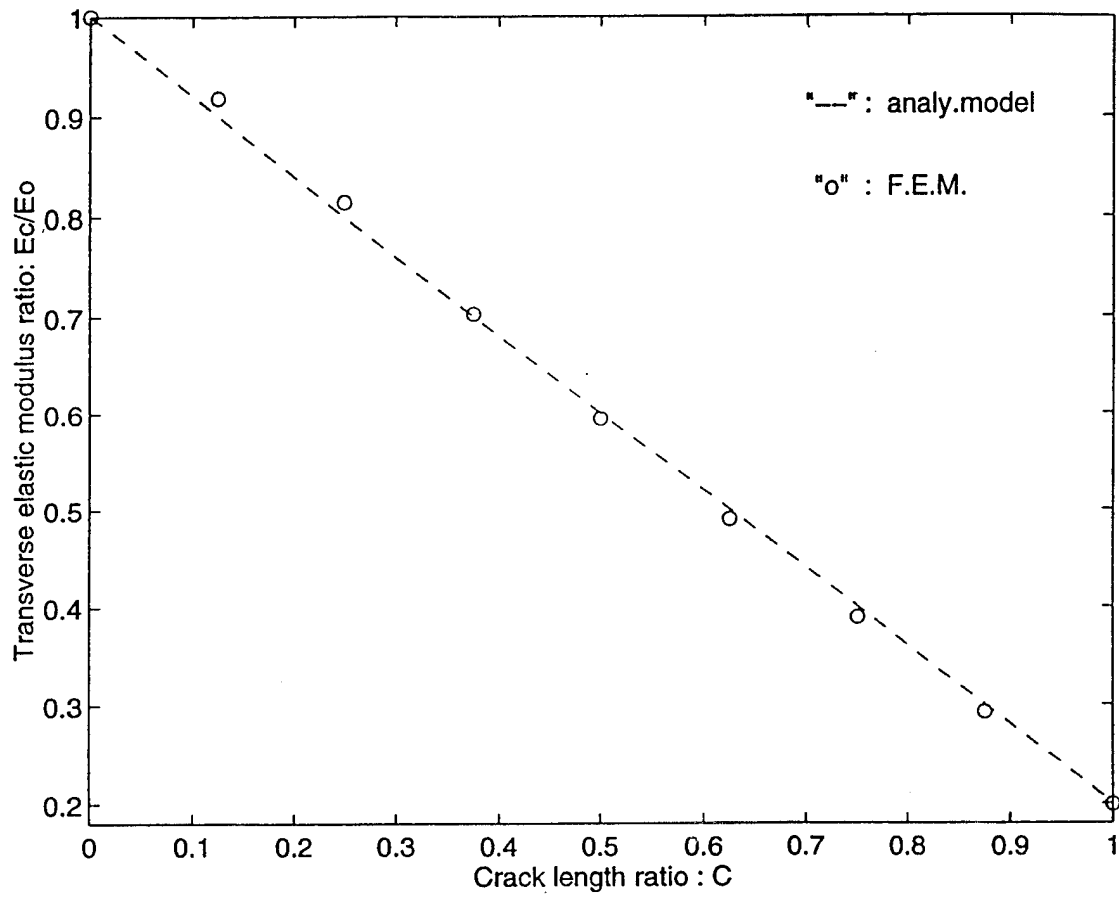
**Figure 53. Transverse Elastic Modulus Ratio of a Glass/Epoxy Composite With
=0.64**
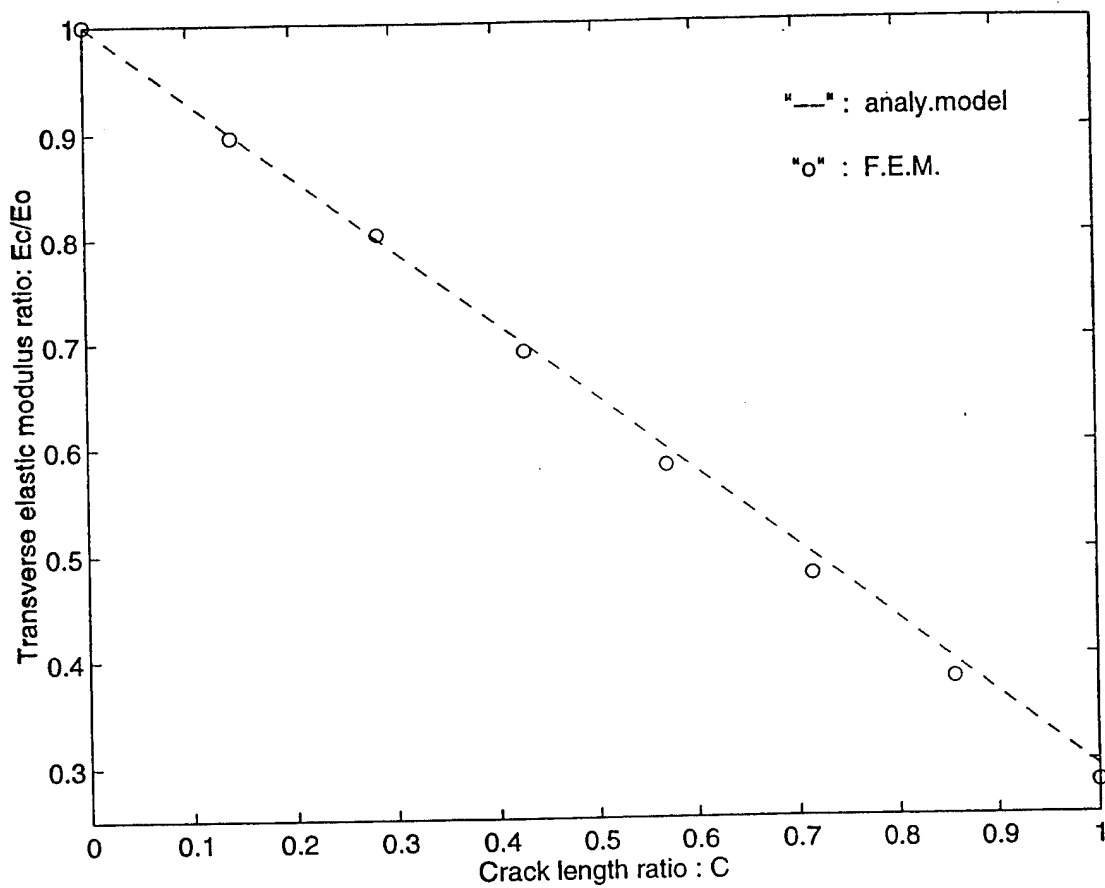
Figure 54. Transverse Elastic Modulus Ratio of a Boron/Epoxy Composite With V_f $= 0.49$

Figure 55. Transverse Elastic Modulus Ratio of a Boron/Epoxy Composite With V_f = 0.64

APPENDIX G. SPRING CONSTANT OF A COMPOSITE.
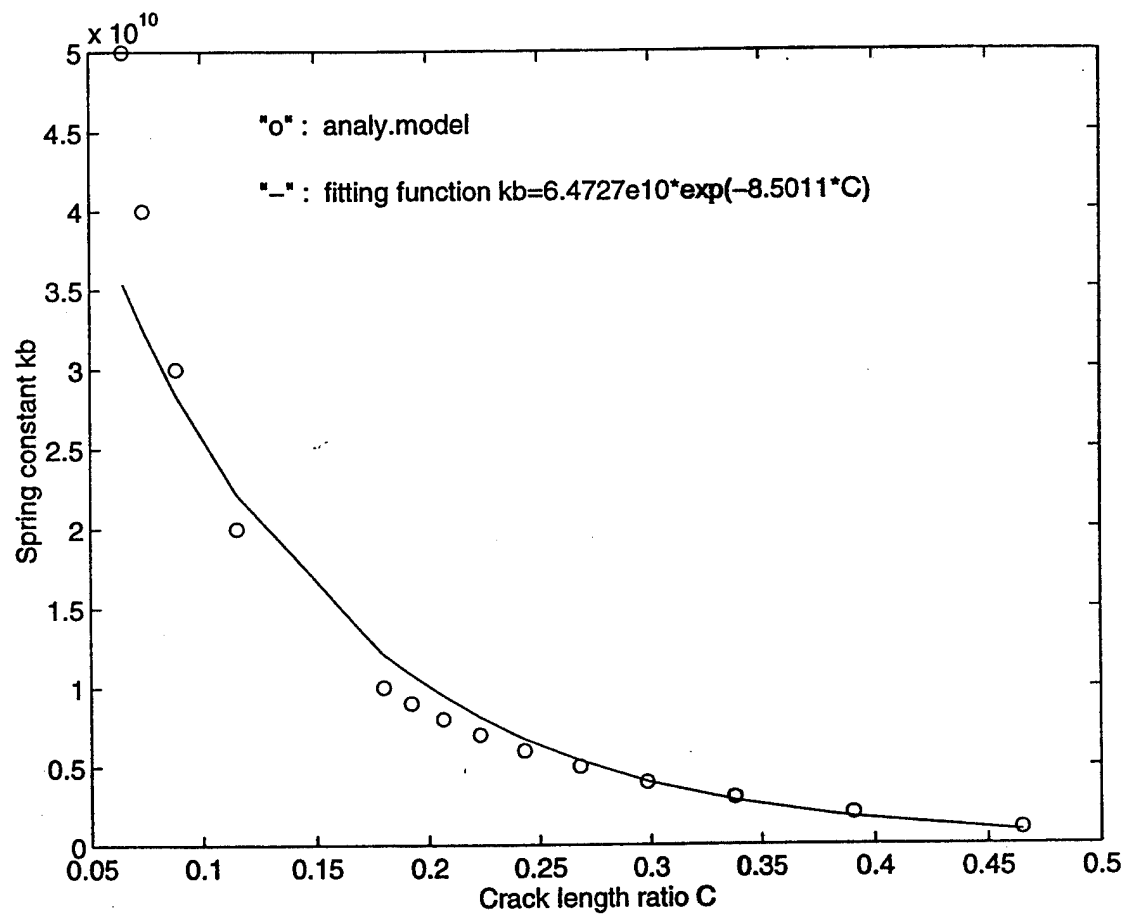
Figure 56. Spring Constant of a Graphite /Epoxy Composite with V_f=0.49 (Low crack case)
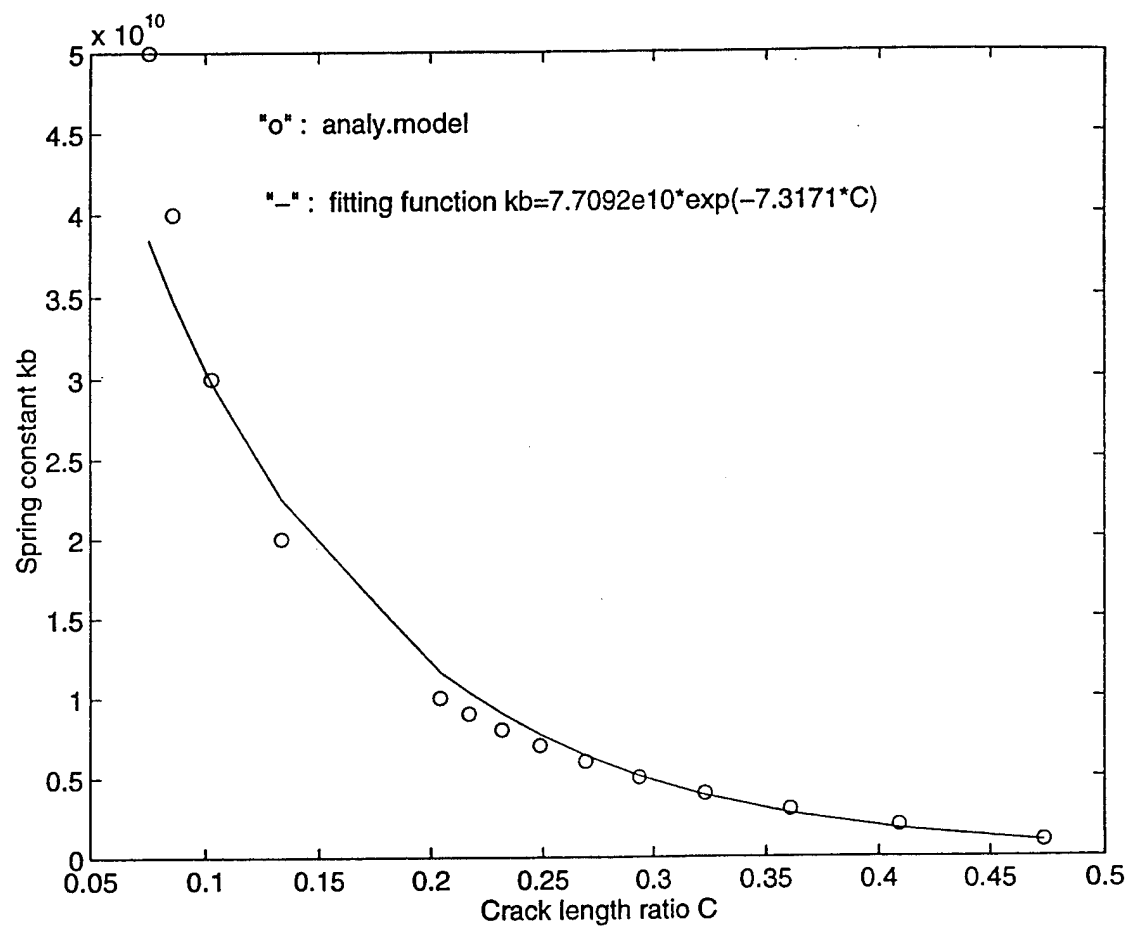
Figure 57. Spring Constant of a Graphite/Epoxy Composite with V_f=0.64 (Low crack case)
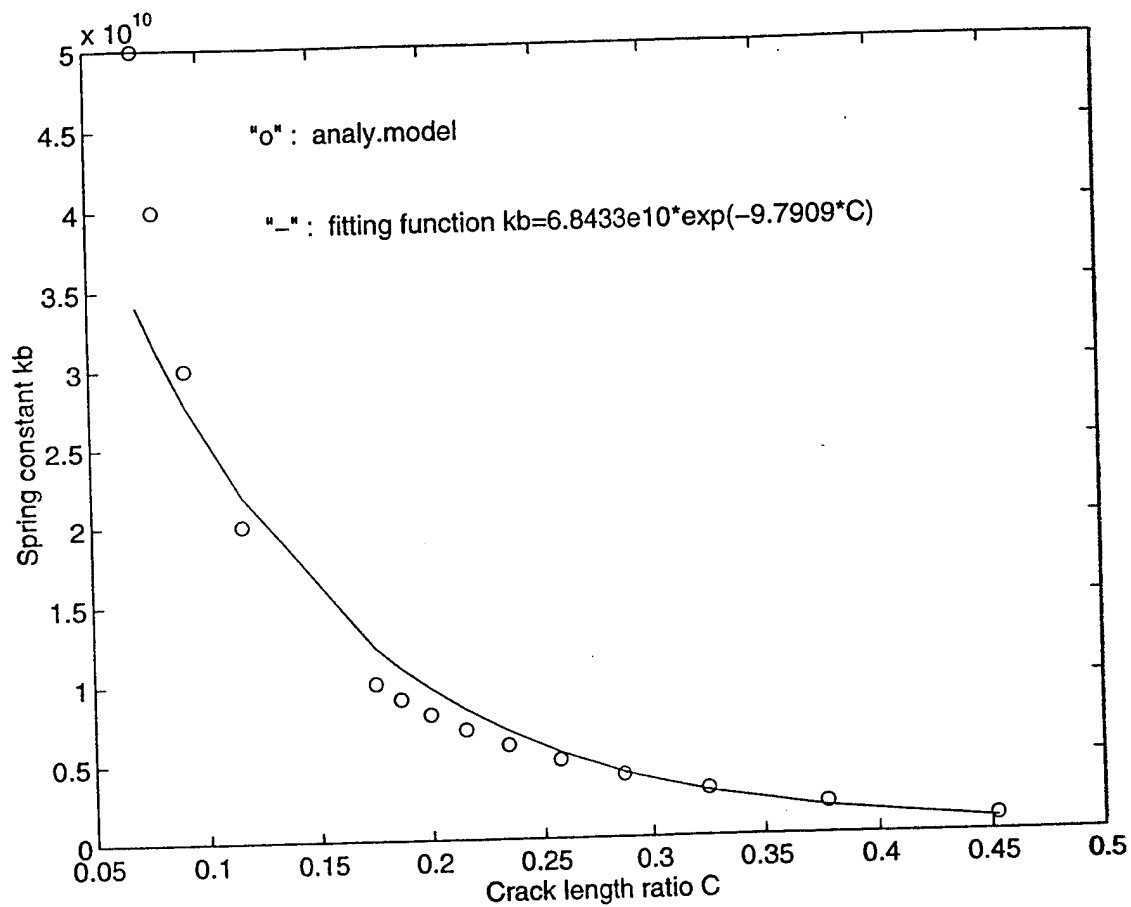
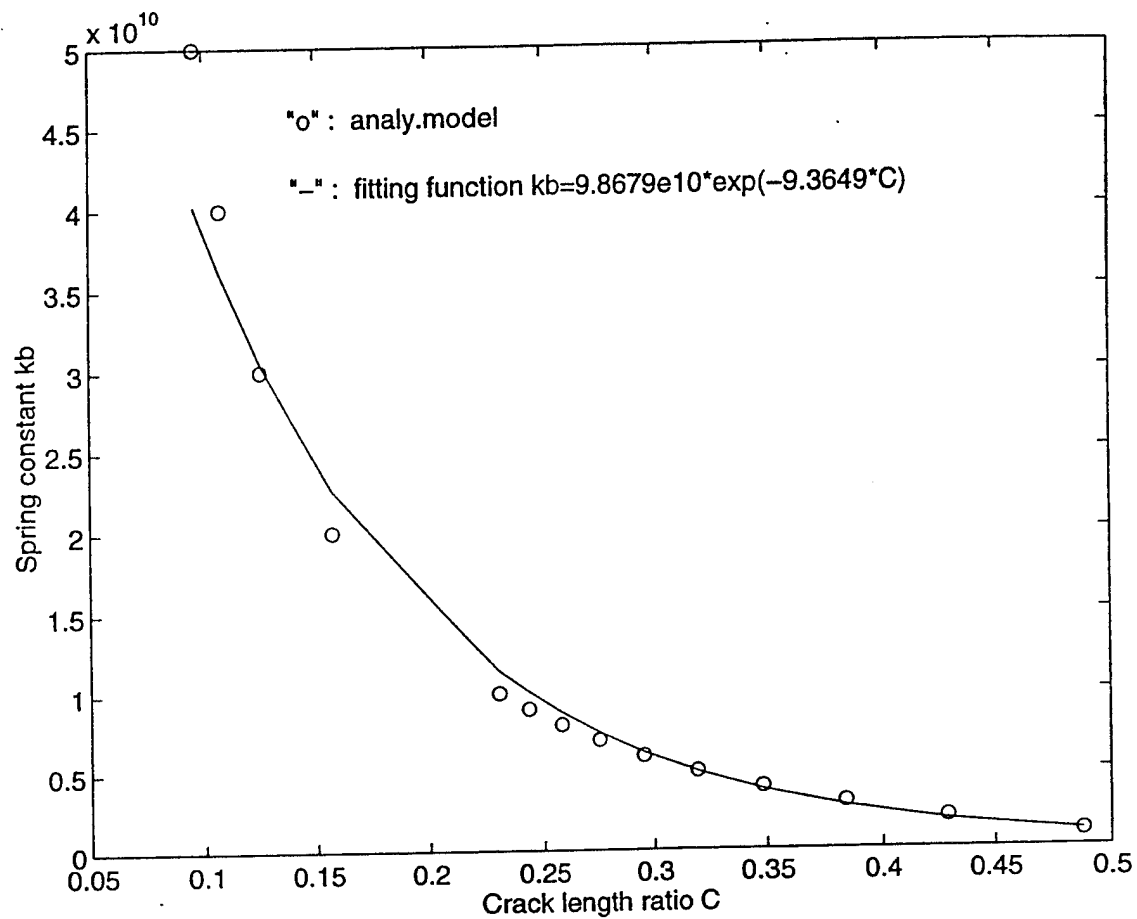**Figure 58. Spring Constant of a Glass /Epoxy Composite with** V_f=0.49 **(Low crack case)**

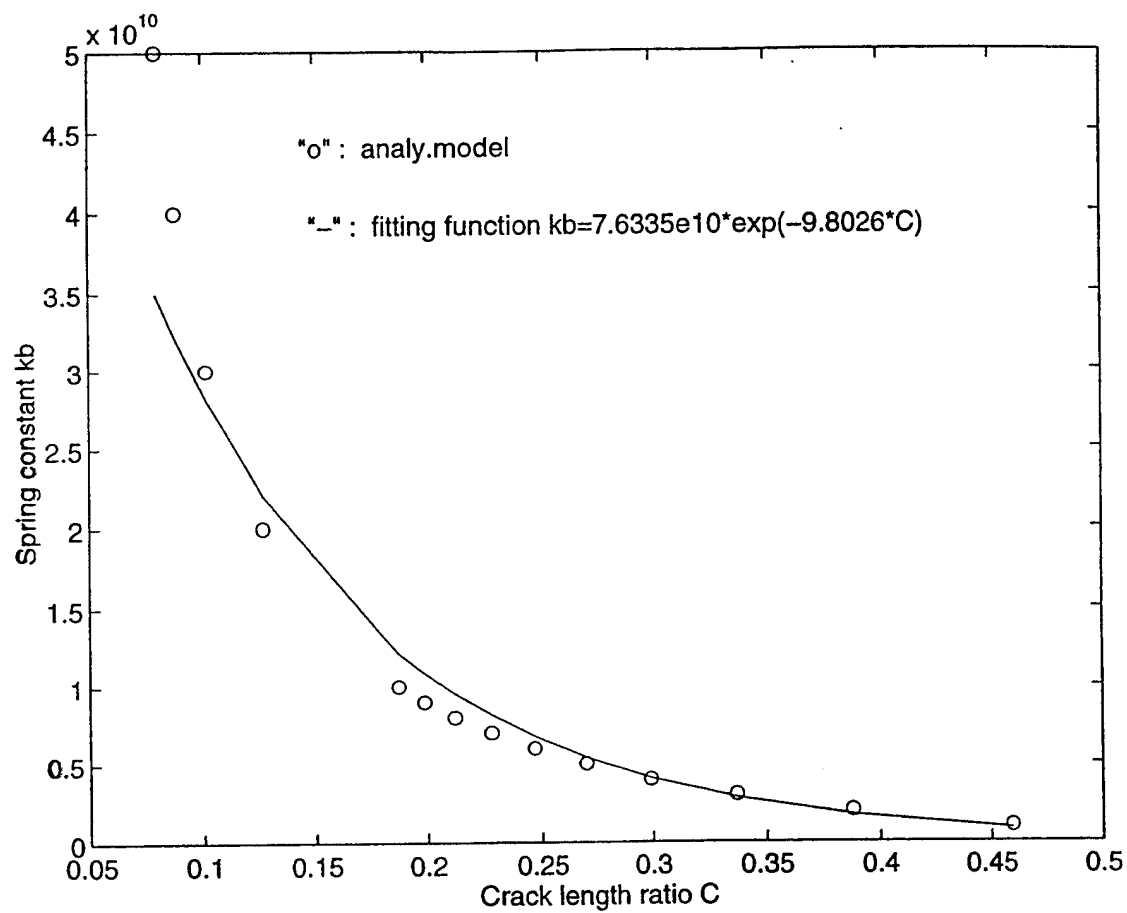**Figure 59. Spring Constant of a Glass /Epoxy Composite with V_f=0.64 (Low crack case)**

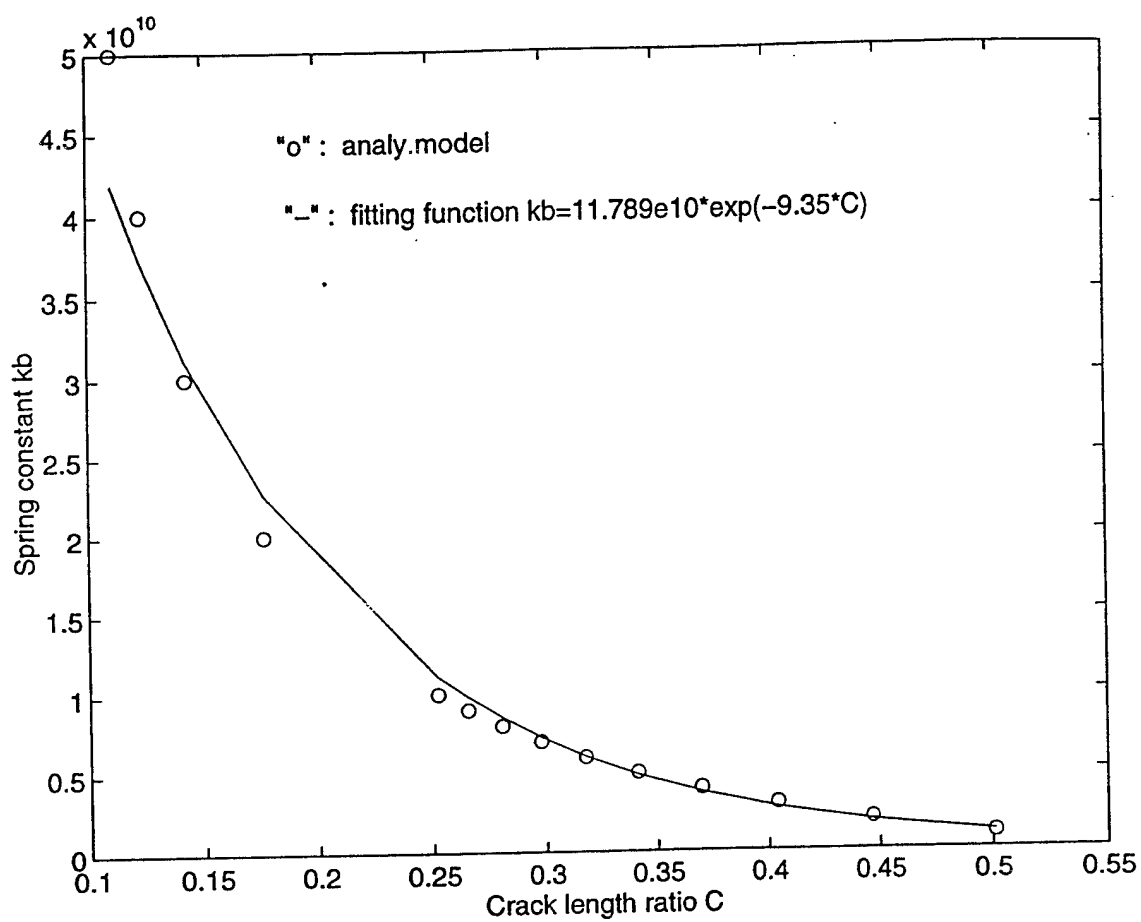Figure 60. Spring Constant of a Boron /Epoxy Composite with V_f=0.49 (Low crack case)

Figure 61. Spring Constant of a Boron /Epoxy Composite with V_f=0.64 (Low crack case)
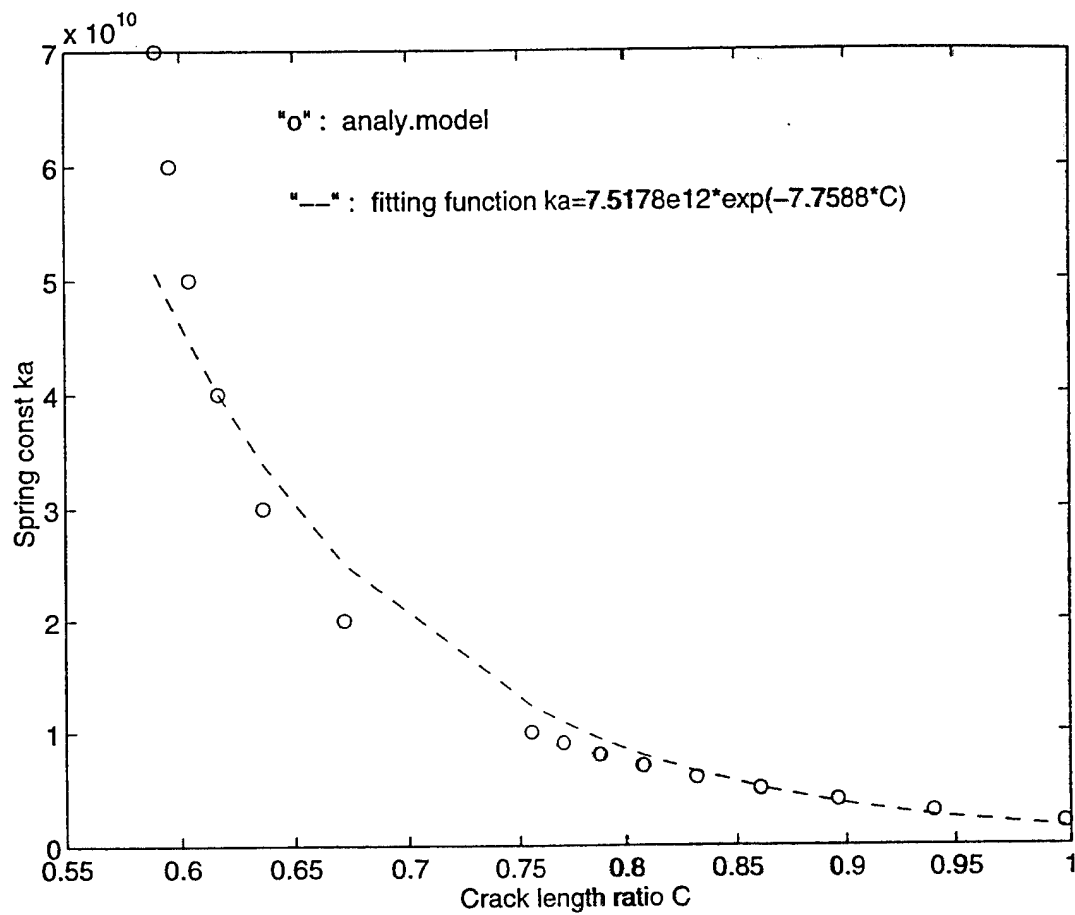
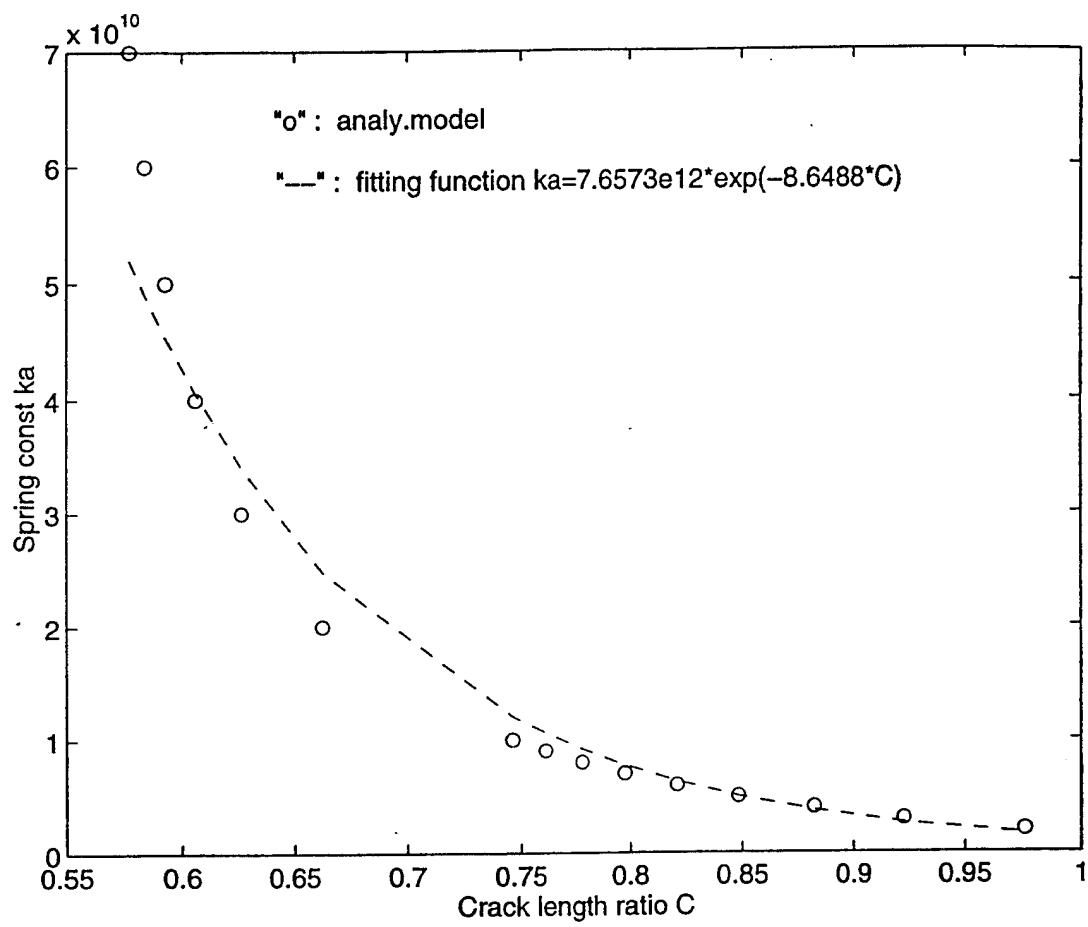**Figure 62. Spring Constant of a Graphite /Epoxy Composite with V_f=0.49 (Upper crack case)**

Figure 63. Spring Constant of a Graphite /Epoxy Composite with V_f=0.64 (Upper crack case)
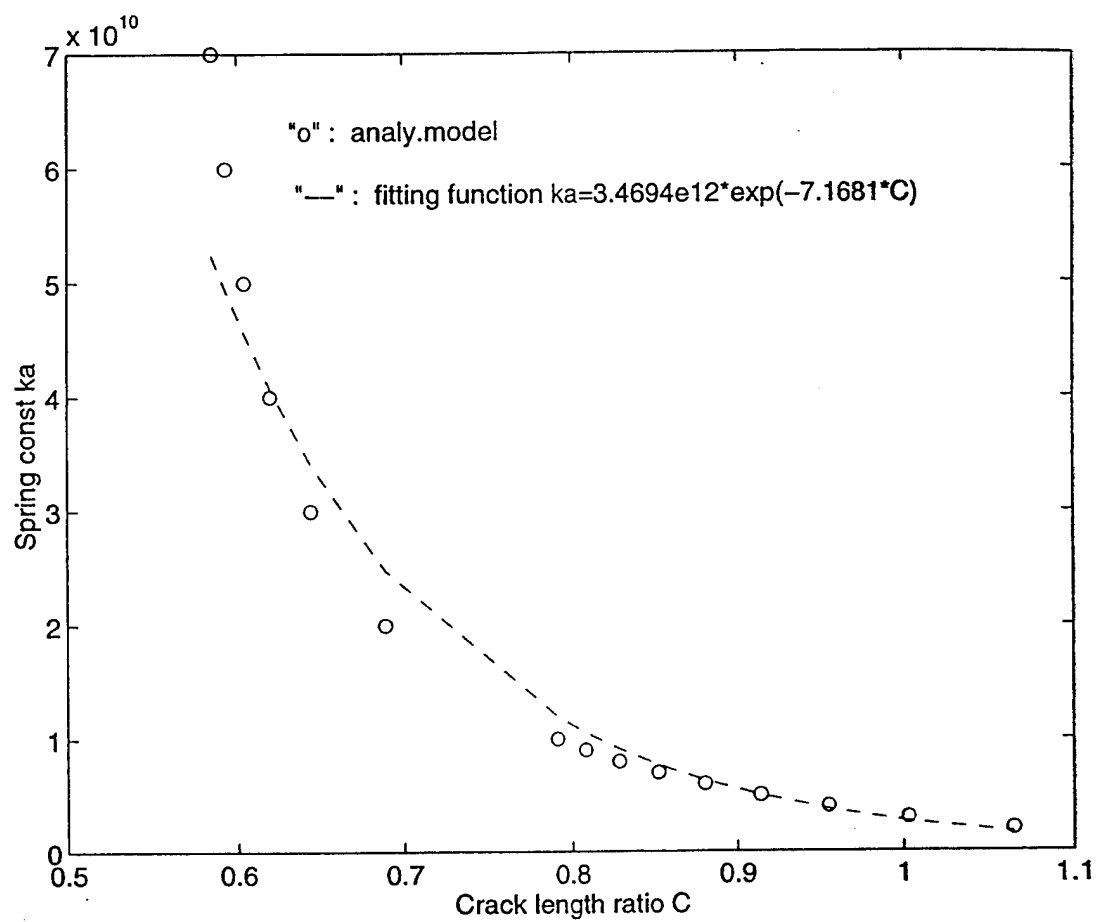
Figure 64. Spring Constant of a Glass /Epoxy Composite with V_f=0.49 (Upper crack case)
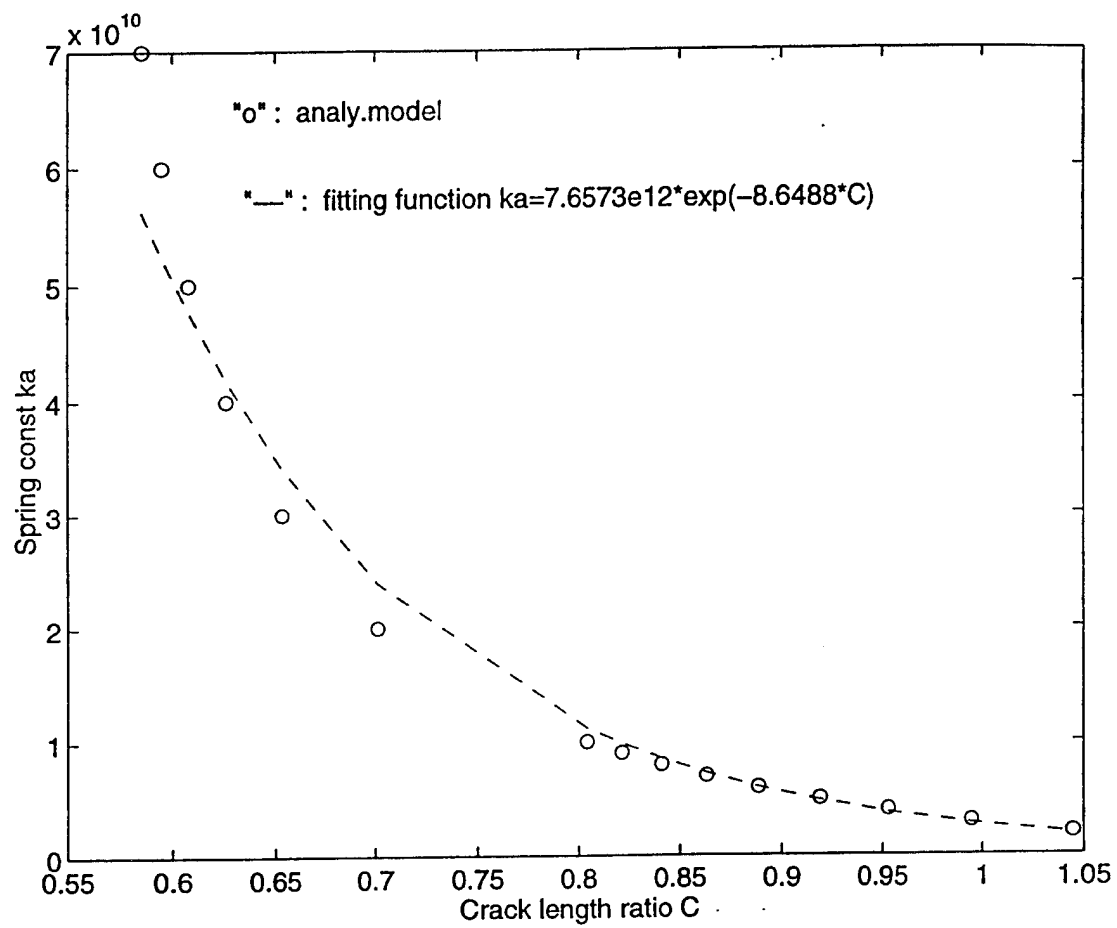
Figure 65. Spring Constant of a Glass /Epoxy Composite with V_f=0.64 (Upper crack case)
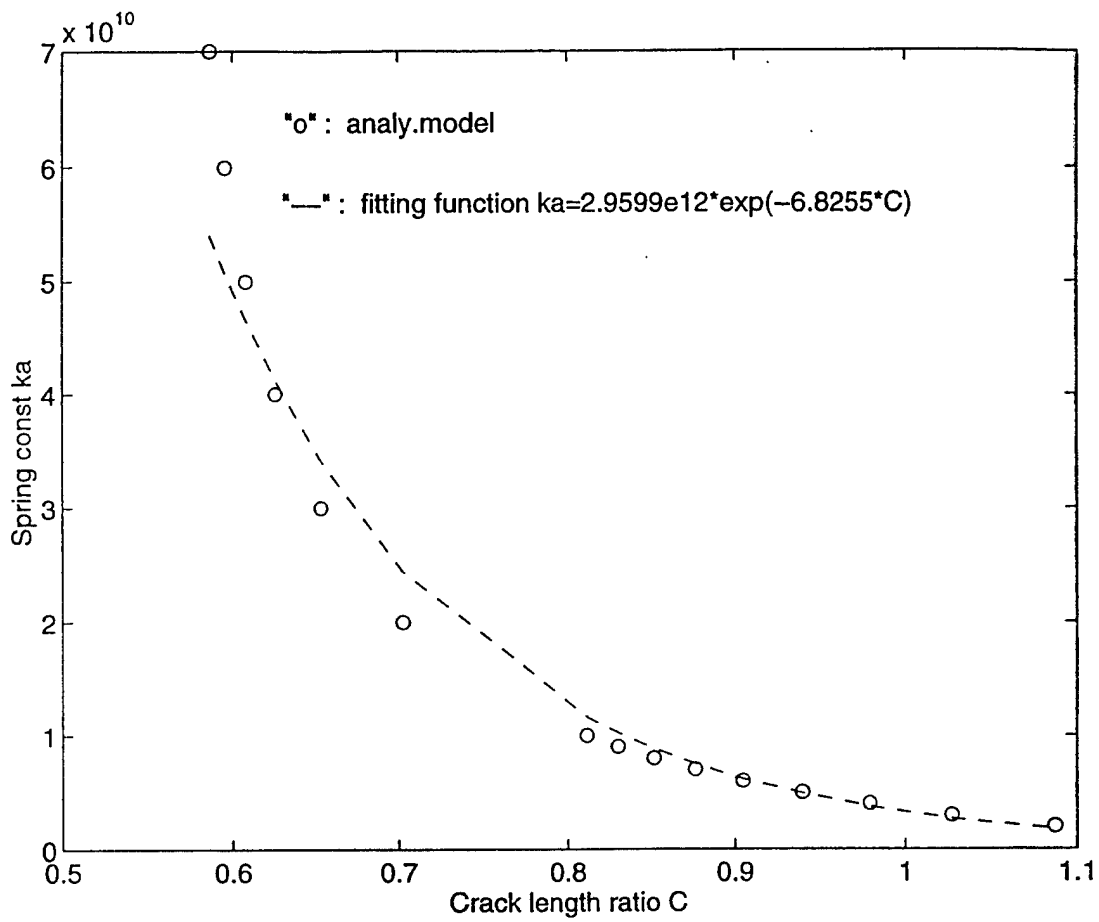
Figure 66. Spring Constant of a Boron /Epoxy Composite with V_f=0.49 (Upper crack case)
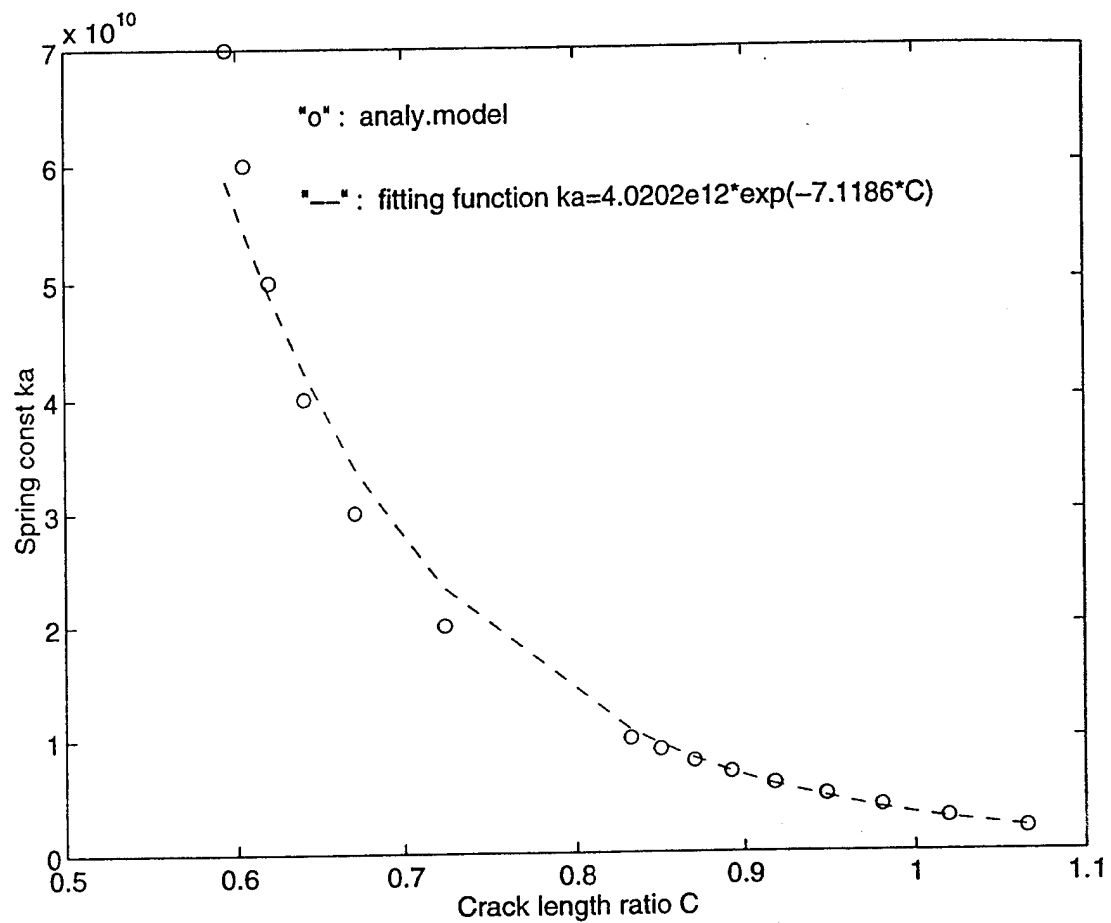
Figure 67. Spring Constant of a Boron /Epoxy Composite with V_f=0.64 (Upper crack case)

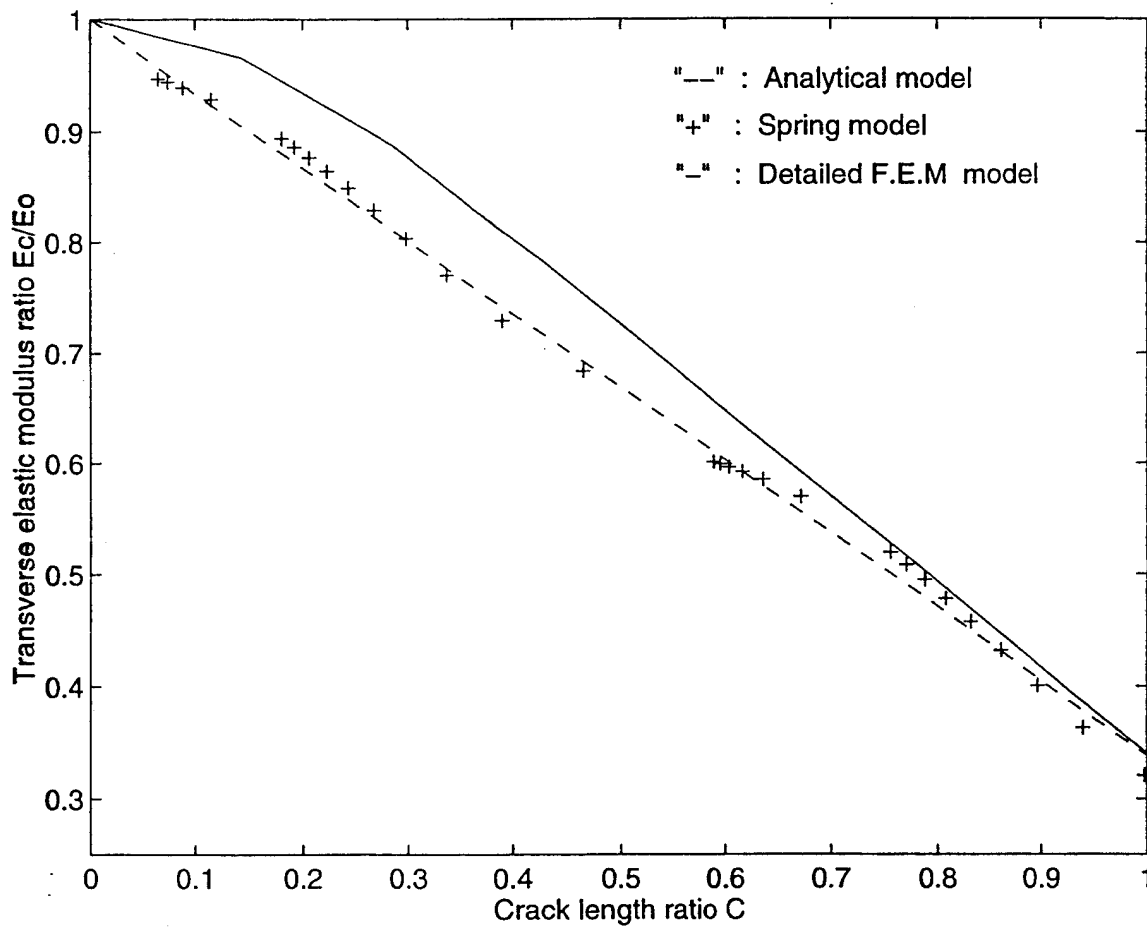# APPENDIX H. TRANSVERSE ELASTIC MODULUS OF COMPOSITE.

Figure 68. Transverse Elastic Modulus of a Graphite/Epoxy Composite of Three Models ($V_f = 0.49$)
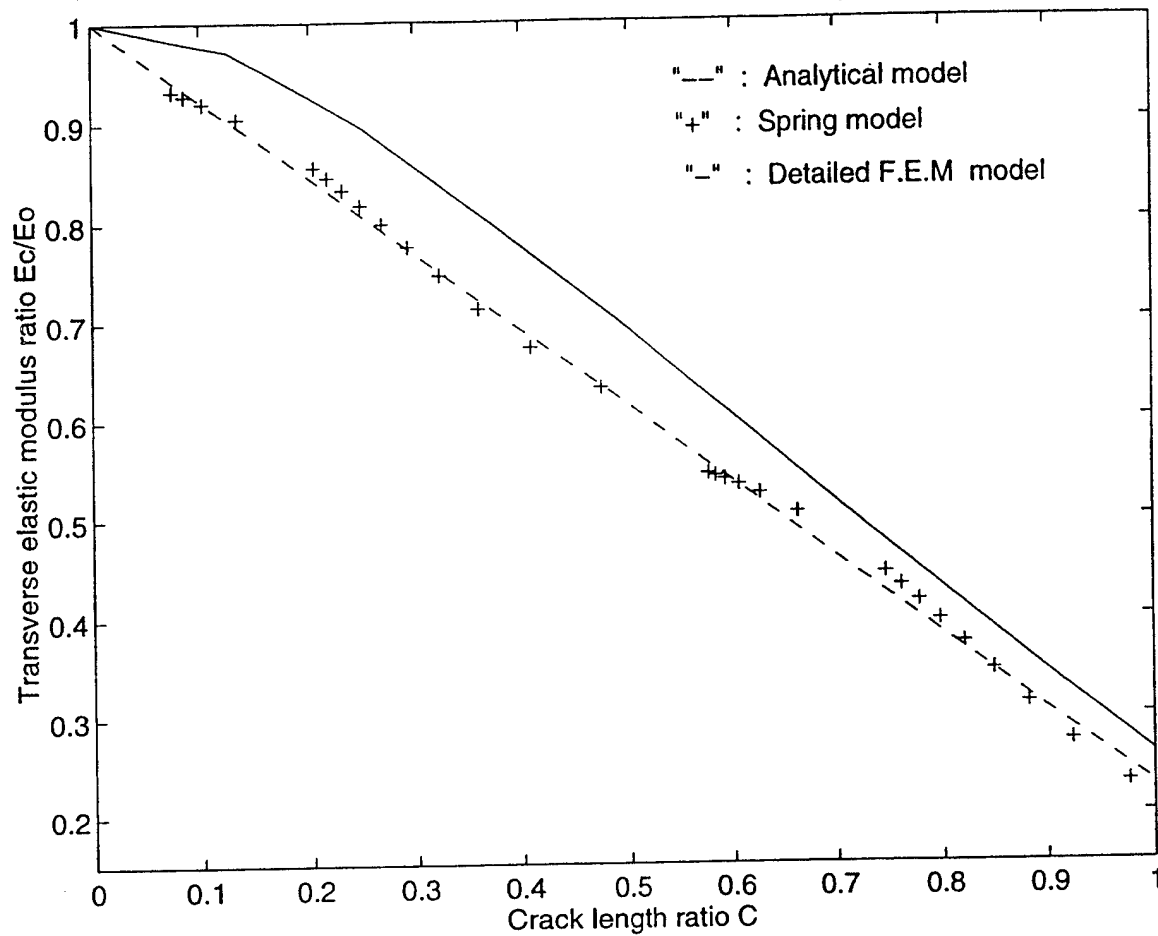
91

Figure 69. Transverse Elastic Modulus of a Graphite/Epoxy Composite of Three Models ($V_f = 0.64$)

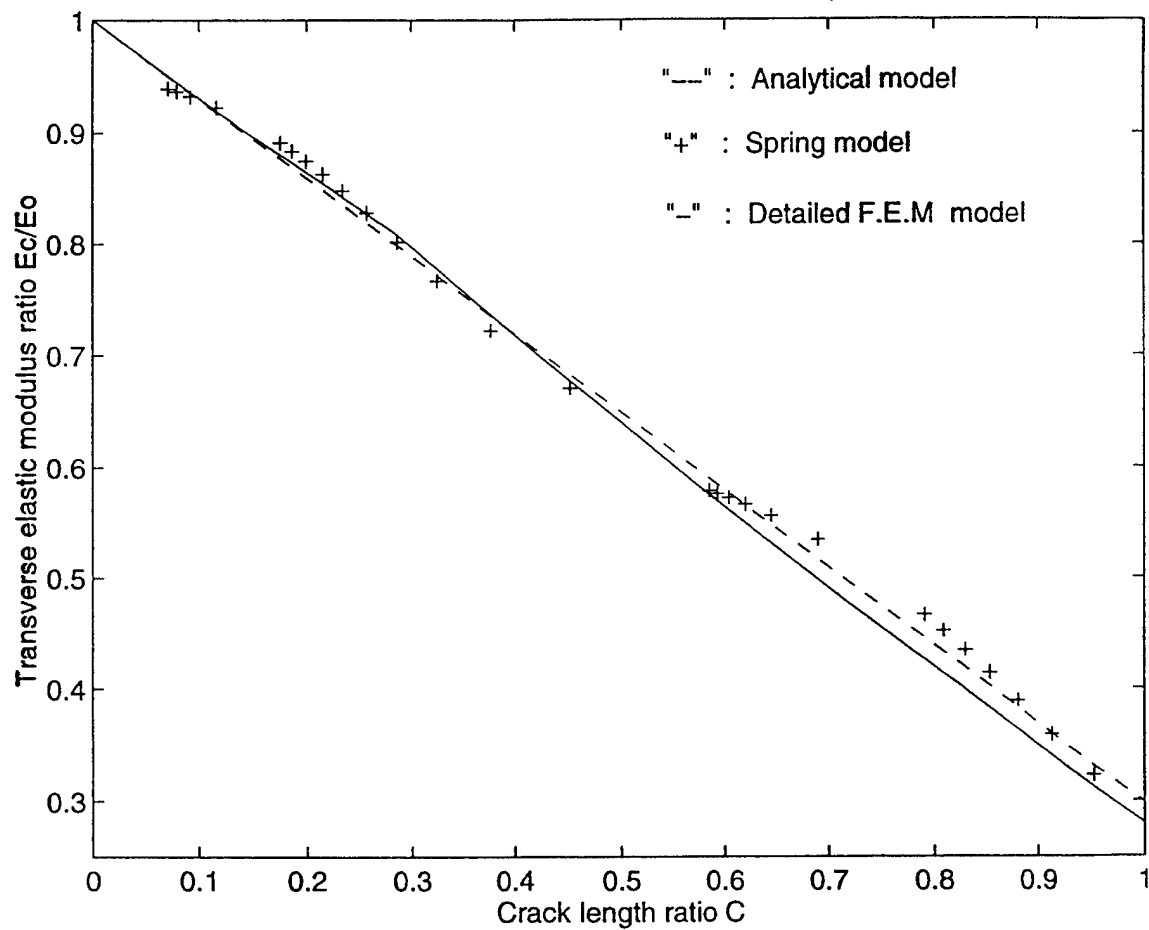**Figure 70. Transverse Elastic Modulus of a Glass/Epoxy Composite of Three Models**
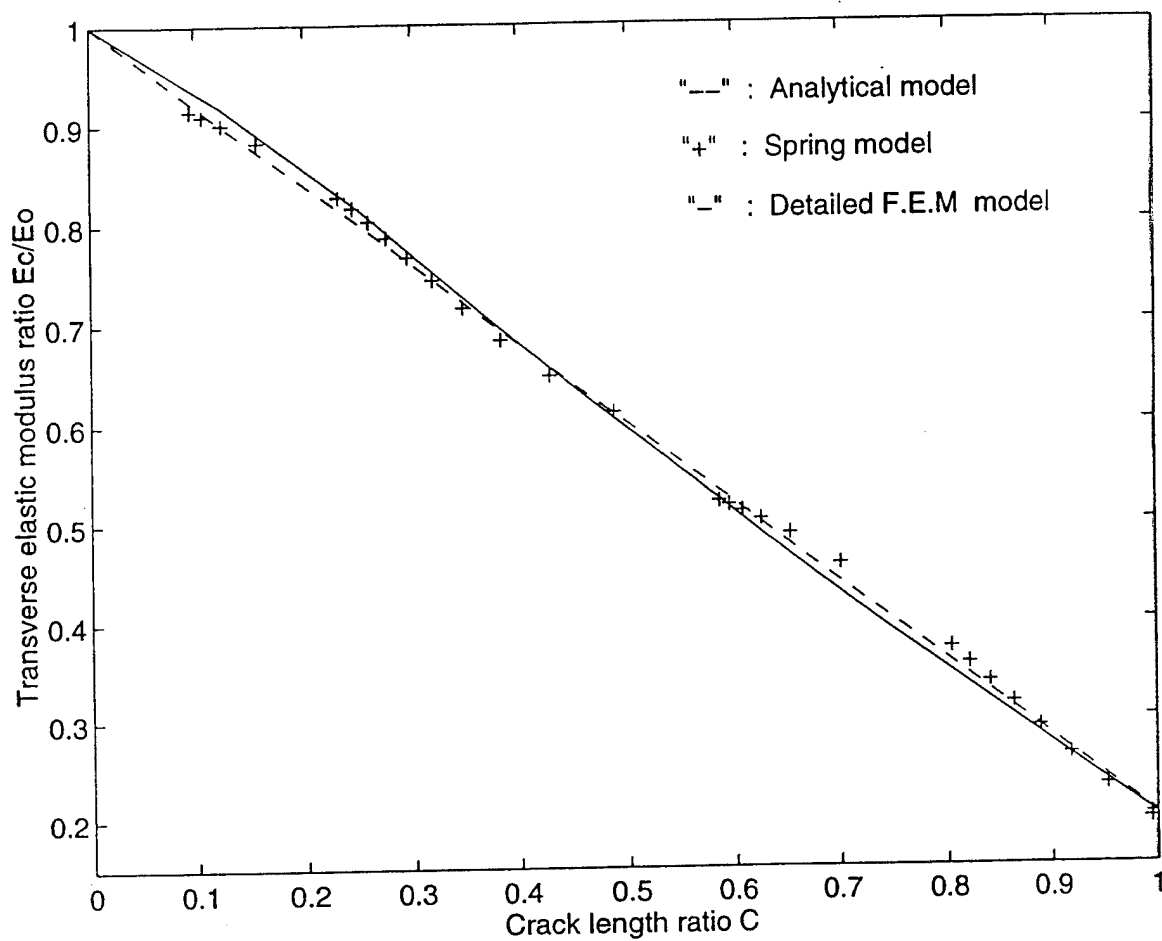$$(V_f = 0.49)$$

93

Figure 71. Transverse Elastic Modulus of a Glass/Epoxy Composite of Three Models
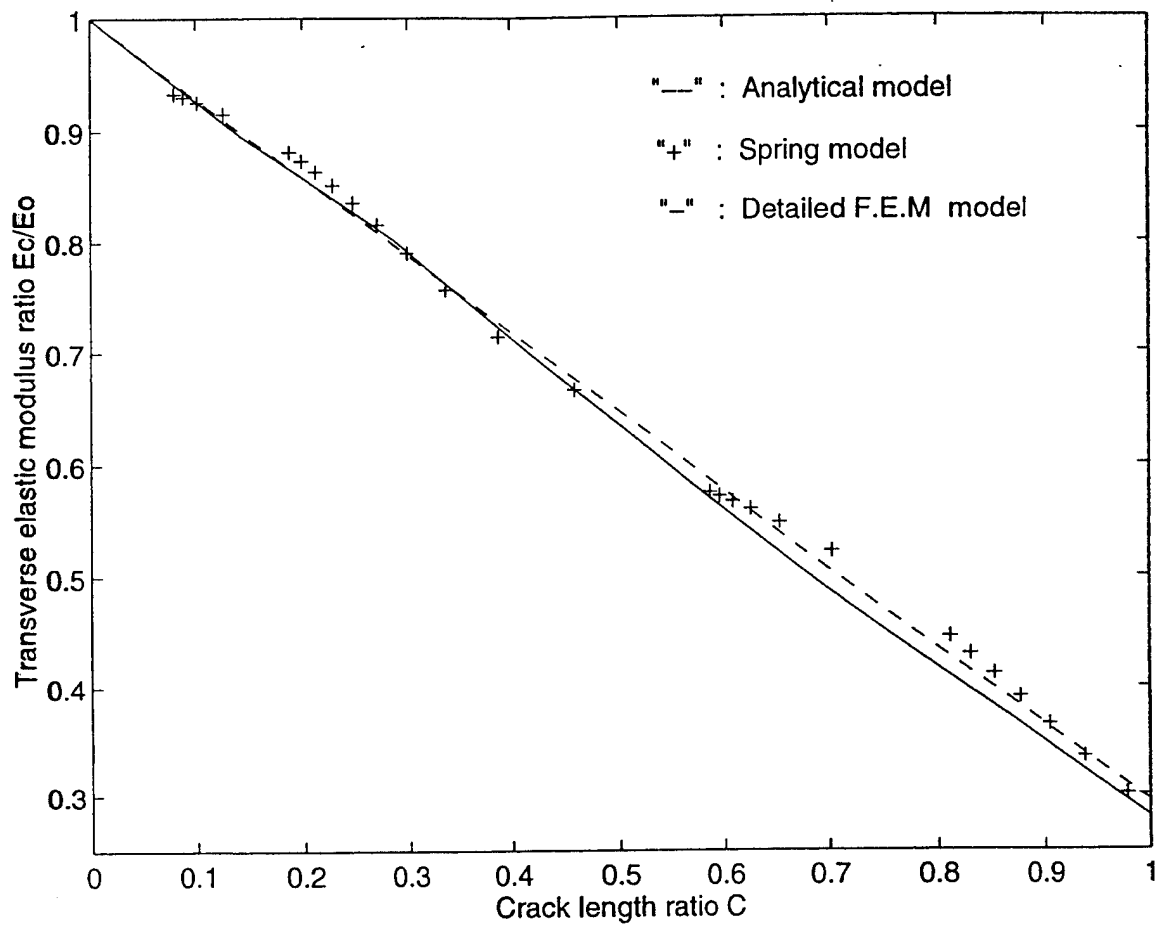$(V_f = 0.64)$

Figure 72. Transverse Elastic Modulus of a Boron/Epoxy Composite of Three Models ($V_f = 0.49$)
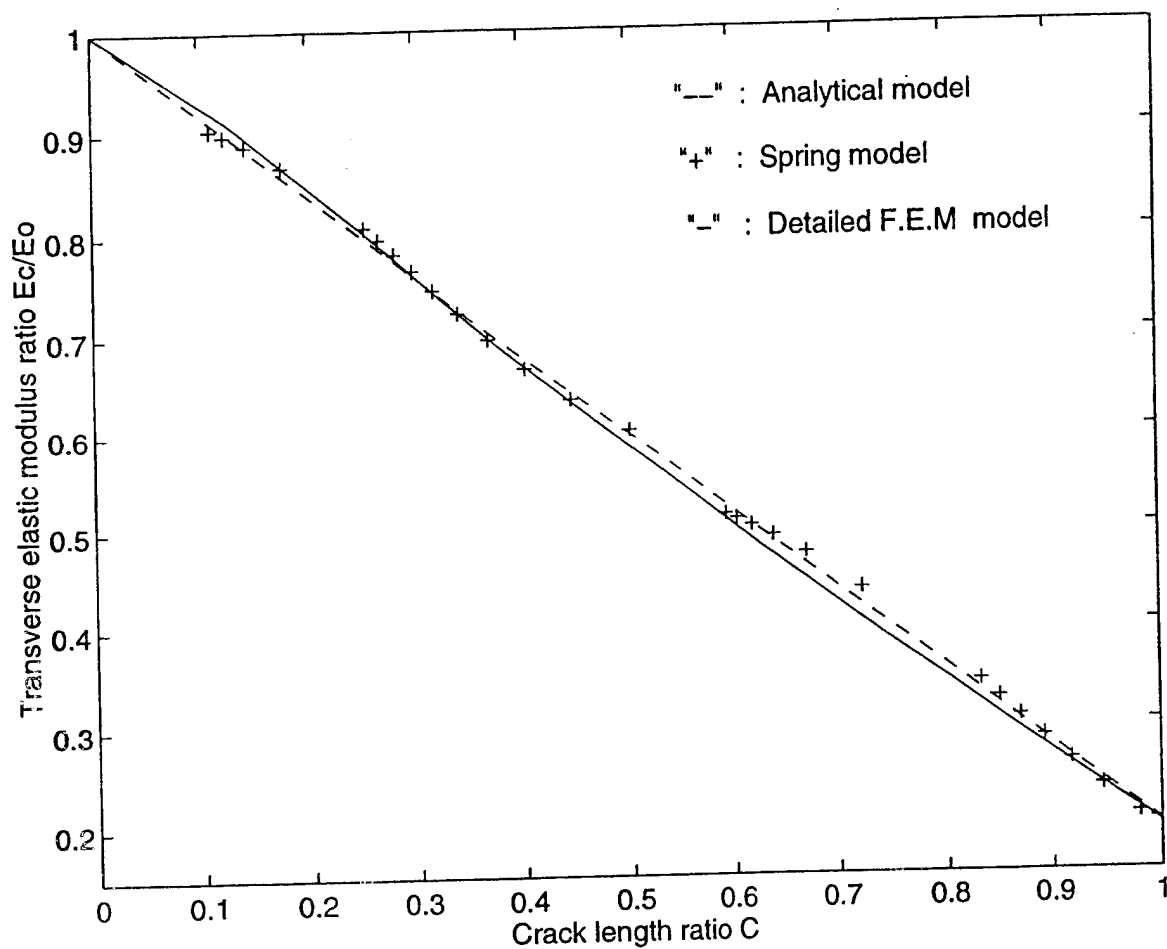
Figure 73. Transverse Elastic Modulus of a Boron/Epoxy Composite of Three Models ($V_f = 0.64$)

REFERENCE LIST

1. Kwon, Y. W., "Calculation of Effective Moduli of Fibrous Composites With or Without Micro-Mechanical Damage," *Composite Structures*, Vol. 25 (1993) pp. 637-650.

2. Broutman, L. J. & Sahu, S., Progressive damage of a glass reinforced plastic during fatigue, SPI, 24th Annual Technical Conference, Washington, D.C., February 1969, Section 11-D.

3. Highsmith, A.L. & Reifsnider, K.L., "Stiffness-Reduction Mechanisms In Composite Laminates. In Damage In Composite Materials," ASTM STP 775, American Society for Testing and Materials, Philadelphia, PA, 1982, pp. 103-17.

4. Talreja, R., "Transverse Cracking And Stiffness Reduction In Composite *Laminates." Journal Composite Materials*, 19 July 1985, 355-75.

5. Talreja, R., "Stiffness Properties Of Composite Laminates With Matrix Cracking And Interior Delamination." *Engng Fract. Mech.*, 25 (5/6) (1986) 751-62.

6. Kwon, Y. W. and J. M. Berner, "Numerical Modeling of Stiffness Reduction Due to Transverse Cracking in Unidirectional Composites," *Computational Engineering*, ed. B. M. Kwak and M. Tanaka, New York: 1994.

7. Bickford, W. B., *A First Course in the Finite Element Method*, Boston, Massachusetts: Irwin, 1990.

INITIAL DISTRIBUTION LIST

		No. Copies
1.	Defense Technical Information Center 8725 John J. Kingman Rd., STE 0944 Ft. Belvoir, VA 22060-6218	2
2.	Library, Code 13 Naval Postgraduate School Monterey, CA 93943-5101	2
3.	Professor Young W. Kwon, Code ME/kw Department of Mechanical Engineering Naval Postgraduate School Monterey, CA 93943-5000	2
4.	Chairman, Code ME/Kk Department of Mechanical Engineering Naval Postgraduate School Monterey, CA 93943-5000	1
5.	Naval Engineering Curricular Office, Code 34 Naval Postgraduate School Monterey, CA 93943-5000	1
6.	Chinese National Defense Management College Library P.O. Box 90046, Chung-her, Taipe 1 County, Taiwan, R.O.C.	2
7.	Guo, Jia-Yuarn No. 3-4 Aly 15 Pin-Shan Street Fengshan Taiwan, R.O.C.	2